

Analysis techniques for aeroacoustics: noise source identification

P. Jordan

Institut Pprime, UPR-CNRS-3346,
Université de Poitiers, ENSMA, France

1 Introduction

Aeroacoustic analysis is concerned with the problem of *sound source mechanism identification*. Let us consider for a moment what we mean by this, because, depending on the context, the same terminology can be interpreted differently. Two different contexts for the analysis of an aeroacoustic system, or indeed a fluid flow system in general, are: (1) the *kinematic* context; and, (2) the *dynamic* context.

When we are interested in kinematics, we are concerned with description of the space-time structure of a fluid flow, and perhaps with phenomenological explanations *vis-à-vis* our observation of that structure: *this vortical structure interacted with that one to produce this or that result*. Such kinematic descriptions will very often be with regard to some observable; in aeroacoustics that observable is the radiated sound field: *this vortical structure interacted with that one to produce this or that property of the sound field*.

Aeroacoustic theory was constructed from such a kinematic standpoint. Lighthill (1952) states on the second page of his seminal paper that he wishes to provide “...a general procedure for estimating the *intensity* of the sound produced in terms of the details of the fluid flow...”. He makes it clear that the search for sound source mechanisms, as he intends it, “is concerned with uncovering the mechanism of conversion of energy between...the kinetic energy of fluctuating shearing motions and the acoustic energy of fluctuating longitudinal motions.”. The “details of the fluid flow”, the “fluctuating shearing motions”, are considered as given.

However, if we are to consider more broadly the problem of source mechanism identification, we realise that, in order to be able to speak clearly about source mechanisms we need to be able to speak clearly about fluid

dynamics mechanisms, and it is difficult to do so without placing ourselves in the context of dynamics: we would like to be able to explain *why this vortical structure interacted with that one to produce this or that property of the sound field*; i.e. we wish to discern the dynamic law that underpins the observed interactions, *where sound production is concerned*. Of course there is one very simple, correct, but not terribly useful, reply to such an inquiry: the Navier-Stokes equations constitute the underlying dynamic law, both of the “fluctuating shearing motions” of the turbulence and the “fluctuating longitudinal motions” of the sound field. But for high Reynolds number turbulence this law, and the space-time flow structure that it engenders, are—from the point of view of perspicacious phenomenological description, flow-state prediction, or design guidance—invariably too complex to be useful; we are thus forced to seek simplified models.

Lighthill (1952) provided us with a tool that allows the “fluctuating longitudinal motions” of the sound field to be modelled more simply, and then connected to the “fluctuating shearing motions” of the turbulence; but the same tool does not provide an analogous clarification with regard to how the latter should be modelled. His theory and its descendants are probably best thought of as means by which *the connection* between the two kinds of motion can be modelled; and by virtue of this connection-model, some insight can be provided regarding the kinematic structure of the underlying flow motions. However, these theories cannot inform with regard to the dynamic law of the “fluctuating shearing motions” that underpin sound radiation.

These lectures are concerned with the exposition of an analysis methodology which, while it uses aeroacoustic theory as a central tool, attempts to take the problem of source mechanism identification beyond the kinematic limits imposed by that theory. The methodology, whose objective is source mechanism identification on both kinematic and dynamic levels (implicit assumption is that the Navier-Stokes dynamics can be modelled in a simplified manner, that simplification being specifically tailored with respect to the acoustic observable), is largely an exercise in system reduction, and relies both on theoretical considerations and signal-processing tools. The document has therefore been organised as follows. In the next section, §2, an overview of aeroacoustic theory is provided; we focus on the earliest (Lighthill (1952)) and most recent theoretical developments (Goldstein (2003), Goldstein (2005), Sinayoko et al. (2011)). This is followed by a discussion, in section §3, of the source modelling problem, the bulk of the attention being focused on ‘coherent structures’. It is in this section that the analysis methodology evoked above is outlined. Example implementations of the methodology are presented in section §4, where two specific case

studies are considered. The various signal processing tools used to support the analysis methodology, and which are implemented in section §4 without detailed explanation, form the basis of section §5. Finally, a brief outline of two reduced-order dynamical modelling approaches is given in section §6.

Acknowledgements

I would like to acknowledge Laurent Cordier, Joël Delville, Yves Gervais and Bernd Noack, all of whom have contributed to the development of the ideas contained in this document. Anurag Agarwal, Tim Colonius and Jonathan Freund, who continue to stimulate and enrich my general appreciation of aeroacoustics, also deserve to be mentioned. Finally, very special thanks are due to André Cavalieri and Franck Kerhervé, on whose research a good deal of the material contained herein is based.

2 Aeroacoustic theory

In this section we provide a brief presentation of the basic mathematical constructs necessary for an understanding of aeroacoustic theory: the wave equation and its integral solution by means of the free-space Green's function. This is followed by a detailed exposition of the theory of Lighthill (1952), where its dimensional, statistical and instantaneous representations are used to illustrate some aspects of the relationship between turbulence and sound. The first theoretical evolutions of Lighthill's theory, due to Phillips (1960) and Lilley (1974), are then evoked, more briefly, followed by a presentation of the most recent theoretical developments, due to Goldstein (2003) and Goldstein (2005), and which amount to a generalisation of the earlier acoustic analogies. Our exposition of Goldstein's generalised theory follows the slightly modified formulation proposed by Sinayoko et al. (2011), and we use a model problem computed by these authors in order to illustrate some of the essential aspects of aeroacoustic theory as it pertains to subsonic jets.

2.1 The wave equation

The motion of a viscous, compressible, heat-conducting fluid continuum is governed by the equations of mass, momentum and energy conservation, and the equation of state, which are, respectively:

$$\frac{\partial \rho}{\partial t} + \nabla \cdot (\rho \mathbf{u}) = m \quad (1)$$

$$\frac{\partial \rho \mathbf{u}}{\partial t} + \nabla \cdot \rho \mathbf{u} \mathbf{u} + \nabla \cdot \mathbf{P} = \mathbf{f} \quad (2)$$

$$\rho T \left(\frac{\partial s}{\partial t} + \mathbf{u} \cdot \nabla s \right) = -\nabla \cdot \mathbf{q} + \boldsymbol{\tau} : \nabla \mathbf{u} \quad (3)$$

$$dp = c^2 d\rho + \left(\frac{\partial p}{\partial s} \right)_\rho ds, \quad (4)$$

where

$$\mathbf{P} = p\mathbf{I} - \boldsymbol{\tau} \quad (5)$$

represents fluid stresses associated with the thermodynamic pressure, p , and the viscous stresses, $\boldsymbol{\tau}$; \mathbf{q} is the heat flux due to conduction, given by Fourier's law, $\mathbf{q} = -K\nabla T$; T is the temperature, s is the entropy, and

$$c^2 = \left(\frac{\partial p}{\partial \rho} \right)_s. \quad (6)$$

Taken together, these equations constitute a closed system of differential equations that governs all classes of motion of a fluid continuum. The

mechanisms that underpin the generation of propagative acoustic energy are contained within this system. However, due to the non-linear nature of the equations, general solutions are not available; and, furthermore, in the general case it is not clear how to: (1) classify motions as turbulent, thermal and acoustic—this classification being possible only in certain limited cases, as shown by Chu and Kovásznyai (1958); and, (2) identify clear relationships of cause and effect between different regions of a fluid in motion, or between different kinds of fluctuation of that motion (between velocity and pressure for example).

In acoustics, the situation is considerably simplified, as we focus on one particular class of fluid motion: that which is characterised by small amplitude fluctuations of a potential nature. In this case it is legitimate to linearise the equations of motion, which reduce, in the case of a quiescent fluid medium, and in the absence of external sources of mass or momentum, to

$$\frac{\partial \rho'}{\partial t} + \rho_o \nabla \cdot \mathbf{u}' = 0 \quad (7)$$

$$\rho_o \frac{\partial \mathbf{u}'}{\partial t} + \nabla p' = 0 \quad (8)$$

$$\frac{\partial s'}{\partial t} = 0 \quad (9)$$

$$p' = c_o^2 \rho'. \quad (10)$$

The velocity perturbation, \mathbf{u}' , can be eliminated by subtracting the time derivative of the mass conservation equation from the divergence of the momentum conservation equation, giving:

$$\frac{\partial^2 \rho'}{\partial t^2} - \Delta p' = 0. \quad (11)$$

p' and/or ρ' can then be eliminated, by means of the constitutive equation $p' = c_o^2 \rho'$, to give wave equations in either the density or the pressure:

$$\begin{aligned} \frac{\partial^2 p'}{\partial t^2} - c_o^2 \Delta p' &= 0 \\ \frac{\partial^2 \rho'}{\partial t^2} - c_o^2 \Delta \rho' &= 0. \end{aligned} \quad (12)$$

2.2 Green's functions

So, what do these wave equations represent? Well, simply stated: they describe propagative wave-like fluctuations of the density or pressure in a

quiescent fluid medium¹. Such wave-like motion will only be sustained by the medium for space-time scales that satisfy the balance expressed by the equation. A Fourier transform of the wave equation can help illustrate this:

$$\begin{aligned}\omega^2 p' &= c_o^2 |\boldsymbol{\kappa}|^2 p', \\ \omega p' &= c_o |\boldsymbol{\kappa}| p'.\end{aligned}\tag{13}$$

This is known as the dispersion relation for the wave equation, and what it states is that for propagation to be supported in the quiescent, homogeneous fluid medium considered, the time scales of the motion, ω^{-1} , must be matched with the space scales, $\boldsymbol{\kappa}^{-1}$, by the speed of sound, c_o . When such a system is excited by a disturbance that does not satisfy this criterion, the associated motions will not be supported as a propagating wave, and will tend, rather, to evanesce (very rapid decay). This concept is central to understanding the mechanisms by which a given source structure² generates a propagative energy flux, and these mechanisms can be most clearly seen by looking at integral solutions of the wave equation, which can be obtained by means of an appropriate Green's function.

The Green's function, $G(\mathbf{x}, t | \mathbf{y}, \tau)$, describes the wave-like *response* (as described by the wave equation) of the quiescent fluid medium to an impulse localised at $\mathbf{x} = \mathbf{y}$ and at time $t = \tau$. Where the free-field Green's function is concerned, a single clap of your hands in a large open space is an approximate equivalent of this. Mathematically, this can be expressed as:

$$\frac{\partial^2 G}{\partial t^2} - c_o^2 \Delta G = \delta(\mathbf{x} - \mathbf{y}) \delta(t - \tau).\tag{14}$$

Once we have found the Green's function we are equipped with a filter which, when convolved with a given source, will extract the space-time scales of the source structure that *match* the balance expressed by the propagation operator ($\frac{\partial^2 p'}{\partial t^2} = c_o^2 \Delta p'$), and which are therefore capable of producing a propagating wave. For example, consider the physical problem described by

$$\frac{\partial^2 p'}{\partial t^2} - c_o^2 \Delta p' = q(\mathbf{x}, t),\tag{15}$$

where $q(\mathbf{x}, t)$ is some (known) source (this could be an unsteady, spatially-distributed force field, or an unsteady, spatially-distributed, addition of

¹In fact the wave equation can, alternatively, be expressed in terms of a velocity potential, ϕ , from which density ($\rho = \frac{1}{c_o^2} \frac{\partial \phi}{\partial t}$), pressure ($p = \frac{\partial \phi}{\partial t}$) and velocity ($\mathbf{u} = \nabla \phi$) can all be derived.

²In what follows we will see that the flow equations can be manipulated such that this source represents the turbulent jet.

mass), that drives sound waves in a quiescent medium. Multiplying equation 14 by p' , equation 15 by G , integrating in both space and time (neglecting the effect of initial conditions), and subtracting the former from the latter, we get, provided there are no solid boundaries, and after a little manipulation

$$p'(\mathbf{x}, t) = \int_{t_0}^t \int_V q(\mathbf{y}, \tau) G(\mathbf{x}, t | \mathbf{y}, \tau) d\mathbf{y} d\tau. \quad (16)$$

The right hand side of this equation describes the filtering of $q(\mathbf{y}, \tau)$ by $G(\mathbf{x}, t | \mathbf{y}, \tau)$: $G(\mathbf{x}, t | \mathbf{y}, \tau)$ allows us to extract, from the heart of what might be an extremely complex, and largely (acoustically) ineffective, source structure, $q(\mathbf{y}, \tau)$, only those scales that are acoustically-matched.

This is the key to analysing and understanding aeroacoustic systems, experimentally, numerically or theoretically. It is necessary to identify the space-time scales (or flow behaviour that leads to the generation of such scales) that are actually efficient in the generation of sound waves—the vast majority are not. In the context of Lighthill's acoustic analogy the problem is exactly that described here, insofar as the wave equation used has the same form as 15. For the more sophisticated acoustic analogies, while the wave equations and source descriptions change, conceptually we are dealing with the same scenario: the dispersion-relations and Green's functions will change, and this will modify the criterion by which we identify the pertinent space-time scales of the 'source' quantity (which it is then necessary to relate to the turbulence characteristics of the jet). Further discussion on this point is provided in the next section.

2.3 Lighthill's acoustic analogy

Lighthill's acoustic analogy is a peculiar kind of object: it amounts to a model representation of the jet-noise problem, but one which is described by an exact fluid dynamics equation (nothing less than the Navier-Stokes equations is stated). This dual quality constitutes both the elegance of, and the crux of the interpretational difficulties associated with, the acoustic analogy formulations in general.

Lighthill sought to rearrange the equations of mass and momentum conservation—taken in their full, non-linear form—such that the wave operator would appear. In order to do so, he followed the same basic steps used in the derivation of the wave equation, but without performing the linearisation. Taking the time derivative of the mass conservation equation, the divergence of the momentum conservation equation, and combined the

two gives, after a little manipulation,³

$$\frac{\partial^2 \rho'}{\partial t^2} - c_o^2 \Delta \rho' = \nabla \cdot \nabla \cdot (\rho \mathbf{u} \mathbf{u} - \boldsymbol{\tau} + (p' - c_o^2 \rho') \mathbf{I}). \quad (17)$$

In terms of p' , the equation becomes

$$\frac{1}{c_o^2} \frac{\partial^2 p'}{\partial t^2} - \Delta p' = \nabla \cdot \nabla \cdot (\rho \mathbf{u} \mathbf{u} - \boldsymbol{\tau}) + \frac{1}{c_o^2} \frac{\partial^2}{\partial t^2} (p' - c_o^2 \rho'). \quad (18)$$

These inhomogeneous wave equations can be interpreted in terms of a source term (the right hand side) that drives density or pressure fluctuations, as described by the left hand side.

We can now examine integral solutions to Lighthill's equation, and it is at this point that we make a first connection between radiated sound energy and the flow characteristics of a turbulent jet.

These solutions can be considered on three levels: that of (1) elementary dimensional analysis; (2) time-averaged (second and higher order) statistics; and, (3) space-time analysis. The third of these gives us the most direct insight, in so far as it allows a local (in space and time) grasp of the sound production mechanisms; it is most useful for highly organised flows, and/or for understanding the organised component of high Reynolds number flows ('coherent structures'). In the second approach, detailed understanding is hampered by time-averaging, and we are obliged to consider the connection between the radiated sound power and the jet flow via the second and higher order statistical moments of the unsteady flow; this kind of approach is most useful for the more random components of the flow unsteadiness. The first of the approaches is the most elementary of the three, where very little physical insight is provided regarding the underlying mechanisms. In section §3 we will revisit these representations when we discuss the role played by coherent structures in the generation of sound.

Integral solutions to equations 17 and 18 can be obtained using the Green's function formalism outlined earlier. Henceforth we will change to tensor notation, we will only consider the equation expressed in terms of p' , and we will consider the simplified source quantity

$$\frac{\partial^2 \rho u_i u_j}{\partial y_i \partial y_j}(\mathbf{y}, t) : \quad (19)$$

the term associated with viscous effects $\boldsymbol{\tau}$ can be neglected for most flows of interest, and the third term on the right hand side of equation 18 is believed

³See Lighthill (1952) for full details.

to correspond to the effect of temperature fluctuations (this is often referred to as the entropy source term). This is probably an oversimplification, as in high Mach number flows there is evidence to suggest that the first and third terms on the right hand side of equation 18 are correlated (cf. Bodony and Lele (2005)). However, as our objective in this lecture is to make as clear as possible, and in as simple a manner as possible, the essential workings of acoustic analogies, we will continue to use this simplified scenario. Once the reasoning has been clearly understood in terms of the simplified source term, it is conceptually straightforward to extend to more complex source terms.

The free-field Green's function is $G_o = \frac{\delta}{4\pi|\mathbf{x}-\mathbf{y}|}$, and so solution to Lighthill's equation can be written as follows:

$$\begin{aligned} p'(\mathbf{x}, t) &= \int_{-\infty}^{\infty} \int_{V_y} \frac{\partial^2 \rho u_i u_j}{\partial y_i \partial y_j}(\mathbf{y}, t) \delta\left(t - \tau - \frac{|\mathbf{x} - \mathbf{y}|}{c_o}\right) \frac{dV_y d\tau}{4\pi|\mathbf{x} - \mathbf{y}|} \\ &= \int_{V_y} \frac{\partial^2 \rho u_i u_j}{\partial y_i \partial y_j}\left(\mathbf{y}, t - \frac{|\mathbf{x} - \mathbf{y}|}{c_o}\right) \frac{dV_y}{4\pi|\mathbf{x} - \mathbf{y}|}. \end{aligned} \quad (20)$$

From equation 20 we can proceed in two ways: (1) we can do the most basic kind of dimensional analysis, which will lead to the simplest expressions of the relationship between radiated sound power and flow characteristics; or, (2) we can take things from the statistical standpoint. We will here do both.

First, however, we introduce two simplifications that are frequently used. The first exploits the reciprocity property of the Green's function, which means that source and observer can be interchanged. This allows the double divergence in equation 20, which is in terms of the source coordinates \mathbf{y} , to be expressed in terms of the observer coordinates, \mathbf{x} , at which point it can be taken outside the volume integral:

$$p'(\mathbf{x}, t) = \frac{1}{4\pi} \frac{\partial^2}{\partial x_i \partial x_j} \int_{V_y} \rho u_i u_j \left(\mathbf{y}, t - \frac{|\mathbf{x} - \mathbf{y}|}{c_o}\right) \frac{dV_y}{|\mathbf{x} - \mathbf{y}|}. \quad (21)$$

Now that differentiation is being performed in the observer frame (assumed to be in the farfield), where fluctuations are entirely acoustic, the spatial derivatives are related to temporal derivatives through

$$\frac{\partial}{\partial x_i} = -\frac{x_i}{|\mathbf{x}|} \frac{1}{c_o} \frac{\partial}{\partial t}, \quad (22)$$

because we are dealing with a non-dispersive wavefield: if you want to know the spatial gradient of the waveform, rather than walk along the wave and measuring the slope as you go, you can simply stay put, letting the

wavefield pass you by, at the speed of sound; by then measuring its temporal rate of change, knowing its propagation speed and considering that the sound waves are locally plane, you immediately have access to the spatial derivative. The solution can thus be written, because we are in the farfield ($|\mathbf{x} - \mathbf{y}| \approx |\mathbf{x}|$), in the following simplified form:

$$p'(\mathbf{x}, t) = \frac{x_i x_j}{4\pi c_o^2 |\mathbf{x}|^3} \frac{\partial^2}{\partial t^2} \int_{V_y} \rho u_i u_j \left(\mathbf{y}, t - \frac{|\mathbf{x}|}{c_o} \right) dV_y. \quad (23)$$

Dimensional analysis Let us consider the problem of the subsonic propulsive jet, which is the system that Lighthill's analogy was first used to assess. If we consider that a characteristic eddy dimension in the turbulent jet plume is of the order of the jet diameter, D , which corresponds, approximately, to the vorticity thickness of the mixing-layer at the end of the potential core of a subsonic jet⁴, a characteristic frequency is $f = U_o/D$, where U_o is the exit velocity of the jet, and $Df/c_o = U_o/c_o = M$, where M is the Mach number (a measure of compressibility). This means that

$$p' \sim \frac{f^2}{c_o^2} \rho_o U_o^2 \frac{D^3}{|\mathbf{x}|} \quad (24)$$

$$\sim \rho_o U_o^2 \frac{f^2}{c_o^2} \frac{M^2 c_o^2}{f^2} \frac{D}{|\mathbf{x}|} \quad (25)$$

$$\sim \rho_o U_o^2 M^2 \frac{D}{|\mathbf{x}|}, \quad (26)$$

and so the acoustic intensity, $I = \frac{\langle p'^2 \rangle}{\rho_o c_o}$, should scale as

$$I \sim \rho_o U_o^3 M^5 \left(\frac{D}{|\mathbf{x}|} \right)^2 \sim U_o^8. \quad (27)$$

This very simple analysis immediately shows the very strong dependence of the sound power radiated on the velocity and Mach number of a jet. This was the first major result of Lighthill's theory. In terms of jet noise control, if we are to judge an analysis in terms of the impact it has had on the design of the application, it remains *the most significant* result to date: it was clear from this analysis that the jet velocity and Mach number would need to be reduced, and that moderate reductions could lead to significant reductions

⁴This region is now known to be one of the most important in terms of sound production, but was not known at the time of Lighthill's first estimates of the sound power radiated by a flow

in sound power. In order to do so, without losing thrust, larger diameter jets would be required: the introduction, and subsequent optimisation of, the (low and high) by-pass jet engine led, between 1950 and 2000, to a 20dB reduction in the sound power radiated by jets exhausts at take-off.

Statistical analysis We now consider the second way in which it is possible to relate radiated sound power to flow/source characteristics. Using equation 23, expressions for the autocorrelation of the farfield pressure (which is related to the power spectrum of the pressure by a Fourier transform) can be obtained; this can then be related to the turbulence through the term $\rho u_i u_j$. Assuming constant density in the source term ($\rho = \rho_o$), the autocorrelation function of the farfield pressure fluctuation is given by

$$\begin{aligned} C(\mathbf{x}, \tau) &= \langle p'(\mathbf{x}, t) p'(\mathbf{x}, t + \tau) \rangle \\ &= \rho_o \frac{x_i x_j x_k x_l}{16\pi^2 c_o^4 |\mathbf{x}|^6} \int_{V_{y''}} \int_{V_{y'}} \left\langle \frac{\partial^2 u_i u_j}{\partial t^2} \left(\mathbf{y}', t - \frac{|\mathbf{x} - \mathbf{y}'|}{c_o} \right) \right. \\ &\quad \left. \frac{\partial^2 u_k u_l}{\partial t^2} \left(\mathbf{y}'', t - \frac{|\mathbf{x} - \mathbf{y}''|}{c_o} + \tau \right) \right\rangle d\mathbf{y}' d\mathbf{y}''. \end{aligned} \quad (28)$$

And, if the turbulence is considered to be statistically stationary, the equation can be rewritten as

$$\begin{aligned} C(\mathbf{x}, \tau) &= \rho_o \frac{x_i x_j x_k x_l}{16\pi^2 c_o^4 |\mathbf{x}|^6} \int_{V_{y''}} \int_{V_{y'}} \frac{\partial^4}{\partial \tau^4} \left\langle u_i u_j \left(\mathbf{y}', t - \frac{|\mathbf{x} - \mathbf{y}'|}{c_o} \right) \right. \\ &\quad \left. u_k u_l \left(\mathbf{y}'', t - \frac{|\mathbf{x} - \mathbf{y}''|}{c_o} + \tau \right) \right\rangle d\mathbf{y}' d\mathbf{y}''. \end{aligned} \quad (29)$$

By virtue of this equation we now have a far more detailed description of how the sound power radiated by a jet flow is related to that flow: for a single observer in the farfield, at \mathbf{x} , the sound power, as a function of frequency,⁵ is given by a volume integral, over the entire extent of the jet, of the two-point, two-time correlation of the Reynolds stress field.

Instantaneous analysis The two approaches presented above, both of which involve considerable data compression when compared to the full space-time fields from which they begin (and where mechanisms show themselves most exactly), necessarily hide a certain amount of information.⁶

⁵The power spectrum is given by taking the Fourier transform

⁶In 1952 measurement and computational capabilities were such that it was not possible to access full-field data; the two-point correlations were about the best that could be achieved.

Some kind of compression is of course indispensable: the formidable complexity of the full space-time structure of turbulence is such that useful assimilation and description is only possible at the expense of some such information loss. However, the ever-increasing capabilities of numerical simulation, experimental data acquisition and data post-processing, mean that new kinds of analysis and modelling methodologies, which deal more directly with the local space-time details of flow mechanisms, can be considered. Such methodologies and tools, which are outline sections §3, §5 and §6, are essential from the point of view of real-time, closed-loop control, towards which fluid dynamics research is headed. It is therefore useful to consider the space-time-local representation of the solution to Lighthill's equation 20.

As outlined above, the physical system described by an inhomogeneous wave equation, such as Lighthill's, involves a coupling between a source term—which in this sub-section we will simply refer to as $q(\mathbf{x}, t)$ —and some base-flow medium that can sustain propagative, wavelike perturbations in accordance with the balance expressed by the wave equation. In the context of Lighthill's formulation, the mechanism by which a propagative wave is set up, in the quiescent medium, by the source, amounts to the acoustic matching described earlier. In order therefore to have access to what is happening in real time, we need to examine the integral solution in its most primitive form

$$p(\mathbf{x}, t) = \frac{1}{4\pi} \int_V \frac{q(\mathbf{y}, t - \frac{|\mathbf{x}-\mathbf{y}|}{c})}{|\mathbf{x}-\mathbf{y}|} d^3\mathbf{y}. \quad (30)$$

What this equation tells us is that if we consider the excitation field in a distorted space-time reference frame, $q(\mathbf{y}, t - \frac{|\mathbf{x}-\mathbf{y}|}{c})$, the farfield pressure is given by simply summing all the points of that distorted field. If the source field is considered in undistorted space-time, additional time-delays, corresponding to wave-propagation times, weight the summation. Physically, this summation corresponds to the time-delayed constructive and destructive interference phenomena that underpin, respectively, loud or quiet source activity. We will discuss this in the next section when we consider the antenna-like wavepacket radiation associated with 'coherent structures'.

2.4 Acoustic analogies of Phillips and Lilley

A difficulty with the Lighthill analogy, for the problem of jet noise, is that the wave equation describes propagation through a medium at rest. While this model is approximately correct outside the region of turbulent flow, it is not so within the turbulent jet. Two subsequent developments, due to Phillips (1960) and Lilley (1974), were aimed at improving this aspect of

the model. Both were motivated by the desire to explicitly describe effects associated with interactions between the sound field and the jet.

Phillips (1960) proposed an alternative rearrangement of the Navier-Stokes equations, leading to:

$$\frac{d}{dt} \frac{d^2 \pi}{dt^2} - \frac{\partial}{\partial x_i} \left(c^2 \frac{\partial \pi}{\partial x_j} \right) = \frac{\partial u_i}{\partial x_j} \frac{\partial u_j}{\partial x_i} - \frac{\partial}{\partial x_i} \left(\frac{1}{\rho} \frac{\partial \tau_{ij}}{\partial x_j} \right) + \frac{d}{dt} \left(\frac{1}{C_p} \frac{ds}{dt} \right), \quad (31)$$

where $\pi = \log(p)$. This equation comprises, explicitly, in the wave operator, some effects of the mean velocity (via the material derivative), in addition to the effects of variable speed of sound that can occur due to temperature or Mach number gradients. The right hand side, which again is considered a source term, comprises, as did Lighthill's source term, terms associated with non-linear momentum fluctuations, viscous stresses and a term due to entropy unsteadiness.

The modification due to Lilley (1974) comes about from recognising that if we linearise Phillips' equation about some mean flow, and we consider the fluctuation to be entirely acoustic, the source contains a term associated with flow-acoustic interaction in the form of refraction of the small-amplitude acoustic disturbances by mean shear. To see this, consider acoustic disturbances propagation in two-dimensional shear-flow with mean velocity profile $U(y) \cdot \vec{x}$. Linearising Phillip's equation about this mean flow, and neglecting thermal and viscous effects, the LHS reduces to

$$\frac{1}{c_o^2} \frac{d^2 p}{dt^2} - \frac{\partial^2 p}{\partial x_i^2}, \quad (32)$$

while the RHS reduces to

$$2\rho_o \frac{\partial v}{\partial x} \frac{dU(y)}{dy}. \quad (33)$$

When it is possible to verify that the perturbation about the mean flow is indeed an acoustic disturbance, this term describes the refraction of sound by the mean flow, and one can argue that it should appear on the LHS, in the wave operator.

With this in mind, Lilley took the material derivative of Phillips' equation:

$$\frac{d}{dt} \left[\frac{d^2 \pi}{dt^2} - \frac{\partial}{\partial x_i} \left(c^2 \frac{\partial \pi}{\partial x_j} \right) \right] + 2 \frac{\partial v_j}{\partial x_i} \frac{\partial}{\partial x_j} \left(c^2 \frac{\partial \pi}{\partial x_i} \right) = -2 \frac{\partial v_j}{\partial x_i} \frac{\partial v_k}{\partial x_j} \frac{\partial v_i}{\partial x_k} + \Psi, \quad (34)$$

where

$$\Psi = 2 \frac{\partial v_j}{\partial x_i} \frac{\partial}{\partial x_j} \left(\frac{1}{\rho} \frac{\partial \tau_{ij}}{\partial x_k} \right) - \frac{d}{dt} \left[\frac{\partial}{\partial x_i} \left(\frac{1}{\rho} \frac{\partial \tau_{ij}}{\partial x_j} \right) \right] + \frac{d^2}{dt^2} \left[\frac{1}{c_p} \frac{ds}{dt} \right], \quad (35)$$

and we see that by linearising this equation about a base-flow comprising mean shear, we obtain a wave operator that describes acoustic propagation in that shear-flow. It is important to point out however, that a Reynolds decomposition of the velocity field (into $U+u$), does not correspond to a split into hydrodynamic and acoustic disturbances, and so it is not clear that the linear term so obtained does indeed correspond to a refraction effect in the case of a turbulent jet, where the fluctuation about the time-averaged mean, within the jet, is largely hydrodynamic. This problem of decomposing a flow into acoustic and non-acoustic components lies at the heart of much of the controversy that surrounds acoustic analogy approaches for the description and study of aeroacoustic systems. The most recent attempt to address this difficulty has been proposed by Goldstein (2003) and Goldstein (2005).

2.5 The generalised acoustic analogy

Goldstein (2003, 2005) has shown how the formulations typified by the efforts of Phillips (1960) and Lilley (1974) amount to particular cases in a more general framework. In what follows we provide, firstly, a compact exposition of this generalised formulation, in order to facilitate description and interpretation. We then proceed to give a more complete presentation, following the work of Sinayoko et al. (2011). We end with an overview of a model problem, proposed by these authors, which serves as an instructive illustration of the differences between different acoustic analogy formulations.

In a nutshell Consider the Navier-Stokes equations, expressed in the compact form

$$\mathcal{N}(\mathbf{q}) = 0, \quad (36)$$

where \mathbf{q} is here a vector containing all of the dependent flow variables, and \mathcal{N} represents the Navier-Stokes operator. Goldstein's generalisation of the acoustic analogy proceeds as follows.

The full solution is first decomposed into a (possibly unsteady) base-flow and a perturbation:

$$\mathbf{q} = \bar{\mathbf{q}}_D + \mathbf{q}_A, \quad (37)$$

the subscript D indicating non-linear fluid dynamics, as opposed to linear acoustic dynamics, which are denoted by the subscript A . From this

decomposition an equation of the following form can be written

$$\mathcal{L}_{\bar{\mathbf{q}}_D}(\mathbf{q}_A) = s(\bar{\mathbf{q}}_D), \quad (38)$$

where $\mathcal{L}_{\bar{\mathbf{q}}_D}$ is a linear operator describing the evolution of \mathbf{q}_A , a disturbance generated and carried by $\bar{\mathbf{q}}_D$. Let us consider this equation for a moment, as it has certain uses, but also some limitations.

A first difficulty associated with an equation constructed in this manner is that, if we are to interpret it in terms of a non-acoustic, causal, source, $s(\bar{\mathbf{q}}_D)$, that drives an acoustic effect, \mathbf{q}_A , we need to be sure that the full flow solution has been decomposed into acoustic and non-acoustic, or radiating and non-radiating, components: there is presently no consensus as to how such a decomposition might be unambiguously effected.

A second difficulty becomes apparent when we consider what has been gained by identifying $s(\bar{\mathbf{q}}_D)$ in this way. If we consider equation 38 to be physically pertinent—in other words we believe that we have successfully decomposed the flow solution into acoustic and non-acoustic components—at best we can consider the decomposition of equation 37 to provide us with the kinematic structure of the flow, $\bar{\mathbf{q}}_D$, that underpins sound radiation. However, as we will see in the following example, $\bar{\mathbf{q}}_D$ is almost identical to \mathbf{q} , the full flow solution, as one would expect given the large amplitude disparity between hydrodynamic and acoustic fluctuations at the heart of the flow; and so the question that arises is the following: in what way does the information provided by decomposition 37 and equation 38 enlighten us with regard to the physical flow mechanisms associated with sound production? The answer appears to be: it constitutes a powerful means by which the radiating flow structure can be *visualised* and probed. For instance, by superposing $s(\bar{\mathbf{q}}_D)$ and $\bar{\mathbf{q}}_D$, and studying, simultaneously, the space-time (or frequency-wavenumber) structure of the two, it may be possible to gain some insight regarding what it was about the flow motions $\bar{\mathbf{q}}_D$ that led to the radiating source structure $s(\bar{\mathbf{q}}_D)$: *this structure ($\in \bar{\mathbf{q}}_D$) interacted with that structure ($\in \bar{\mathbf{q}}_D$) to produce this or that aspect of the source field ($\in s(\bar{\mathbf{q}}_D)$)*.

However, having clarified the kinematics in this way, it is then necessary to address the question of the dynamics, as the flow motions associated with the generation of sound can only be fully understood in the context of their underlying dynamic law. In the context of high Reynolds number turbulent jets, $\bar{\mathbf{q}}_D$ will be no less complex than \mathbf{q} , and thus the dynamic law of the source is approximately the Navier-Stokes operator; in which case we arrive at the conclusion that the sound-source mechanism is the turbulence! The point on which we insist is the same evoked in the introduction: while the acoustic analogies can provide simplified models for the propagation

and connection-to-turbulence parts of the problem, they do not directly provide any such simplification where the “fluctuating shearing motions” are concerned. These points will be further discussed in section §3.

Full derivation The following derivation, taken from Sinayoko et al. (2011), shows, in detail, how a generalised acoustic analogy, such as that evoked more compactly above, can be formulated for a homentropic fluid medium. The derivation is followed by the presentation and discussion of a model problem chosen by those authors; the problem considered constitutes a useful illustration of the differences between this and more conventional acoustic analogies; it also serves to illustrate the limitations of acoustic analogies in general.

Unsteady, non-radiating base-flow

The flow equations are written as:

$$\frac{\partial \rho}{\partial t} + \frac{\partial}{\partial x_j} \rho v_j = 0 \quad (39)$$

$$\frac{\partial}{\partial t} \rho v_i + \frac{\partial}{\partial x_j} \rho v_i v_j + \frac{\partial p}{\partial x_i} = \frac{\partial}{\partial x_j} \sigma_{ij} \quad (40)$$

$$\frac{\partial p}{\partial t} + v_j \frac{\partial p}{\partial x_j} + \gamma p \frac{\partial v_j}{\partial x_j} = 0. \quad (41)$$

Using a modified pressure variable $\pi = p^{1/\gamma}$, the momentum and energy equations can be rewritten as

$$\frac{\partial}{\partial t} \rho v_i + \frac{\partial}{\partial x_j} \rho v_i v_j + \frac{\partial}{\partial x_i} \pi^\gamma = 0 \quad (42)$$

$$\frac{\partial \pi}{\partial t} + \frac{\partial}{\partial x_j} \pi v_j = 0. \quad (43)$$

Note that the pressure equation now appears in conservative form.

For the moment consider that a filter capable of extracting acoustic, or radiating, disturbances, \mathbf{q}' , from the full flow variable, \mathbf{q} , exists: $\mathcal{L}' = \mathcal{I} - \mathcal{L}$.

Application of this filter to the conservation equations gives:

$$\frac{\partial \rho'}{\partial t} + \frac{\partial}{\partial x_j}(\rho v_j)' = 0 \quad (44)$$

$$\frac{\partial}{\partial t}(\rho v_i)' + \frac{\partial}{\partial x_j}(\rho v_i v_j)' + \frac{\partial}{\partial x_i}(\pi^\gamma)' = 0 \quad (45)$$

$$\frac{\partial(\pi)'}{\partial t} + \frac{\partial}{\partial x_j}(\pi v_j)' = 0. \quad (46)$$

The non-linear momentum flux term can be expanded as

$$\rho v_i v_j = \bar{\rho} \tilde{v}_i \tilde{v}_j + \tilde{v}_j(\rho v_i)' + \tilde{v}_i(\rho v_j)' - \tilde{v}_i \tilde{v}_j \rho' + O(\rho'^2), \quad (47)$$

where

$$\tilde{v}_i = \frac{\overline{(\rho v_i)}}{\bar{\rho}}. \quad (48)$$

$O(\rho'^2)$ terms, being quadratic in the radiating (acoustic variables), are several orders of magnitude smaller than radiating components, and can be neglected. Thus, application of the filter \mathcal{L}' to the expanded momentum flux term gives

$$(\rho v_i v_j)' \approx \underbrace{(\bar{\rho} \tilde{v}_i \tilde{v}_j)'}_A + \underbrace{(\tilde{v}_j(\rho v_i)' + \tilde{v}_i(\rho v_j)' - \tilde{v}_i \tilde{v}_j \rho')'}_B. \quad (49)$$

Term A is the acoustically-matched part of the non-linear momentum flux term, i.e. it comprises only those components of the triple correlation $\bar{\rho} \tilde{v}_i \tilde{v}_j$ that present radiation-capable space-time scales, and that can thereby couple with the sound field. The second group of terms, B, corresponds to acoustically-matched components of hydrodynamic-acoustic interaction terms: refraction, scattering, convective transport, etc.

Similarly the modified pressure term, which is also non-linear, can be expanded and filtered:

$$\pi^\gamma = (\bar{\pi} + \pi')^\gamma = \bar{\pi}^\gamma + \gamma \bar{\pi}^{\gamma-1} \pi' + O(\pi'^2), \quad (50)$$

$$(\pi^\gamma)' = \underbrace{(\bar{\pi}^\gamma)'}_A + \underbrace{(\gamma \bar{\pi}^{\gamma-1} \pi')'}_B. \quad (51)$$

On account of the homentropic character of the fluid medium, it can be shown (see Sinayoko et al. (2011) for details) that the radiating component

arising due to the non-linearity of the non-radiating pressure term, A , is equal to zero:

$$(\bar{\pi}^\gamma)' = \frac{\pi_\infty}{\rho_\infty} (\bar{\rho}^\gamma)' = \left(\frac{\rho_\infty}{\pi_\infty} \right)^{\gamma-1} (\bar{p})' = 0. \quad (52)$$

Similarly, the energy flux term, $(\pi v_j)'$, can be decomposed as follows

$$(\pi v_j)' \approx \underbrace{(\bar{\pi} \tilde{v}_j)'}_A + \underbrace{\left(\frac{\bar{\pi}}{\bar{\rho}} (\rho v_j)' + \tilde{v}_j \pi' - \frac{\bar{\pi}}{\bar{\rho}} \tilde{v}_j \rho' \right)'}_B, \quad (53)$$

and the radiating component of the non-linear part shown also to be equal to zero:

$$(\bar{\pi} \tilde{v}_j)' = \frac{\pi_\infty}{\rho_\infty} (\bar{\rho} \tilde{v}_j)' = \frac{\pi_\infty}{\rho_\infty} (\bar{\rho} v_j)' = 0. \quad (54)$$

The filtered Navier Stokes equations can now be re-written, placing all of the non-zero sound source terms, A (which comprise radiating components of non-linear interactions of non-radiating components) on the right hand side, and the flow-acoustic interaction terms, B , on the left:

$$\frac{\partial \rho'}{\partial t} + \frac{\partial}{\partial x_j} (\rho v_j)' = 0, \quad (55)$$

$$\begin{aligned} \frac{\partial}{\partial t} (\rho v_i)' + \frac{\partial}{\partial x_j} (\tilde{v}_j (\rho v_i)' + \tilde{v}_i (\rho v_j)' - \tilde{v}_i \tilde{v}_j \rho')' \\ + \gamma \frac{\partial}{\partial x_i} (\bar{\pi}^{\gamma-1} \pi')' = - \frac{\partial}{\partial x_j} (\bar{\rho} \tilde{v}_i \tilde{v}_j)', \end{aligned} \quad (56)$$

$$\frac{\partial \pi'}{\partial t} + \frac{\partial}{\partial x_j} \left(\frac{\bar{\pi}}{\bar{\rho}} ((\rho v_j)' - \tilde{v}_j \rho') + \tilde{v}_j \pi' \right)' = 0. \quad (57)$$

This is a generalised acoustic analogy, the source and propagator components of which depend on how the filter, \mathcal{L}' is defined.

Time-averaged base-flow

In order to compare the above formulation with more conventional approaches, Sinayoko et al. (2011) repeat the same derivation where the decomposition into base-flow and perturbation follows a simple Reynolds decomposition. The result leads to a formulation synonymous with the Linearised Euler Equations.

Base flow and perturbation are thus defined by

$$q = q_0 + q'', \quad (58)$$

where q_0 and q'' denote, respectively, the steady (time-averaged) and unsteady part of q . Following the previous procedure leads to

$$\frac{\partial \rho''}{\partial t} + \frac{\partial(\rho v_j)''}{\partial x_j} = 0, \quad (59)$$

$$\frac{\partial(\rho v_i)''}{\partial t} + \frac{\partial(\rho v_i v_j)''}{\partial x_j} + p_\infty \frac{\partial(\pi^\gamma)''}{\partial x_i} = 0, \quad (60)$$

$$\frac{\partial \pi''}{\partial t} + \gamma \frac{\partial(\pi v_j)''}{\partial x_j} = 0. \quad (61)$$

The term $\rho v_i v_j$ can be decomposed as

$$\begin{aligned} \rho v_i v_j &= \frac{\rho v_i \rho v_j}{\rho} \\ &= \begin{cases} (a) & \rho_0 \hat{v}_i \hat{v}_j + \\ (b) & \hat{v}_j (\rho v_i)'' + \hat{v}_i (\rho v_j)'' - \hat{v}_i \hat{v}_j \rho'' + \\ (c) & \frac{1}{\rho_0} (\rho v_i)'' (\rho v_j)'' - \frac{\hat{v}_j}{\rho_0} (\rho v_i)'' \rho'' - \frac{\hat{v}_i}{\rho_0} (\rho v_j)'' \rho'' + \frac{\hat{v}_i \hat{v}_j}{\rho_0} \rho''^2 + O(\rho''^3), \end{cases} \end{aligned} \quad (62)$$

where

$$\hat{v}_i = \frac{(\rho v_i)_0}{\rho_0}, \quad (63)$$

which is analogous to \tilde{v}_i but uses a steady base flow rather than a non-radiating base flow.

Term (a) is steady and so cannot contribute to sound production or propagation; term (b) is an interaction term, between the time-averaged mean flow and the fluctuation, although it is clearly incorrect to speak of flow-acoustic interaction, the fluctuation in this case being dominated by hydrodynamic unsteadiness (turbulence). Term (c) contains quadratic and higher order non-linearities dominated by hydrodynamic unsteadiness. It is terms of this kind that are referred to as ‘source’ in acoustic analogies that involve time-averaged base-flows, or Linearised Euler formulations.

The term $(\pi^\gamma)''$ is decomposed as:

$$\pi^\gamma = (\pi_0 + \pi'')^\gamma = \pi_0^\gamma + \gamma \pi_0^{\gamma-1} \pi'' + \frac{1}{2} \gamma(\gamma-1) \pi_0^{\gamma-2} \pi''^2 + O(\pi''^3) \quad (64)$$

$$(\pi^\gamma)'' \approx \gamma \pi_0^{\gamma-1} \pi'' + \frac{1}{2} \gamma(\gamma-1) \pi_0^{\gamma-2} (\pi''^2)''. \quad (65)$$

Finally, the term πv_j is decomposed as follows:

$$\pi v_j = \frac{\pi \rho v_j}{\rho} = \begin{cases} (a) & \frac{\pi_0}{\rho_0}(\rho v_j)_0 \\ (b) & \frac{\pi_0}{\rho_0}(\rho v_j)'' + \hat{v}_j \pi'' - \frac{\pi_0}{\rho_0} \hat{v}_j \rho'' \\ (c) & \frac{1}{\rho_0} \pi''(\rho v_j)'' - \frac{\hat{v}_j}{\rho_0} \rho'' \pi'' - \frac{\pi_0}{\rho_0^2} \rho''(\rho v_j)'' + \frac{\pi_0 \hat{v}_j}{\rho_0^2} \rho''^2 + O(\rho''^3), \end{cases} \quad (66)$$

where (a) has no unsteady part, (b) corresponds to interaction terms and (c) to source terms; however, Sinayoko *et al.* show that term (c) can be shown to be equal to zero.

Equations (59–61) are now re-written, the quadratic non-linear terms being placed on the right hand side, the interaction terms, between the mean-flow and the perturbation, being retained as ‘propagation terms’ on the left hand side:

$$\frac{\partial \rho''}{\partial t} + \frac{\partial}{\partial x_j}(\rho v_j)'' = 0, \quad (67)$$

$$\frac{\partial}{\partial t}(\rho v_i)'' + \frac{\partial}{\partial x_j}(\hat{v}_j(\rho v_i)'' + \hat{v}_i(\rho v_j)'' - \hat{v}_i \hat{v}_j \rho'') + \gamma \frac{\partial}{\partial x_i} \pi_0^{\gamma-1} \pi'' = f_{2i}, \quad (68)$$

$$\frac{\partial \pi''}{\partial t} + \frac{\partial}{\partial x_j} \left(\frac{\pi_0}{\rho_0}(\rho v_j)'' + \hat{v}_j \pi'' - \frac{\pi_0}{\rho_0} \hat{v}_j \rho'' \right) = 0, \quad (69)$$

where the momentum equation source term f_{2i} is defined as

$$f_{2i} \equiv -\frac{\partial}{\partial x_j} \left(\frac{1}{\rho_0}(\rho v_i)''(\rho v_j)'' - \frac{\hat{v}_j}{\rho_0}(\rho v_i)''\rho'' - \frac{\hat{v}_i}{\rho_0}(\rho v_j)''\rho'' + \frac{\hat{v}_i \hat{v}_j}{\rho_0} \rho''^2 \right) - \frac{1}{2} \gamma(\gamma-1) \frac{\partial}{\partial x_i} (\pi_0^{\gamma-2} (\pi'')^2). \quad (70)$$

Application of the two foregoing formulations to a model flow, where the flow is manipulated in such way that the sound-production mechanisms are clear, will help to more fully appreciate what the two formulations involve.

Application to a model problem We here provide a brief exposition of the model problem and main results. For more complete details the reader should refer to Sinayoko *et al.* (2011).

A Direct Numerical Simulation is performed wherein a laminar, axisymmetric jet is driven at the inflow by two different frequencies. The response of the jet comprises the growth of two hydrodynamic instabilities; these

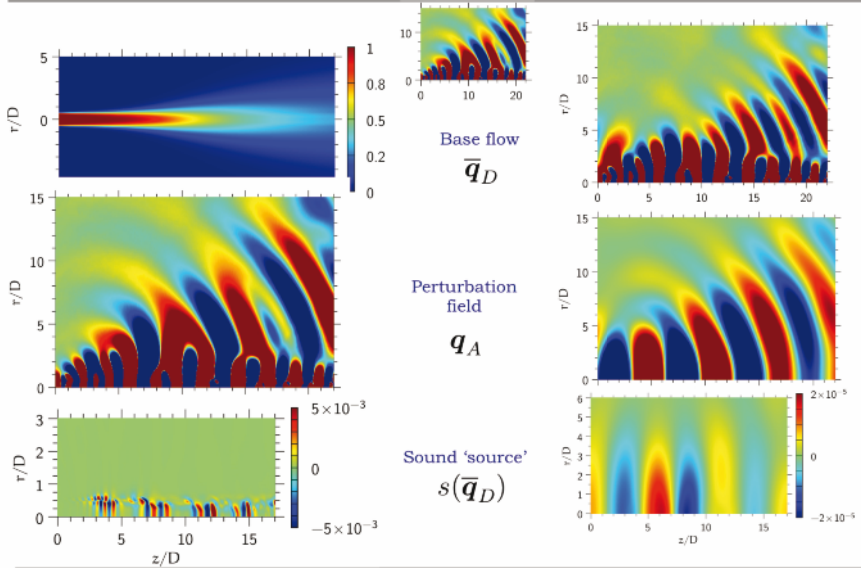


Figure 1. Top center: full flow solution; Left and right columns show, from top to bottom: base flow, perturbation and sound source corresponding to the two flow decompositions; left column: $\mathbf{q}_0 + \mathbf{q}''$; right column: $\bar{\mathbf{q}}_D + \mathbf{q}_A$.

undergo a non-linear interaction which results in a difference wave, and it is this difference wave that dominates the generation of sound waves. The instability waves each couple directly with the sound field, but this linear mechanism is weaker than that of the non-linear interaction.

The full solution of the model problem is shown in figure 1. The filtering operation used to separate ‘radiating’ and ‘non-radiating’ components of the flow is based on the free-space Green’s function, and in this particular implementation the ‘perturbation’ is defined as the radiating component of the flow *at the dominant radiation frequency only*. It is for this reason that some radiating components remain in the base flow, $\bar{\mathbf{q}}_D$.

The considerable differences between what is referred to as ‘base flow’, ‘perturbation’ and, consequently, ‘source’ are illustrative of the degree to which different acoustic analogies will yield different interpretational frameworks: the mechanisms that we infer from the equations can differ as widely as the decompositions, base-flows, perturbations and sources with which they are associated. Much contemporary debate regarding the true physics

of sound production is fueled by this lack of universality.

We here draw attention to one importance difference in particular. In the case of the time-averaged base flow (which is what is used in Lilley or Linearised Euler formulations), the fluctuation is largely dominated, as stated earlier, by hydrodynamic unsteadiness, whereas the radiating fluctuation obtained by means of an acoustic filter is mainly acoustic. The difference in both amplitude and space-time structure between the two attests to this. As seen in figure 1, when a time-averaged base-flow is considered, the perturbation within the jet is dominated by hydrodynamic, convective scales. When the radiating/non-radiating decomposition is used, the perturbation shows an acoustic (radiating) scale throughout the jet. A corresponding difference in amplitude between the two perturbations (not shown in the figure, where colour scales are saturated) is also observed. This illustrates the extent to which it is incorrect to think of interactions terms of the kind $\mathbf{q}_0 \mathbf{q}''$ as corresponding to mean-flow/acoustic interaction; the correct interpretation is that these terms are dominated by mean-flow/turbulence interactions, as is the interpretation attributed to such terms by students of incompressible turbulence (cf. George et al. (1984)), where such terms are referred to as slow-pressure terms.

Finally, Sinayoko et al. (2011) verify that when the time-averaged base flow is driven by the two source terms, the correct result is obtained in the acoustic field. Figure 2 shows this.

2.6 Conclusion

Two things are worth pointing out with regard to the results of the model problem considered above. The first is the difference between the two source terms; it clearly cannot be correct to refer to both of these as the ‘source of sound’. Furthermore, because in this model problem the flow has been carefully manipulated so that the fluid dynamics and acoustic mechanisms are clear, we know that the dominant source mechanism comprises a non-linear interaction between two hydrodynamic instabilities; this interaction creates an acoustically-matched difference wave. The source identified by the formulation based on the decomposition into a predominantly non-radiating unsteady base-flow and a monochromatic, purely radiating disturbance resembles such a difference wave. The source obtained using a time-averaged base flow and corresponding disturbance does not. The former system does therefore appear to constitute a more physically pertinent description of the problem than the latter. The causal reading of the problem, as a one way transmission of fluctuation energy from ‘source’ to ‘sound’, also appears to be more justified by the former formulation. As evoked earlier,

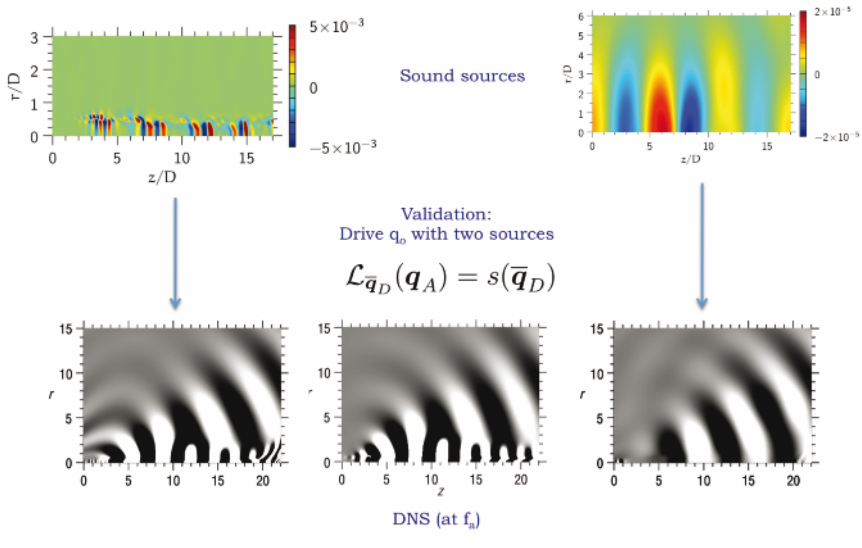


Figure 2. Result of driving the time-averaged base flow by both sources. Result is compared with the DNS result at the peak acoustic frequency. While the source term constructed from the non-radiating, unsteady base flow elicits a purely acoustic response, the source term associated with the time-averaged base flow causes the mean-flow to respond with both hydrodynamic and acoustic components. Both give the correct result in the acoustic field.

this improved consistency is also manifest in the response of the base-flow to excitation by the two sources; in the former case the response is purely acoustic, consistent with what has been denoted ‘perturbation’, whereas in the latter case the response is dominated, within the flow, by hydrodynamics: we therefore have a case in the latter situation where the cause is part of the effect and *vice versa*; this is clearly problematic. It should also be noted, however, that in both cases the correct solution is obtained in the sound field. This shows, as has been borne out over the past 10 years or so by means of numerical simulation, that all acoustic analogies are capable of providing a link between turbulence and sound; however, the differences illustrated by the foregoing study shows that we need to be careful with regard to the physical interpretations that we infer from analysis based on

acoustic analogies.

Where the question of the relationship between \bar{q}_D and $s(\bar{q}_D)$ is concerned, further visualisation and analysis will always be necessary. The same is true with regard to the question of the dynamic law that underpins \bar{q}_D . These observations constitute useful departure points for the experimental approach, and the remainder of these lectures will be concerned with outlining methodologies and tools that can be useful in this regard.

3 The modelling challenge

3.1 Introduction

As outlined in the previous section, estimation of the sound radiation from a turbulent flow, using an acoustic analogy, requires the solution of a propagation equation given a corresponding source term. If the source is not known exactly (such exact knowledge implies knowledge of the full Navier Stokes solution) it must be modelled, and the question of how best to construct this model arises.

Regardless of the acoustic analogy used, the source is a function of the flow turbulence, and so the question of source modelling is inseparable from that of turbulence modelling. In this section we consider the turbulent jet, and the link between this and sound sources. The way turbulence is perceived and modelled has changed considerably in the last fifty years, as has, correspondingly, our understanding of the jet as a source of sound. We therefore briefly trace out these evolutions, providing examples of some recent developments where the source modelling question is concerned.

3.2 A systematic approach to modelling

Analysis of aeroacoustic systems is, like that of most of complex fluid systems, largely an exercise in system reduction. We are interested in discerning the essential aspects of the fluid system with regard to the quantity (observable) that interests us (the radiated sound in the present case), our end objective being to come up with a simplified model of the flow (both *kinematically* and *dynamically*). And, of course, it is a prerequisite that this simplified model provide as accurate as possible a prediction of the radiated sound field: how best to model the flow turbulence as a sound source. The acoustic analogy can be useful as an aid, but, as we saw in the previous section, used in isolation it is not sufficient.

The information neglected in a simplified model of an aeroacoustic system can be seen as an error, and the success or failure of that model will be reflected by the degree to which the acoustic analogy considered is sensitive to that error. Note, however, that such errors can arise, or be perceived, in two quite different contexts. The errors might be due to there being incomplete flow information available to us. Or, alternatively, the ‘error’ might be something that we intentionally introduce, through the removal of flow information that we consider non-essential where the sound production problem is concerned. In the latter case, the missing information is something that we are required to consider and choose carefully. An analysis methodology is outlined in this section, concerned with such a *considered*

removal of non-essential information: we intentionally introduce considered and calculated ‘errors’.

The sensitivity issue has been studied in an *ad hoc* manner by Samanta et al. (2006) with the former idea in mind: how sensitive are acoustic analogies to unwanted errors? The authors considered a DNS of a two-dimensional mixing layer, which they used in conjunction with a number of acoustic analogy formulations (Lighthill-like and Lilley-like formulations were assessed); the sound fields computed by all analogies showed good agreement with the DNS, consistent with the results of the model problem considered in the previous section. The full solution of the DNS was then artificially modified so as to introduce an error, which we here denote $\delta s(\mathbf{q})$. This error was produced through a manipulation of the coefficients of the POD modes ⁷ of the full solution. The sound field was then recomputed, by means of the different acoustic analogies, using the contaminated flow data, and the error in the sound field so computed was assessed in each case.

Different kinds of source error were explored: effects analogous to low-pass filtering, and the reduction of energy in narrow frequency bands, are two examples. In many cases the resultant error in the sound field was found to be similar for all of the acoustic analogies considered. For one particular case, however, where the error corresponds to a division of the first POD mode coefficient by 2 (this amounts to a significant reduction of the low frequency fluctuation energy of the flow), the Lighthill-like formulation showed greater sensitivity than the other formulations.

The problem can be thought about as follows. Consider an acoustic analogy, written in the general form $\mathcal{L}p = s(\mathbf{q})$. The parameter space of the source, $s(\mathbf{q})$, can be expressed in terms of an orthonormal basis, to which there corresponds an inner product; such is the case, for instance, for the POD basis of Samanta et al. (2006). If we now consider the eventual impact of the introduction of a small disturbance (which simulates a modelling error) to the source, $\delta s(\mathbf{q})$ (as per Samanta et al. (2006)), we are interested in the impact that this will have on the acoustic field, i.e. δp . The problem comes down to the following situation: if $\delta s(\mathbf{q}) \parallel \nabla \mathcal{L}$ then the sound field will be sensitive to small perturbations in the source, $\delta s(\mathbf{q})$. $\delta s(\mathbf{q})$ is in this case aligned with the direction of maximum sensitivity of the propagation operator \mathcal{L} in the parameter space considered. If, on the other hand, $\delta s(\mathbf{q}) \perp \nabla \mathcal{L}$, then changes in $s(\mathbf{q})$ will have no impact on the sound field, p . ⁸

This way of viewing the aeroacoustic problem means that the modelling

⁷see section 5 for an exposition of POD

⁸This shows that the arbitrary introduction of disturbances to, and subsequent comparison of, two different analogies cannot provide an unambiguous assessment, in an absolute sense, of the relative robustness of the two formulations. For, if the gradients

problem can be formulated in the following way: beginning with full flow information \mathbf{q} , from a numerical simulation for example, we are required to find the directions (in a suitably chosen parameter space) of the flow solution that can be eliminated without adversely affecting the quality of sound prediction. We must identify the ‘errors’ $\delta\mathbf{q}$, such that we obtain a simplified flow field, $\hat{\mathbf{q}} = \mathbf{q} - \delta\mathbf{q}$; the source computed from this simplified flow field, $s(\hat{\mathbf{q}})$, has an associated error, and this error must be such that the component of $s(\hat{\mathbf{q}})$ aligned with the propagation operator is unaffected.

The following analysis methodology, based on the above reasoning, is intended as a guide for the analysis of complex aeroacoustic systems, from the point of view of source mechanism identification and the design of simplified models (from both kinematic and dynamic standpoints).

Analysis methodology

1. Obtain full or partial information associated with the complete flow solution, \mathbf{q} (whose dynamic law we know: the Navier-Stokes operator, $\mathcal{N}(\mathbf{q}) = 0$); this data could be provided by experimental measurements or from a numerical simulation;
2. Identify and extract, from \mathbf{q} , the observable of interest: the radiated sound in our case, \mathbf{q}_A ;
3. Construct an observable-based filter, $\mathcal{F}_{\mathbf{q}_A}$, which, applied to the full solution removes information not associated with sound production, and thereby provides a reduced-complexity sound-producing flow skeleton (*kinematics*), $\hat{\mathbf{q}}_D = \mathcal{F}_{\mathbf{q}_A}(\mathbf{q})$;
4. Analyse $\hat{\mathbf{q}}_D$ with a view to postulating a simplified *ansatz* for the source, $s(\hat{\mathbf{q}}_D)$;
5. Using an acoustic analogy, compute $\hat{\mathbf{q}}_A = \mathcal{L}^{-1}s(\hat{\mathbf{q}}_D)$, and verify that $\min\|\mathbf{q}_A - \hat{\mathbf{q}}_A\|$;
6. Determine a reduced-complexity dynamic law, $\hat{\mathcal{N}}(\hat{\mathbf{q}}_D) = 0$, that governs the evolution of $\hat{\mathbf{q}}_D$.

Let us consider step 3 for a moment, as the observable-based filter, $\mathcal{F}_{\mathbf{q}_A}$, can be defined with varying degrees of rigour. The following are some possible scenarios. (i) In some situations the application of $\mathcal{F}_{\mathbf{q}_A}$ might be quite heuristic, e.g. no more than the simple observation of the flow—we see with relative ease that *this structure interacted with that to produce this aspect of the sound field*, whence we propose a model. (ii) Alternatively,

$\nabla\mathcal{L}_1$ and $\nabla\mathcal{L}_2$ (where the subscripts 1 and 2 indicate the two analogies) have different directions in the parameter space, one will always be able to find a perturbation that causes one operator to appear less robust than the other.

it could comprise a more sophisticated flow visualisation, or perhaps a series of measurements giving quantitative access to the flow solution, from which a simplified model might be proposed, provided the essential mechanisms show themselves clearly in this data. However, in the context of high Reynolds number turbulent flows, it is frequently necessary to approach the design of $\mathcal{F}_{\mathbf{q}_A}$ in a more rigorous, methodological and objective, manner. Two further avenues can be pursued in this regard: (iii) it may be possible, using a purely theoretical deduction, to identify flow (or source) information that can be safely removed (examples are provided in what follows); and, (iv) signal processing tools can be used to decompose the complex system into more easily manageable ‘building blocks’, whose relative importance for sound production can then be tested.

Early analysis in aeroacoustics (1950s-1980s) was largely undertaken in contexts (i) and (iii), due to the limited capabilities of measurement and signal-processing. With the progressive improvement of the two latter disciplines, analysis in contexts (ii) and (iv) has become more common. In what follows we will show how a complete analysis will generally involve a combination of (i)-(iv).

In the following, we provide a short historical sketch (contexts (i) and (iii) are preponderant) outlining how the complexity of the turbulent jet was observed, considered, discerned and finally modelled with respect to both its internal turbulence mechanisms and the associated sound sources.

3.3 Turbulence: as a space-time chaos

When Lighthill first provided us with a theoretical foundation from which to model, study and understand jet noise, turbulence, both generally and in the specific case of the round jet, was considered to comprise a space-time chaos, devoid of any underlying order. The standard at that time for the kinematic description of turbulence structure could be found in turbulence theories such as that of Batchelor (1953): attempts to understand and model turbulence were based on the Reynolds Averaged Navier-Stokes (RANS) equations, where the only conceptual constructs invoked, aside from those expressed in the conservation equations, are those required for closure (Boussinesq’s notion of eddy viscosity, for instance) on one hand, and, on the other, the flow entities supposed to participate in the physical processes associated with the various terms that appear in the RANS equations: fluctuation energy is ‘produced’, ‘transported’, ‘dissipated’ by virtue of interactions between stochastic flow ‘scales’ or ‘eddies’.

Figure 3(a), which shows a schlieren photograph of a turbulent jet, gives a visual sense of this stochastic character. Source terms in acoustic analogies

were constructed in accordance with this conceptual picture of turbulence. Lighthill (1952) assumed a statistical distribution of uncorrelated eddies throughout the source region, and this led to the well known U^8 power law for the isothermal turbulent jet. However, predictions based on Lighthill's analogy, using such kinematic models for the turbulence, do not explain all of the features of subsonic jet noise: at low emission angles (with respect to the downstream jet axis), for example, the U^8 power law does not hold, and the narrower spectral shape is generally not well predicted. Something is missing from this combination of acoustic-analogy formulation and source representation.

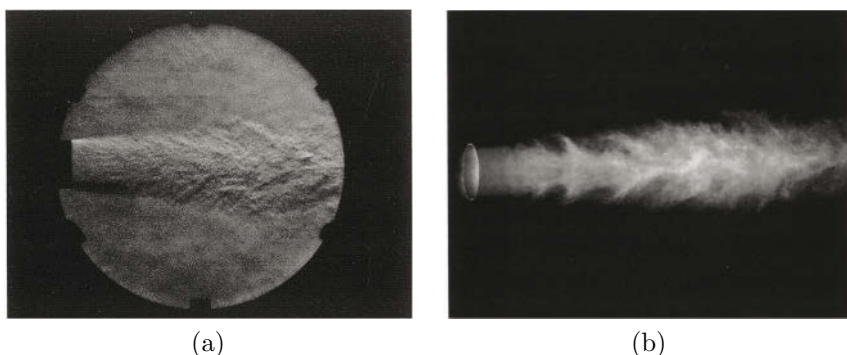


Figure 3. Different visualisation techniques of jets at similar Reynolds number, taken from Crow and Champagne (1971). (a) Schlieren photography; $Re = 1.06 \times 10^5$; (b) CO_2 fog visualisation using sheet illumination; $Re = 7.5 \times 10^4$.

3.4 Turbulence and ‘coherent structures’

Soon after the first attempts by Lighthill and his successors to predict the sound radiated by turbulent jets a change occurred in the way turbulence is perceived. Turbulent flows were observed to be more ordered than had previously been believed, and a new conceptual flow entity was born, sometimes referred to as a ‘coherent structure’, or, alternatively, a ‘wave-packet’. Mollo-Christensen (1967) was one of the first to report such order in the case of the round jet: “...although the velocity signal is random, one should expect to see intermittently a rather regular spatial structure in the shear layer.”. A series of papers followed, confirming these observations and postulating on the nature of this order (Crow and Champagne (1971), Brown

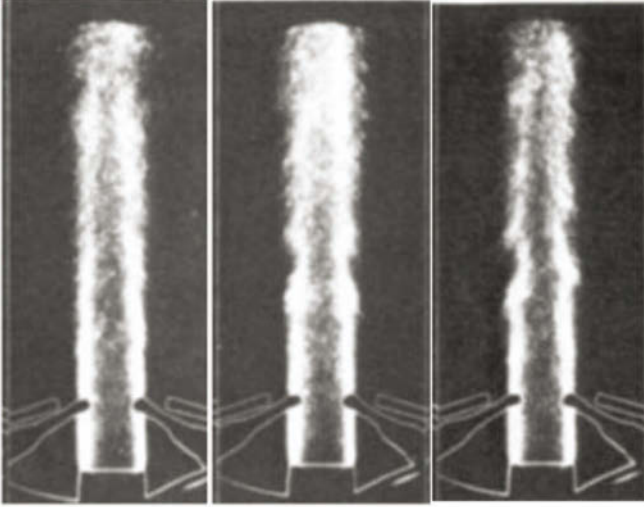


Figure 4. Flash Schlieren images of jets ($Re = 5 \times 10^5$; $M = 0.83$), taken from Moore (1977). Left: random ensemble average; middle: conditional average using axisymmetric nearfield pressure signature as trigger; right: conditional average using a single nearfield microphone as trigger (this reduces the antisymmetric organisation).

and Roshko (1974) and Moore (1977) to cite just a few). Figure 3(b), taken from Crow and Champagne (1971), provides a visual sense of this underlying order: by changing visualisation technique, using sheet illumination and carbon dioxide fog, rather than the fine grained patterns revealed by the schlieren technique, an axially-aligned waveform with wavelength of the order of the jet diameter is observed.

A further illustration of the underlying organisation present in high Reynolds number jets is shown in figure 4, which shows the difference between time-averaged and conditionally-averaged images of round jets at high Reynolds and Mach numbers. We will discuss conditional averaging techniques later in more detail.

Order in chaos

The following series of citations gives a sense of the impression that this

discovery made on researchers working in the field of both turbulence and aeroacoustics.

“The apparently intimate connexion between jet stability and noise generation appears worthy of further investigation” – Mollo-Christensen and Narasimha (1960)

“[jet noise] is of interest as a problem in fluid dynamics in the class of problems which involve the interaction between instability, turbulence and wave emission” – Mollo-Christensen (1963)

“There appear to be at least two distinguishable types of emitted sound, one dominating at very low frequencies and another dominating at high frequencies. A relation which gives a smooth interpolation between these asymptotic ranges would prove useful, if one could be invented.” – Mollo-Christensen (1963)

“The data suggest that one may perhaps represent the fluctuating [hydrodynamic] pressure field in terms of rather simple functions. For example, one may consider the jet as a...semi-infinite antenna for sound...” – Mollo-Christensen (1967)

“...although the velocity signal is random, one should expect to see intermittently a rather regular spatial structure in the shear layer.” – Mollo-Christensen (1967)

“We therefore decided to stress measurements near and in the jets, hoping to discern some of the simpler features of the turbulent field. We also did measure for field pressures, and intended to see if we could not connect the two sets of observations somehow, using the equations of sound propagation.” – Mollo-Christensen (1967)

“It is suggested that turbulence, at least as far as some of the lower order statistical measures are concerned, may be more regular than we may think it is, if we could only find a new way of looking at it.” – Mollo-Christensen (1967)

“The mechanics of turbulence remains obscure, so that it comes as a matter of some relief to find that the motions which now interest us are coherent on a large scale...Such large eddies might be readily recognisable as a coherent transverse motion more in the category of a complicated laminar

flow than chaotic turbulence. In any event the eddies generating the noise seem to be much bigger than those eddies which have been the subject of intense turbulence study. They are very likely those large eddies which derive their energy from an instability of the mean motion..." – Bishop et al. (1971)

"These [measurements] suggest that hidden in the apparently random fluctuations in the mixing layer region is perhaps a very regular and ordered pattern of flow which has not been detected yet" – Fuchs (1972)

"Whether one views these structures as waves or vortices is, to some extent, a matter of viewpoint." – Brown and Roshko (1974)

"All this evidence suggests that the turbulence in the mixing layer of the jet behaves like a train similar to the hydrodynamic stability waves propagating in the shear flow." – Chan (1974)

"The dominant role of the dynamics and interaction of the large structure in the overall mechanism that eventually brings the two fluids into intimate contact becomes apparent. It is clear that any theoretical attempts to model the complex mixing process in the shear layer must take this ubiquitous large structure into account." – Dimotakis and Brown (1976)

"Turbulence research has advanced rapidly in the last decade with the widespread recognition of orderly large-scale structure in many kinds of turbulent shear flows...some measure of agreement seems to have been reached among investigators on the general properties of the coherent motions." – Crighton and Gaster (1976)

"...the turbulence establishes an equivalent laminar flow profile as far as large-scale modes are concerned." – Crighton and Gaster (1976)

"In the last years our understanding of turbulence, especially in jets, has changed rather dramatically. The reason is that jet turbulence has been found to be more regular than had been thought before." – Michalke (1977)

"This 'new-look' in shear-flow turbulence, contrary to the classical notion of essentially complete chaos and randomness, has engendered an unusually high contemporary interest in the large-scale structures." – Hussain and Zaman (1981)

"The last twenty years of research on turbulence have seen a growing

realisation that the transport properties of most turbulence shear flows are dominated by large-scale vortex motions that are not random.” – Cantwell (1981)

“Suddenly it was feasible and reasonable to draw a picture of turbulence! The hand, the eye, and the mind were brought into a new relationship that had never quite existed before; cartooning became an integral part of the study of turbulence.” – Cantwell (1981)

As we see from many of the above citations, stability theory is frequently evoked as a possible theoretical framework for the dynamical modelling of the flow behaviour described above. However, a full treatment of hydrodynamic stability is beyond the scope of this lecture, and so we will simply list, briefly, a few of the different kinds of stability frameworks that are sometimes used to model the organised component of turbulent shear flows. We would also point out that the application of stability theory to turbulent flows, where the stability of a time-averaged mean-flow is considered, is not entirely rigorous (hydrodynamic stability analysis is self-consistent only when applied to laminar flows), involving a number of assumptions: one of these is that there exists a scale-separation between a large-scale organised component of the flow and a finer-grained, stochastic, ‘background’ component; the latter establishes a mean-flow profile that can sustain large-scale instabilities, and acts, furthermore, as a kind of eddy viscosity that damps the large-scale instabilities.

The first stability calculations with respect to the round jet were performed by Batchelor and Gill (1962) who studied the temporal stability problem for a plug flow. Michalke and Timme (1967) looked at the temporal instability of a finite-thickness, two-dimensional shear layer, while Michalke (1971) considered the spatial instability of a finite thickness axisymmetric shear-layer. Crighton & Gaster (1976) took account of the slow axial variation of the shear-layer thickness. Mankbadi and Liu (1984) made an attempt to include the effect of non-linearities. Tam and Morris (1980) used matched asymptotic expansions to obtain the acoustic field of a two-dimensional compressible mixing-layer; Tam and Burton (1984) then extending this effort to the case of a round jet. More recent approaches have been based on linear and non-linear Parabolised Stability Equations, as used by Colonius et al. (2010) for example, and Global Stability approaches, applied for instance to the problem of heated jets by Lesshafft et al. (2010).

3.5 Coherent structures as a sound source

We now turn our attention to the mechanisms by which such coherent structures may be active as sound sources. We will work in the context of Lighthill's acoustic analogy, whence by means of theoretical considerations it will be possible to gain some insight regarding pertinent simplifications. We are, therefore, in what follows, working in the context of steps 3, 4 and 5 of the analysis methodology outlined earlier; and with regard to the filtering operation, $\mathcal{F}_{\mathbf{q}_A}$, we are in context (iii).

The wavepacket source *ansatz* Mollo-Christensen (1967) appears to have been first to propose a mechanism by which coherent structures might be active as a source of sound. Observing that the nearfield pressure signature of the subsonic jet presents a surprising degree of organisation in the (y_1, τ) plane, he suggested that such organisation could result in the jet behaving as a 'semi-infinite antenna for sound'. Where this kind of sound production is concerned, a convected wavepacket constitutes a pertinent model for the organised component of the flow. Such a model, first explored by Michalke (1971) and Crow (1972), continues to be widely used by researchers today, even if there is probably some disagreement with regard to the salient sound-producing features and dynamic law of such wavepackets.

Our presentation of the wavepacket sound source is organised as follows:

- We begin by introducing the basic wavepacket source *ansatz*, as proposed by Michalke (1971), Crow (1972) (see also Crighton (1975)),
- We then outline some of the arguments used to justify its simple line-source form: the elimination of the radial dimension is a good example of observable-based simplification,
- We next present a comparison of experimentally obtained acoustic data with the sound field characteristics of the wavepacket model,
- We then discuss, in greater detail, the radiation mechanism associated with wavepackets, exploring a number of different kinds of behaviour which lead to its being enhanced:
 1. Spatial modulation,
 2. Temporal modulation,
 3. Temporally-localised wavepacket truncation,
 4. Space-time 'jitter'.
- Finally, we present, in section §4, two case studies, in which a number of numerical databases (obtained both by Large Eddy Simulation and by Direct Numerical Simulation) are analysed, following the methodology outlined earlier, and the salient sound-producing features of wavepackets thereby deduced.

The basic wavepacket model First attempts to explore the wavepacket *ansatz* as a kinematic model for the organised component of the jet were made by Michalke (1971), Crow (1972) (see also Crighton (1975)). The physical problem considered is that of small amplitude acoustic disturbances propagating through a quiescent, homogeneous medium, as a result of an externally-imposed source term:

$$\frac{1}{c_0^2} \frac{\partial^2 p(\mathbf{x}, t)}{\partial t^2} - \nabla p(\mathbf{x}, t) = s(\mathbf{y}, t), \tag{71}$$

where the source takes the following form:

$$s(\mathbf{y}, t) = \frac{\partial^2}{\partial y_1^2} 2\rho_0 U \tilde{u} \frac{\pi D^2}{4} \delta(y_2) \delta(y_3) e^{(\omega t - \kappa_y y_1)} e^{(-y_1^2/l^2)}. \tag{72}$$

The solution of the spherical wave equation to an externally-imposed excitation of this kind is:

$$p(\mathbf{x}, t) = -\frac{\rho_0 U \tilde{u} M_c^2 (kD)^2 L \sqrt{\pi} \cos^2 \theta}{8|\mathbf{x}|} e^{-\frac{L^2 k^2 (1 - M_c \cos \theta)^2}{4}} e^{i\omega(t - \frac{|\mathbf{x}|}{c})}, \tag{73}$$

where M_c is the Mach number based on the phase velocity of the convected wave, U_c .

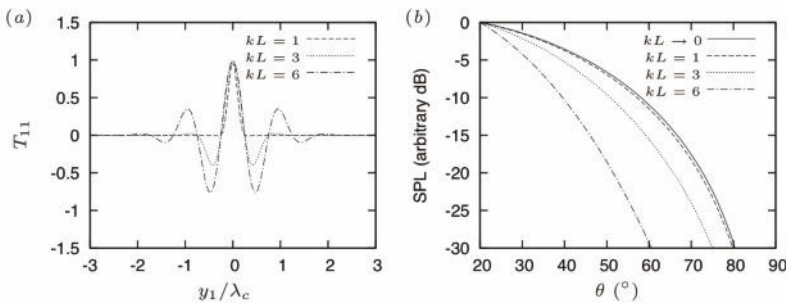


Figure 5. Effect of axial compactness parameter, kL , on directivity.

As outlined in section §2, equation 73 results from a convolution of the source *ansatz* with the free-space Green’s function, this operation identifying the source characteristics to which the radiated sound field is sensitive.

One of these characteristics, visible in the solution, is the source compactness, kL . Figure 5 shows how for small values of kL the source is compact, while for larger values it becomes non-compact, exhibiting numerous oscillations over its spatial extent. The corresponding dependence of the sound field directivity is shown in the right-hand figure: the less compact the source, the more the sound field is ‘beamed’, due to an antenna effect, to shallow axial angles. For $kL = 6$ the directivity pattern is close to exponential; sources exhibiting such exponential directivity are termed superdirective (Crighton and Huerre (1990)).

It can be seen in equation 72 that the source is concentrated on a line (by $\delta(y_2)\delta(y_3)$). This may seem strange considering that the turbulent region of a propulsive jet fills a volume that is approximately bounded by a conical surface. This simplification can be justified, however, by appealing to the radiation efficiency of different azimuthal modes of a cylindrical source (which is a slightly better approximation to the real dimensions of a jet, particularly when one considers the regions of maximal turbulence intensity: these lie on such a cylindrical surface). In the following section we outline this justification; this is an exercise in system reduction based purely on theoretical arguments: we use the Lighthill acoustic analogy formulation to demonstrate how certain ‘directions’ of the source system can be disregarded: the conclusion that we come to is that equation 72 is a reasonable approximation for the coherent structures where low-angle sound emission is concerned.

Radiation efficiency of azimuthal modes The following is taken from Cavalieri et al. (2010b) and Cavalieri et al. (2011a), similar analysis being found in Michalke (1970). Consider a source term of the form

$$T_{11}(\mathbf{y}, \tau) = \rho_0 U \tilde{u} R \delta(r - R) e^{i(\omega\tau - ky_1)} e^{-\frac{y_1^2}{L^2}} C_m e^{im\phi}. \quad (74)$$

Where m denotes azimuthal Fourier mode number, and C_m the corresponding Fourier coefficient. The corresponding solution of the wave equation can be written

$$p(\mathbf{x}, t) = \frac{\rho_0 U \tilde{u} R^2}{4\pi c^2 |\mathbf{x}|} \frac{\partial^2}{\partial t^2} \iint e^{i[\omega(t - \frac{|\mathbf{x}-\mathbf{y}|}{c}) - ky_1]} e^{-\frac{y_1^2}{L^2}} C_m e^{im\phi} d\phi dy_1. \quad (75)$$

We assume, without loss of generality, that the observer is at $\Phi = 0$ and $x_2 = 0$ in cartesian coordinates, where $\Phi = \tan^{-1}(x_2/x_3)$. The distance can be expressed, with a far-field assumption, as,

$$|\mathbf{x} - \mathbf{y}| \approx |\mathbf{x}| - y_1 \cos \theta - R \cos \phi \sin \theta, \quad (76)$$

where θ is the angle of \mathbf{x} to the jet axis. The solution thus becomes

$$p(\mathbf{x}, t) = \frac{\rho_0 U \tilde{u} R^2}{4\pi c^2 |\mathbf{x}|} \frac{\partial^2}{\partial t^2} \int \int e^{i\left[\omega\left(t - \frac{|\mathbf{x}| - y_1 \cos \theta - R \cos \phi \sin \theta}{c}\right) - ky_1\right]} e^{-\frac{y_1^2}{L^2}} C_m e^{im\phi} d\phi dy_1, \quad (77)$$

which can be rearranged as

$$p(\mathbf{x}, t) = \frac{\rho_0 U \tilde{u} R^2}{4\pi c^2 |\mathbf{x}|} \frac{\partial^2}{\partial t^2} \int_{-\infty}^{\infty} e^{i\left[\omega\left(t - \frac{|\mathbf{x}| - y_1 \cos \theta}{c}\right) - ky_1\right]} e^{-\frac{y_1^2}{L^2}} dy_1 \int_0^{2\pi} C_m e^{i\left(m\phi - \omega \frac{R \cos \phi \sin \theta}{c}\right)} d\phi. \quad (78)$$

Evaluation of the azimuthal integral

$$I_1 = \int_0^{2\pi} e^{i\left(m\phi - \omega \frac{R \cos \phi \sin \theta}{c}\right)} d\phi, \quad (79)$$

which can be expressed as

$$I_1 = \int_0^{2\pi} e^{i(m\phi)} e^{(-i\pi \text{St} M \cos \phi \sin \theta)} d\phi, \quad (80)$$

indicates the radiation efficiency of azimuthal mode m ; i.e. the capacity of that azimuthal source mode to couple with the acoustic field.⁹ This integral can be expressed in terms of Bessel functions J_m ,

$$J_m(x) = \frac{1}{2\pi i^m} \int_0^{2\pi} e^{ix \cos \phi} e^{im\phi} d\phi, \quad (81)$$

giving

$$I_1 = (-i)^m 2\pi J_m(\pi \text{St} M \sin \theta). \quad (82)$$

For $\text{St} M \sin \theta = 0$ the I_1 integral yields 2π for $m = 0$, and 0 for all other values of m . This means that, if we neglect retarded time differences along the azimuthal direction, which is justified if this direction is acoustically compact (i.e., the acoustic wavelength is much larger than the azimuthal wavenumber, which being always smaller than the jet diameter, D , allows

⁹Or, stated otherwise, the extent to which that mode is aligned with the propagation operator. If we find that certain modes are not so aligned, this will be an indication that there neglect constitutes a pertinent modelling simplification.

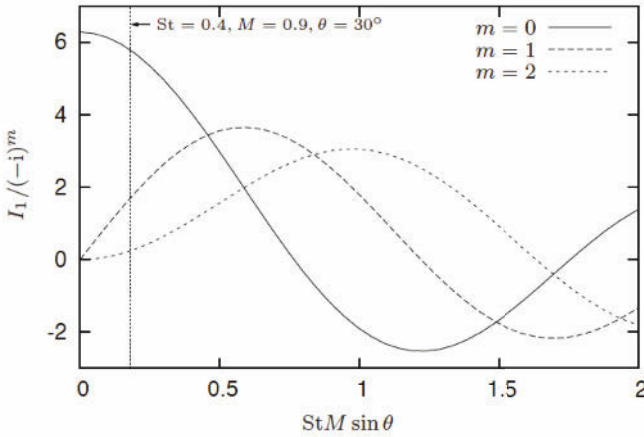


Figure 6. Results for the I_1 integral

the compactness criterion to be expressed in terms of the jet diameter: $D/\lambda = StM$) only axisymmetric wave-packets can radiate. In other words, if the wave-packet diameter D is compact, or, if the observation angle θ is small, only the axisymmetric wave-packet has significant radiation. This is always true for $\theta = 0$ and $\theta = \pi$, i.e. for an observer on the jet axis (Michalke (1970); Michalke and Fuchs (1975); Michel (2009)).

Figure 6 shows the I_1 integral, divided by $(-i)^m$ so as to yield a real quantity. We see that the integral of $m = 0$ decays from its compact value of 2π , eventually goes to zero, and then oscillates. The integrals for the higher azimuthal modes are zero at the compact limit, as expected from the properties of the Bessel functions; they go from zero to a certain value, which is of the same order of the $m = 0$ integral, and then oscillate.

In order to appreciate the implications for a realistic jet flow, consider the sound radiation to low axial angles from a high Mach number subsonic jet. Taking $\theta = \pi/6$, $M = 0.9$ and $St = 0.4$, we have $StM \sin \theta = 0.18$, and in this case, as seen in fig. 6, we can, if we have similar amplitudes C_m for the different m values, neglect all modes $m > 0$ and consider the compact limit ($I_1 = 2\pi$ for $m = 0$) as a first approximation; the I_1 integral for $m = 1$ yields a sound intensity 10dB lower than that for $m = 0$, the integrals for higher m modes being lower still. Suzuki and Colonius (2006) have provided experimental evidence showing that the peak amplitudes, C_m , for azimuthal modes $m = 0$ and $m = 1$ are similar, the amplitudes of mode $m = 2$ being

somewhat lower.

If we retain only the axisymmetric wave-packet and approximate I_1 as 2π , we have

$$p(\mathbf{x}, t) = \frac{\rho_0 U \tilde{u} R^2}{2c^2 |\mathbf{x}|} \frac{\partial^2}{\partial t^2} \int C_0 e^{i\left[\omega\left(t - \frac{|\mathbf{x}| - y_1 \cos \theta}{c}\right) - ky_1\right]} e^{-\frac{y_1^2}{L^2}} dy_1, \quad (83)$$

and integration gives

$$p(\mathbf{x}, t) = -C_0 \frac{\rho_0 U \tilde{u} M_c^2 (kD)^2 L \sqrt{\pi} \cos^2 \theta}{8|\mathbf{x}|} e^{-\frac{L^2 k^2 (1 - M_c \cos \theta)^2}{4}} e^{i\omega\left(t - \frac{|\mathbf{x}|}{c}\right)} \quad (84)$$

which is the same result obtained using the line source in equations 71, 72 and 73. This means that for small values of the parameter $StM \sin \theta$, the use of a wave-packet concentrated on a line leads to the same result as a surface wave-packet, justifying therefore the use of a line distribution for T_{11} , whose amplitude is that of the azimuthal mean of the u fluctuation on the jet lipline. We will see, later, the extent to which this considerably simplified source model, and variants thereof, can mimic the sound-producing behaviour of a turbulent jet. In particular, we will be interested in some important additional modifications, identified thanks to the application of the analysis methodology outlined earlier, which are necessary in order that the *ansatz* be capable of producing quantitative agreement with the sound field radiated by the turbulent jet. First, however, let us examine some experimental data, comparing, qualitatively, with the basic wavepacket *ansatz* outlined above.

Experimental evidence of wavepacket radiation The following results are taken from Cavalieri et al. (2011b). The experiments were performed at the Bruit & Vent jet-noise facility of the Pprime Institute. The setup is shown in figure 7. The exit diameter of the jet is $D = 0.05m$, the flow is isothermal, and the exit velocity is varied over the Mach number range $0.3 < M < 06$; the corresponding Reynolds number range is $3.7 \times 10^5 < Re < 5.7 \times 10^5$, and the boundary layer is tripped in all cases so as to ensure that at the outlet it is fully turbulent. Acoustic measurements are performed by means of an azimuthal distribution of six microphones at a radial distance of $35D$, and the axial position of the ring array was variable. In this way the directivity of the sound field, decomposed into azimuthal Fourier modes, can be studied. These measurements can then be compared with the sound field of the wavepacket *ansatz* discussed above; in particular we focus on the axisymmetric component. Figure 7(b) shows the directivity in terms of both the overall SPL and the contributions from

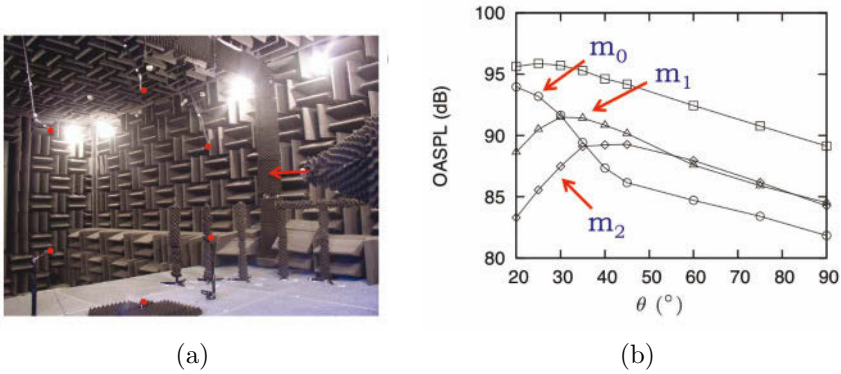


Figure 7. (a) Jet noise experiment assessing azimuthal structure of the acoustic field radiated by moderate Mach number jets; $0.3 < M < 06$, $< Re <$. Red arrow shows direction of jet; red circles indicate the positions of the 6 azimuthally-distributed microphones; (b) OASPL: squares: total; contributions from azimuthal modes $m=0$, $m=1$ & $m=2$ indicated in figure. Note dominance of axisymmetric mode in downstream radiation.

each of the first three azimuthal Fourier modes, $m = 0$, $m = 1$ and $m = 2$. The axisymmetric component, $m = 0$, dominates the downstream radiation, sideline radiation comprising larger contributions from modes $m = 1$ and $m = 2$.

The dominance of the low-angle radiation by the axisymmetric mode is consistent with the foregoing analysis of the efficiency of azimuthal source modes, suggesting the existence of wavepacket radiation. By continuing to interrogate the experimental data with respect to the wavepacket model characteristics, we can evaluate the extent to which this model is pertinent.

Concentrating now on the lower emission angles, assessing the power spectral density as a function of emission angle and azimuthal Fourier mode, we obtain the result shown in figure 8. As we move from 40° to 20° we observe the progressive emergence of the axisymmetric component of the power spectrum, and we note that this emergence occurs over a relatively narrow spectral range, with peak frequency $St_D = 0.2$. The energy of the axisymmetric component of the sound field finds itself concentrated at low angles (highly directive) and across a relatively narrow range of frequency. At the lowest emission angles the peak of the overall spectrum is almost entirely axisymmetric, the energy of mode $m = 0$ being $10dB$ (that is one

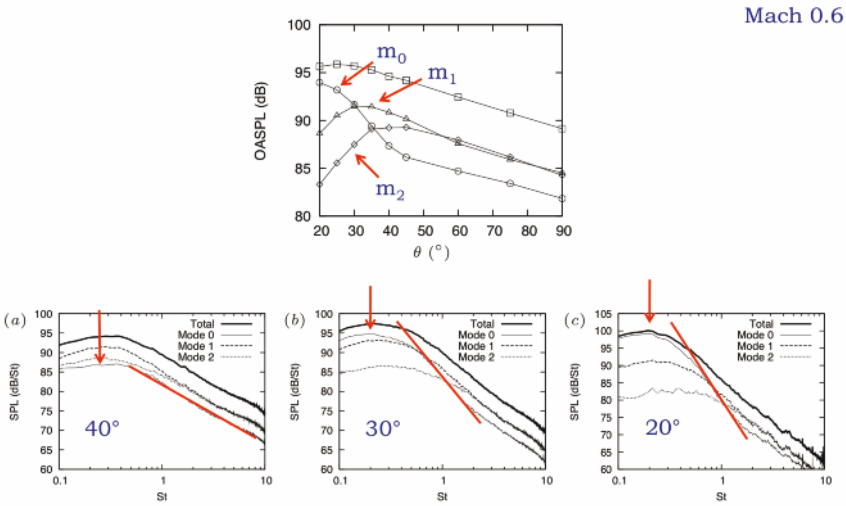


Figure 8. Power spectra of azimuthal modes 0, 1 & 2 at low emission angles.

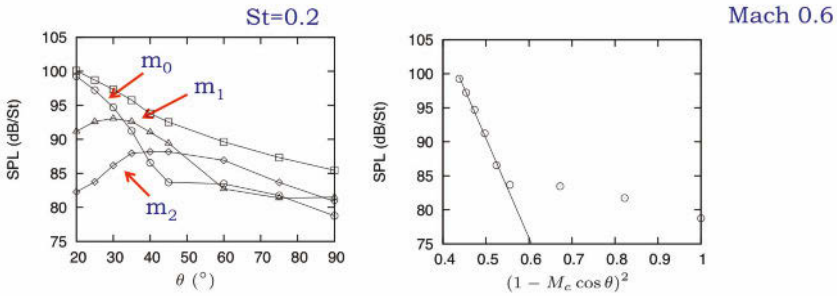


Figure 9. Narrowband-filtered (at $St_D = 0.2$) directivity of azimuthal modes and comparison of axisymmetric mode with wavepacket *ansatz*. Axisymmetric component of experimentally obtained sound field is superdirective (exponential polar decay) in agreement with the wavepacket model

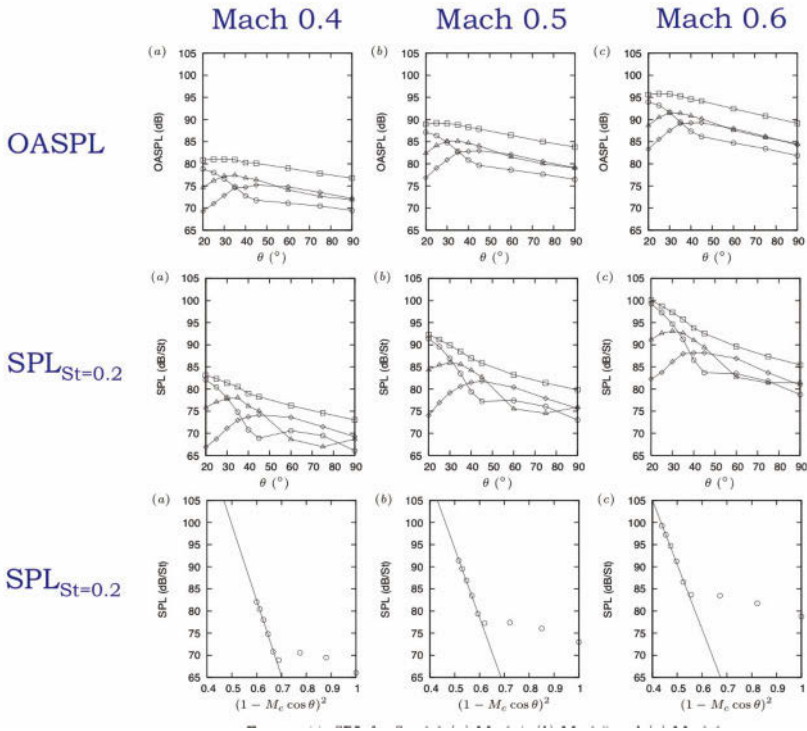


Figure 10. Azimuthal mode directivities as a function of Mach number. Axisymmetric mode is superdirective for all Mach numbers; indicates wavepacket radiation even at low Mach number

order of magnitude) greater than the next most energetic azimuthal mode, $m = 1$. The narrowband character of the emergence of the axisymmetric mode, whose energy is concentrated at $St_D = 0.2$, justifies an assessment of the directivity of the SPL in a narrow frequency range centered at this frequency. The result is shown in figure 9(a), where the downstream directivity of the axisymmetric component at this frequency is even more marked. Comparison can now be made with the directivity factor of the wavepacket *ansatz*, $(1 - M_c \cos \theta)^2$; this is done in figure 9(b). The exponential character of the axisymmetric component of the sound field, when plotted as a function of this wavepacket directivity factor again suggests that the associated underlying source mechanism is associated with an axially extended

wavepacket of the kind modelled by equation 72. The term *superdirectivity* was coined by Crighton and Huerre (1990) to describe such directivity.

It is now of interest to study two further aspects of the experimental sound field: the Mach number dependence and the spectral scaling; both will allow further insight with regard to the possibility that the downstream radiation is underpinned by these relatively simply wavepacket source functions. Figure 10 shows the OASPL and narrowband-filtered SPL as a function of emission angle for the different azimuthal Fourier modes of the sound field, as a function of jet Mach number. The result shows that precisely the same behaviour observed at Mach 0.6 is also observed at lower Mach number, suggesting that wavepacket radiation is a dominant mechanism for low-angle emission, even at low Mach number.

Finally, we assess the scaling of spectra for the modes m_0 and m_1 , as a function of Mach number, for emission angle $\theta = 30^\circ$. The result is shown in figure 11, where both Strouhal ($St_D = fD/U_j$) and Helmholtz ($He = D/\lambda$) numbers are assessed. For the axisymmetric component of the sound field we find that Helmholtz scaling best collapses the sound spectra. As the Helmholtz number is the ratio of a characteristic flow scale to a characteristic scale of the sound field, the fact that this parameter collapses the axisymmetric component of the sound field suggests that the associated source is non-compact, as it suggests that this component of the sound field is sensitive to the ratio between flow scales and acoustic scales; this would not be so for a compact source, where a clear scale separation exists between acoustic waves and flow eddies.

By comparing the experimental data with the details of the wavepacket *ansatz*, it is possible to make a quantitative estimate of the wavepacket compactness parameter, kL , which can be written as

$$Lk = \frac{2\pi}{M_c} He \frac{L}{D}. \quad (85)$$

Considering the jet at $M = 0.6$, we have, $M_c = 0.36$, $He = 0.12$ and $D = 0.05$. For the same jet the directivity of the axisymmetric mode is characterised by a decrease of $15.6dB$ over the angular range $20^\circ < \theta < 45^\circ$, which allows us to estimate that the compactness parameter, $Lk = 6.5$. Comparison with figure 5, gives a sense of the corresponding wavepacket structure; this value, which suggests that the wavepacket extends over an axial region of about $6D$, is consistent with the analysis of Hussain and Zaman (1981), who deduced coherent structures from low Mach number turbulent jets by means of conditional averaging of hotwire measurements.

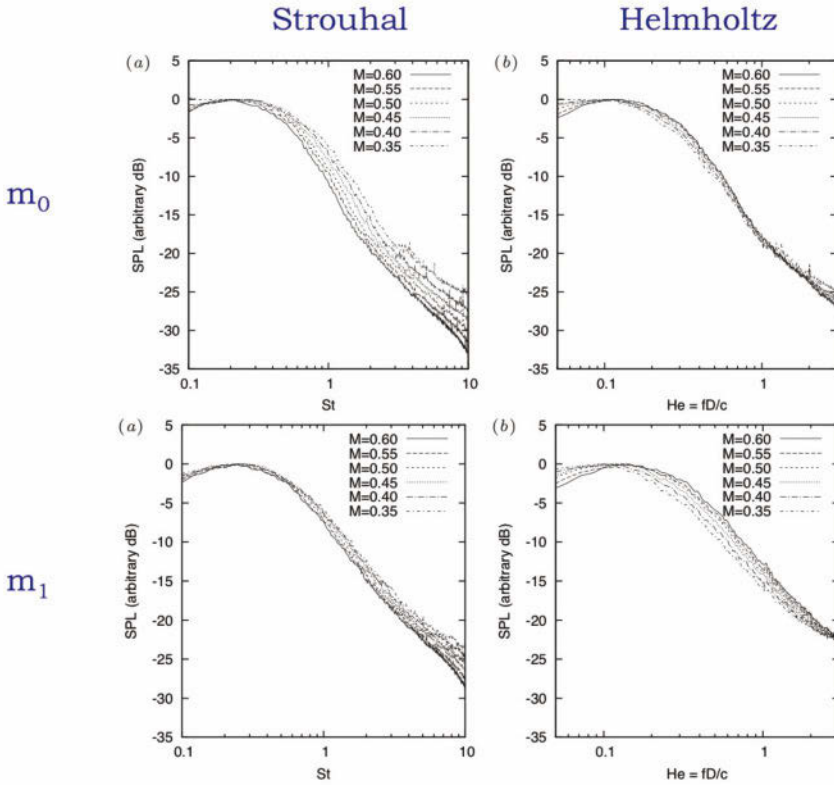


Figure 11. Scaling of azimuthal modes 0 and 1. Axisymmetric mode scales best with Helmholtz number, $He = D/\lambda$, suggesting that it is associated with a non-compact source. Substituting the experimental parameters into the wavepacket model we can deduce that $Lk = 6.5$; comparison with figure5 shows that this implies wavepacket with a spatial structure comprising about three oscillations, extended over approximately $6D$, i.e. from the jet exit to beyond the end of the potential core.

The radiation mechanism Let us now consider the details of the mechanism by which sound sources, and in particular, ‘coherent structures’, excite acoustic modes in turbulent flows. The mechanism can be understood by considering the acoustic analogy, written down either as a partial differential equation, or expressed in terms of its integral solution; time-domain,

frequency-domain and linear algebraic formulations of both the inhomogeneous PDE and its integral solution can be helpful in understanding the essentials: the sound production mechanism can be thought about in three different ways; we can say that:

1. Space-time inhomogeneity of the source field is such that cancellation (in time-delayed coordinates) between regions of positive and negative stresses is incomplete; the fluid medium thus finds itself subjected to compressions and rarefactions that engender a propagative energy flux,
2. The propagation operator has an acoustic response to only those components of the source field that are acoustically-matched: those that satisfy the dispersion relation $\omega^2 = c_0^2 |\boldsymbol{\kappa}|^2$; in terms of the integral solution we can say that the Green's function filters out, from the full range of source scales, only those that satisfy that dispersion relation,
3. In terms of linear algebra we can say that the propagator maps to the farfield those components of the source with which it is aligned: $\mathcal{L} \parallel s(\mathbf{q})$.

In the case of the wavepacket, these different scenarios can be represented schematically as in figure 12.

Let us now consider a number of different kinds of physical wavepacket behaviour that can lead to such radiation, before going on to explore data from turbulent jets. The following is taken from Cavalieri et al. (2011a) and Cavalieri et al. (2010b).

Spatial modulation The wavepacket characteristic most often referred to in the literature as important for the production of radiating sound energy is its spatial modulation. A subsonically-convected spatial sinusoid of constant amplitude and infinite spatial extent contains only non-radiating scales, because $\omega < k_x c$. However, any truncation or spatial modulation of the amplitude of that wavepacket will cause its axial wavenumber spectrum to broaden, and in this way some of the wavepacket energy will find itself in the acoustically-matched region of the spectrum. Figure 12 illustrates this: (a) shows non-radiating and radiating space-time structures; (b) shows the frequency-wavenumber spectrum of a radiating wavepacket—the tail of the spectrum that finds itself in the radiating sector causes sound radiation.

Temporal modulation A further feature of the unsteadiness associated with the orderly part of a turbulent jet is its intermittency. The earlier citations from Mollo-Christensen recognise this. A further citation from Crow

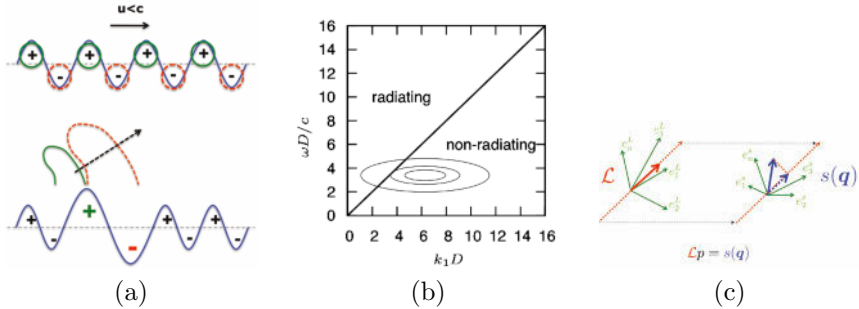


Figure 12. Different ways of thinking about the wavepacket radiation mechanism: (a) Space-time representation: amplitude inhomogeneities lead to incomplete cancellation, and associated compressions and rarefactions; (b) frequency-wavenumber representation; mechanism can be thought of as a filter that only passes the source components that satisfy $\omega^2 = c_0^2 |\boldsymbol{\kappa}|^2$; (c) Representation in terms of linear algebra: mapping to the farfield of source by propagation operator: directions of the source, $s(\mathbf{q})$, that are parallel to the propagator, \mathcal{L} , get mapped to the farfield.

and Champagne (1971) is also relevant; they observed, by means of flow visualisation, the appearance of a train of coherent ‘puffs’ of turbulence. These were characterised by an average Strouhal number of 0.3, but the authors noted how “three or four puffs form and induct themselves downstream, an interval of confused flow ensues, several more puffs form, and so on”.

The effect of such intermittency can be considered in a number of ways. Ffowcs Williams and Kempton (1978) were the first to consider a kinematic model for such behaviour; this took the form of a random variation of the phase velocity of the convected wavepacket, as shown in equation 86. In this case the wave envelope remains time-invariant.

$$s(\mathbf{y}, \tau) = \frac{\partial^2}{\partial y_1^2} 2\rho_0 U \tilde{u} \frac{\pi D^2}{4} \delta(y_2) \delta(y_3) \frac{[1 + \epsilon(t - y_1/U)]}{U} e^{(\omega t - \kappa_y y_1)} e^{(-y_1^2/l^2)}. \tag{86}$$

Figure 13, which shows data taken from the DNS of Freund (2001) and the experimental measurements of Tinney and Jordan (2008), illustrates how intermittency is also manifest in an unsteadiness of the wavepacket envelope: a pattern of convected waves is observed from $x \approx D$ to $x \approx 6D$. These are characterised by some average frequency, but they undergo a modulation which is both spatial and temporal: the maximum amplitude of the wave

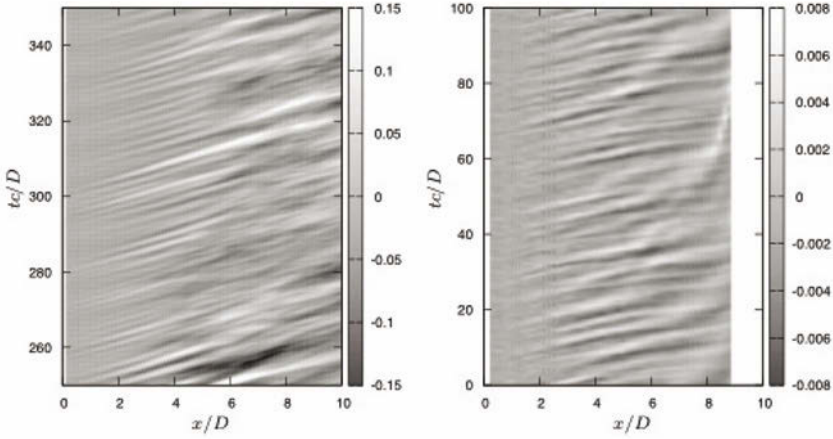


Figure 13. Left: axisymmetric axial velocity fluctuation at $r/D = 0.5$, from DNS of Freund (2001); $Re = 3600$. Right: nearfield pressure signature of jet at $Re = 5.10^6$, from measurements of Tinney and Jordan (2008). Note in both cases the time variation of wavepacket amplitudes and spatial extension.

changes in time, as does the position where it breaks down. A model for the former effect is

$$T_{11}(\mathbf{y}, \tau) = 2\rho_0 U \tilde{u} \frac{\pi D^2}{4} \delta(y_2) \delta(y_3) e^{i(\omega\tau - ky_1)} e^{-\frac{y_1^2}{L^2}} e^{-\frac{\tau^2}{\tau_c^2}}. \quad (87)$$

Examples of this kind of space and time modulation are shown in figure 14 and this leads to a radiated sound pressure:

$$p(\mathbf{x}, t) = \frac{\rho_0 U \tilde{u} D^2 \cos^2 \theta}{8c^2 |\mathbf{x}|} \frac{\partial^2}{\partial t^2} \int_{-\infty}^{\infty} \left\{ e^{i(\omega\tau - ky_1)} e^{-\frac{y_1^2}{L^2}} e^{-\frac{\tau^2}{\tau_c^2}} \right\}_{\tau=t-\frac{|\mathbf{x}-\mathbf{y}|}{c}} dy_1, \quad (88)$$

where c is the speed of sound in the undisturbed fluid and θ is the angle of \mathbf{x} to the jet axis. Use of the far-field approximation $|\mathbf{x} - \mathbf{y}| \approx |\mathbf{x}| - y_1 \cos \theta$ leads to

$$p(\mathbf{x}, t) = \frac{\rho_0 U \tilde{u} D^2 \cos^2 \theta}{8c^2 |\mathbf{x}|} \frac{\partial^2}{\partial t^2} \left\{ e^{i\omega\left(t-\frac{|\mathbf{x}|}{c}\right) - \frac{\left(t-\frac{|\mathbf{x}|}{c}\right)^2}{\tau_c^2}} \int_{-\infty}^{\infty} f(y_1) dy_1 \right\} \quad (89)$$

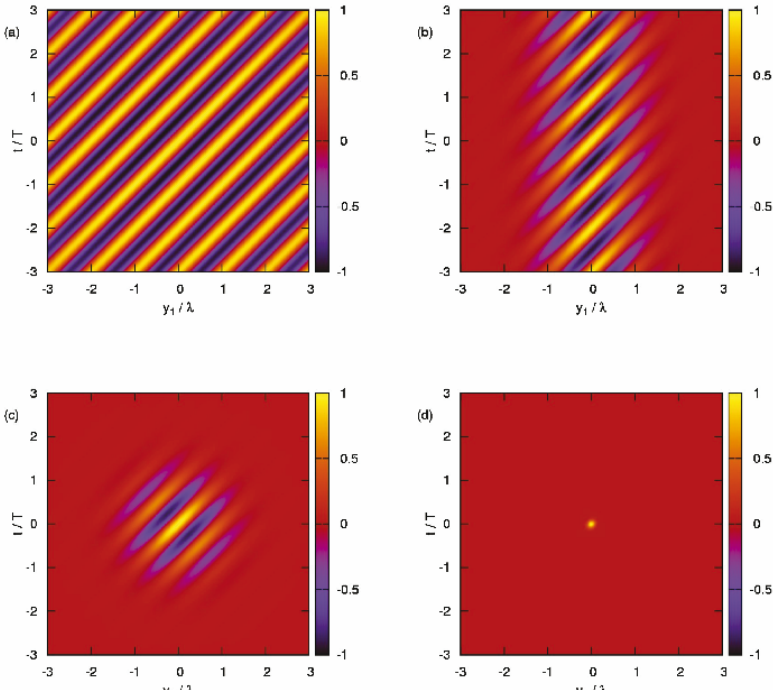


Figure 14. Space- and time-modulated wavepackets.

with

$$f(y_1) = e^{i\left(\frac{\omega y_1 \cos \theta}{c} - ky_1\right)} e^{-\frac{y_1^2}{L^2} - \frac{(y_1 \cos \theta)^2}{c^2 \tau_c^2}} e^{-\frac{2y_1 \cos \theta \left(t - \frac{|\mathbf{x}|}{c}\right)}{c \tau_c^2}}, \quad (90)$$

where c is the speed of sound in the undisturbed fluid and θ is the angle of \mathbf{x} to the jet axis.

Evaluation of the integral of equation 90 leads to an analytical expression for the pressure in the far field:

$$p(\mathbf{x}, t) = PQe^{i\omega t_r - \frac{t_r^2}{\tau_c^2} - \frac{L^2}{4\tau_c^2 \gamma^2} [(ck - \omega \cos \theta)\tau_c^2 - 2it_r \cos \theta]^2} \quad (91)$$

with

$$t_r = t - \frac{|\mathbf{x}|}{c}, \quad (92)$$

$$P = \frac{\rho_0 U \tilde{u} D^2 \tau_c c L \sqrt{\pi} \cos^2 \theta}{4c^2 |\mathbf{x}|^\gamma}, \quad (93)$$

$$Q = \left\{ \left[i\omega - 2 \frac{t_r}{\tau_c} + \frac{iL^2 \cos \theta}{\tau_c^2 \gamma^2} [(ck - \omega \cos \theta)\tau_c^2 - 2it_r \cos \theta] \right]^2 - \frac{2c^2}{\gamma^2} \right\}, \quad (94)$$

and

$$\gamma = \sqrt{\tau_c^2 c^2 + L^2 \cos^2 \theta}. \quad (95)$$

If we calculate the limit with $\tau_c \rightarrow \infty$ of eqs. (91)–(95), we have

$$\gamma \rightarrow \tau_c c \quad (96)$$

and

$$P \rightarrow \frac{\rho_0 U \tilde{u} D^2 L \sqrt{\pi} \cos^2 \theta}{4c^2 |\mathbf{x}|}, \quad (97)$$

which, after substitution in eq. (91), leads, as expected, to the earlier result for a purely spatially modulated wavepacket,

$$p(\mathbf{x}, t) = -\frac{\rho_0 U \tilde{u} M_c^2 (kD)^2 L \sqrt{\pi} \cos^2 \theta}{8|\mathbf{x}|} e^{-\frac{L^2 k^2 (1 - M_c \cos \theta)^2}{4}} e^{i\omega(t - \frac{|\mathbf{x}|}{c})}, \quad (98)$$

where M_c is the convective Mach number given by $\omega/(kc)$.

We can define a source efficiency as the ratio between the acoustic energy,

$$E_A = \int_0^\infty \int_\Omega \frac{p^2}{\rho_0 c} dS(\mathbf{x}) dt, \quad (99)$$

with the surface integral calculated over a spherical surface Ω in the far field, and the turbulent kinetic energy, or “source” energy, given by

$$E_S = \frac{1}{T} \int_0^\infty \int_{V_S} \frac{\rho_0 u^2}{2} dy d\tau. \quad (100)$$

This allows an evaluation of the impact of changes in the space and time scales of the wavepacket envelope on the acoustic efficiency. Figure 15 shows this dependence. Note that the colour scale is logarithmic: at high Mach number small reductions in either the spatial or temporal extent of the wavepacket can lead to considerably enhanced radiation efficiency; the space-time localisation of a wavepacket is thus an important source parameter: such behaviour in a jet comprises a flow ‘direction’ to which the wave operator is highly sensitive.

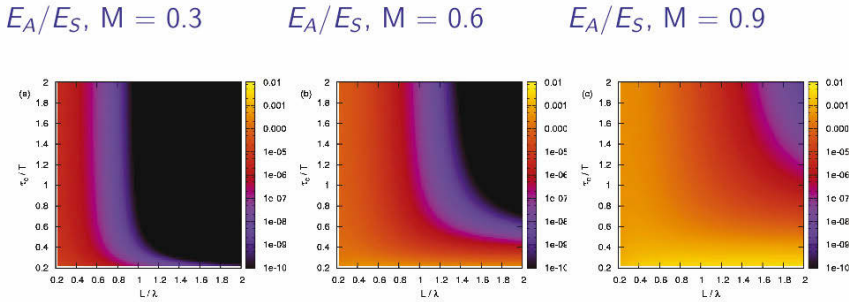


Figure 15. Wavepacket efficiency, as a function of space- and time-envelope scales, for different Mach numbers.

Temporally-localised envelope truncation In order to provide temporal changes in the spatial extent of the envelope function, in an effort to better model the wavepacket characteristics observed in figure 13, we can model T_{11} as

$$T_{11}(\mathbf{y}, \tau) = 2\rho_0 U \tilde{u} \frac{\pi D^2}{4} \delta(y_2) \delta(y_3) e^{i(\omega\tau - ky_1)} e^{-\frac{y_1^2}{L^2(\tau)}}. \quad (101)$$

With this expression the peak amplitude of the convected wave is kept constant, but the characteristic length of the envelope, L , changes with time. We model the changes in L as

$$L(\tau) = L_0 - \kappa e^{-\frac{(\tau - \tau_0)^2}{\tau_L^2}}, \quad (102)$$

where L_0 is an initial envelope width and κ is the maximum envelope reduction, which happens at $\tau = \tau_0$. This reduction of the envelope occurs over an interval characterised by the temporal scale τ_L , and is modelled by a Gaussian function. Examples of this source behaviour are shown in fig. 16. The sound radiation is obtained in this case by numerical integration using this line source. A sample result is shown in figure 16: we note that the envelope truncation also leads to an enhancement of the sound radiation, again suggesting that this kind of unsteadiness, observed in the numerical and experimental data, may underpin the emission of high-amplitude acoustic perturbations to the far field of turbulent jets: again, in the spirit of the system reduction at the heart of the analysis methodology evoked earlier,

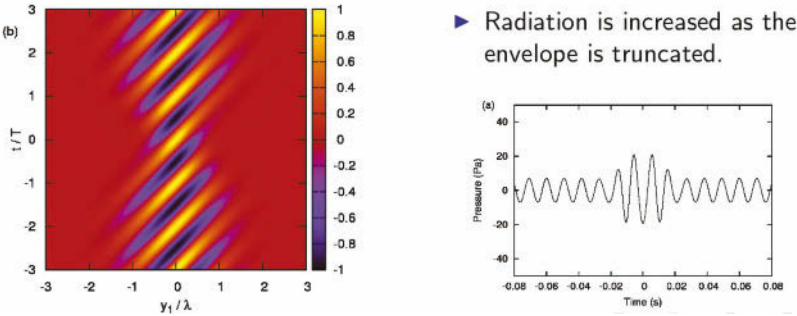


Figure 16. Space- and time-modulated wavepackets.

the propagation operator is sensitive to this kind of flow behaviour, and so such flow ‘directions’ should, again, be retained, i.e. explicitly modelled.

We now consider a final model, which takes us closer again to the behaviour we observe in the data shown in figure 13. We wish to mimic the space-time ‘jitter’ manifest in the data, we must therefore capture the time variation of the wavepacket envelope in terms of both its peak amplitude and its axial extent. This final model combines the effects modelled individually in the two previous models.

Space-time ‘jitter’ T_{11} is now modelled as

$$T_{11}(\mathbf{y}, \tau) = 2\rho_0 U \tilde{u} \frac{\pi D^2}{4} \delta(y_2) \delta(y_3) A(\tau) e^{i(\omega\tau - ky_1)} e^{-\frac{y_1^2}{L^2(\tau)}}, \quad (103)$$

where we allow temporal variations of the amplitude A , and also temporal changes in L . This expression, used in conjunction with the far-field assumption, leads to:

$$p(\mathbf{x}, t) = \frac{\rho_0 U \tilde{u} D^2 \cos^2 \theta}{8c^2 |\mathbf{x}|} \frac{\partial^2}{\partial t^2} \int_{-\infty}^{\infty} A \left(t - \frac{|\mathbf{x}| - y_1 \cos \theta}{c} \right) e^{i \left[\omega \left(t - \frac{|\mathbf{x}| - y_1 \cos \theta}{c} \right) - ky_1 \right]} e^{-\frac{y_1^2}{L^2 \left(t - \frac{|\mathbf{x}| - y_1 \cos \theta}{c} \right)}} dy_1. \quad (104)$$

If the amplitude A and the characteristic length of the envelope, L , change slowly when evaluated at retarded-time differences ($y_1 \cos \theta/c$) along

the wave-packet, we can consider axial compactness for these functions in the integration, such that

$$A\left(t - \frac{|\mathbf{x}| - y_1 \cos \theta}{c}\right) \approx A\left(t - \frac{|\mathbf{x}|}{c}\right) \quad (105)$$

and

$$L\left(t - \frac{|\mathbf{x}| - y_1 \cos \theta}{c}\right) \approx L\left(t - \frac{|\mathbf{x}|}{c}\right). \quad (106)$$

If $*$ is used to denote a function evaluated at the retarded time $t - \frac{|\mathbf{x}|}{c}$, we have

$$p(\mathbf{x}, t) = \frac{\rho_0 U \tilde{u} D^2 \cos^2 \theta}{8c^2 |\mathbf{x}|} \frac{\partial^2}{\partial t^2} \left\{ A^* \int e^{i[\omega(t - \frac{|\mathbf{x}| - y_1 \cos \theta}{c}) - ky_1]} e^{-\frac{y_1^2}{(L^*)^2}} dy_1 \right\} \quad (107)$$

Evaluation of this integral, considering that the temporal changes in L and in A are slower than those related to the harmonic oscillation in ω , leads to

$$p(\mathbf{x}, t) = -A^* \frac{\rho_0 U \tilde{u} M_c^2 (kD)^2 L^* \sqrt{\pi} \cos^2 \theta}{8|\mathbf{x}|} e^{-\frac{(L^*)^2 k^2 (1 - M_c \cos \theta)^2}{4}} e^{i\omega(t - \frac{|\mathbf{x}|}{c})} \quad (108)$$

This means that for sufficiently slow temporal changes in A and in L , the radiated sound field at a given time t is that of a wave-packet whose amplitude and envelope corresponds to the values A^* and L^* , that is, *to the wave-packet at the retarded time $t - |\mathbf{x}|/c$* (compare with eq. (98)).

In the spirit of the analysis methodology outlined earlier the models considered here will be used, in conjunction with an ensemble of data-processing/reduction techniques (outlined in section §5), to analyse data obtained using Large Eddy Simulation and Direct Numerical Simulation.

3.6 Conclusion

In this section we have considered the source modelling problem from the perspective of ‘coherent structures’. It has been shown how considerable simplifications can be justified where the associated sound production mechanisms are concerned, these simplifications being for the most part derived from theoretical reasoning based on Lighthill’s acoustic analogy. In what follows we will explore some numerical databases, from which we will endeavour to extract and evaluate the salient source features through the application of a number of different analysis tools. These analyses closely follow the methodology outlined at the beginning of this section; and a detailed exposition of the various analysis tools implemented are described in section §5.

4 Two case studies

In this section we provide two examples of applications of the analysis methodology outlined earlier, focusing on the organised component of the turbulent jet discussed in the previous section; we also make use of the wavepacket sound source models of that section.

Let us begin by briefly recalling the analysis methodology: (1) we equip ourselves with complete or partial data from full Navier-Stokes solution¹⁰; (2) we then identify the acoustic observable, \mathbf{q}_A , and design a corresponding filter, $\mathcal{F}_{\mathbf{q}_A}$ ¹¹, used to extract the radiating flow skeleton, $\hat{\mathbf{q}}_D$; (3) we construct a simplified kinematic source model, $s(\hat{\mathbf{q}}_D)$ (based on the models developed in section §3), and verify that solution of $\mathcal{L}\hat{\mathbf{q}}_A = s(\hat{\mathbf{q}}_D)$ is such that $|\mathbf{q}_A - \hat{\mathbf{q}}_A|$ be acceptably small. The final stage of the analysis methodology involves identifying the associated dynamic law; this aspect will be outlined briefly in section §6.

We use three different databases for the analysis, two LES and one DNS. The two LES use different numerical schemes, leading to one having higher space-time scale resolution than the other. We will refer to these as LES_{MD} and LES_{HR} , the subscripts denoting, respectively, moderate and high resolution. The DNS and LES_{MR} therefore constitute databases where coherent structures are relatively easy to identify, on account, respectively, of the low Reynolds number and the moderate scale resolution. LES_{HR} is more challenging, as it contains a broader range of turbulence scales, making the coherent structures more difficult to educe. In this case we are required to construct a filter based on Linear Stochastic Estimation (LSE).¹²

4.1 Case study 1. Moderate-resolution LES and DNS

We begin by performing a Large Eddy Simulation of a Mach 0.9, isothermal jet, with nominal Reynolds number, $Re = 400000$. The details of the computation can be found in Cavalieri et al. (2010a). An image of the flow solution is shown in figure 17, where the first stage in the analysis methodology is illustrated. We, of course, verify that the simulation shows good agreement with experimental results: at peak sound radiation frequencies

¹⁰It is true that the LES does not provide a full Navier Stokes solution, being based on filtered equations; we nonetheless consider that it provides a relatively complete representation of the behaviour of the larger structures, which are those we are interested in here.

¹¹In the first study this filter is rather heuristic, being based simply on flow visualisation following the application of Fourier and wavelet transforms; in the second, the filter has a rigorous mathematical definition.

¹²A detailed presentation of LSE is provided in section §5.

the LES is within 2dB of experimentally observed values.

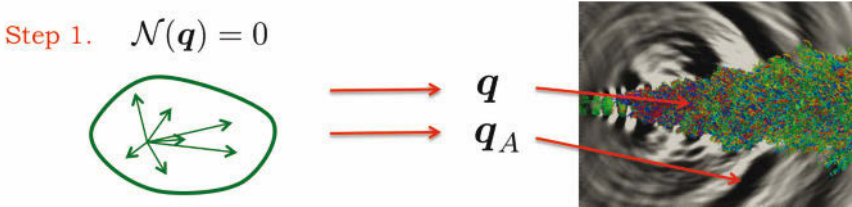


Figure 17. First stage of analysis: obtain Navier Stokes solution, \mathbf{q} , which contains the acoustic observable, \mathbf{q}_A .

The next stage is to analyse the observable, \mathbf{q}_A . To do so we implement the following signal processing: azimuthal Fourier decomposition is performed on the acoustic data on a cylindrical surface of radius, $r = 9D$, and which extends from $x/D = 0$ to $x/D = 20$; wavelet transforms are applied in the time direction, for each azimuthal Fourier mode. The reasons for this choice of data-processing can be found in the previous section: we saw in the experiment that the sound field is dominated by only three azimuthal Fourier modes; this being the case, it is legitimate and useful to break the sound field down into these building blocks. This will allow us to simplify the analysis. Also, we saw that coherent structures in jets display intermittency, and in peak radiation directions much of the overall sound energy arrives in temporally localised bursts. This suggests a link between the intermittency of coherent structures and peak sound radiation, and the models developed in the previous section illustrate how such source behaviour can indeed enhance the sound radiation efficiency of organised flow structures.

We can see in figure 18 that the downstream direction is, in agreement with what was observed experimentally, dominated by axisymmetric sound radiation. We will therefore focus on this component of the sound field, and see if we can ascertain the associated flow kinematics. Note the procedure that is being followed here: we are gradually eliminating flow information, thereby homing in progressively on the dominant aspects of the flow with regard to the acoustic observable. By doing so we simplify the task of analysing and later modelling the jet as a source of sound.

We now consider the temporal structure of the axisymmetric component of the sound field. Application of a wavelet transform¹³ to the time history

¹³The wavelet transform is presented in section §5.

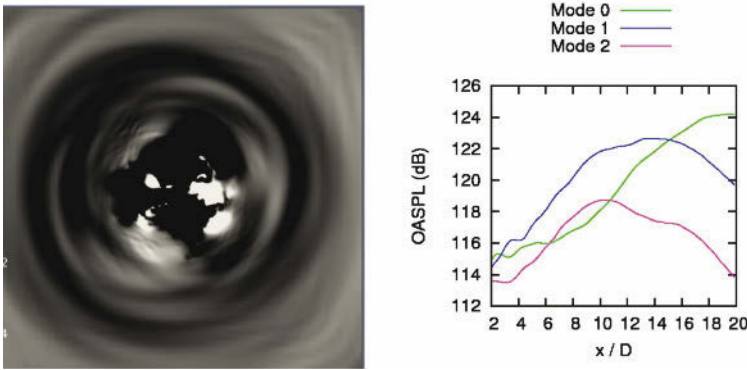


Figure 18. Left: instantaneous image of the jet, taken in a cross-section at $x/D = 7$; note the azimuthal organisation of the radiating pressure wave. Right: jet directivity as a function of azimuthal Fourier mode; note, consistent with image on the left, dominance of the axisymmetric mode in the downstream direction.

of the axisymmetric mode of the sound field at each axial station provides a corresponding scalogram. Figure 19 shows an example for the axial station, $x/D = 17$ (i.e. at low emission angle, $\theta \approx 30^\circ$). A series of high-amplitude events, labelled A - H, stand out. By setting a threshold the scalogram can be filtered and the time signal reconstructed such that only the said events are retained. In what follows we concentrate on the first high-amplitude event. This filtering procedure is applied to the sensors at all axial stations and the result is shown in figure 20. We have here isolated one particular piece of the observable, $\mathbf{q}_A(m = 0; 19 < tc_0/D < 30)$, and from this filtered information we will now work our way back into the flow, \mathbf{q}_D , in order to analyse and understand the flow events that caused the high-amplitude sound pressure fluctuation.

Figure 21 shows the flow at four consecutive times during the production of the said fluctuation. The following behaviour is observed. At $t = 8.576$ (top left) we see an axisymmetric wavepacket extending out to about $x/D = 5$, downstream of which the structures are tilted into something closer to mode 1. As far as the axisymmetric component of the flow is concerned we therefore have a truncated wavepacket. We saw in section §3 how such behaviour can lead to enhanced acoustic efficiency, and, indeed, consistent with this, a high-amplitude depression is emitted from the flow

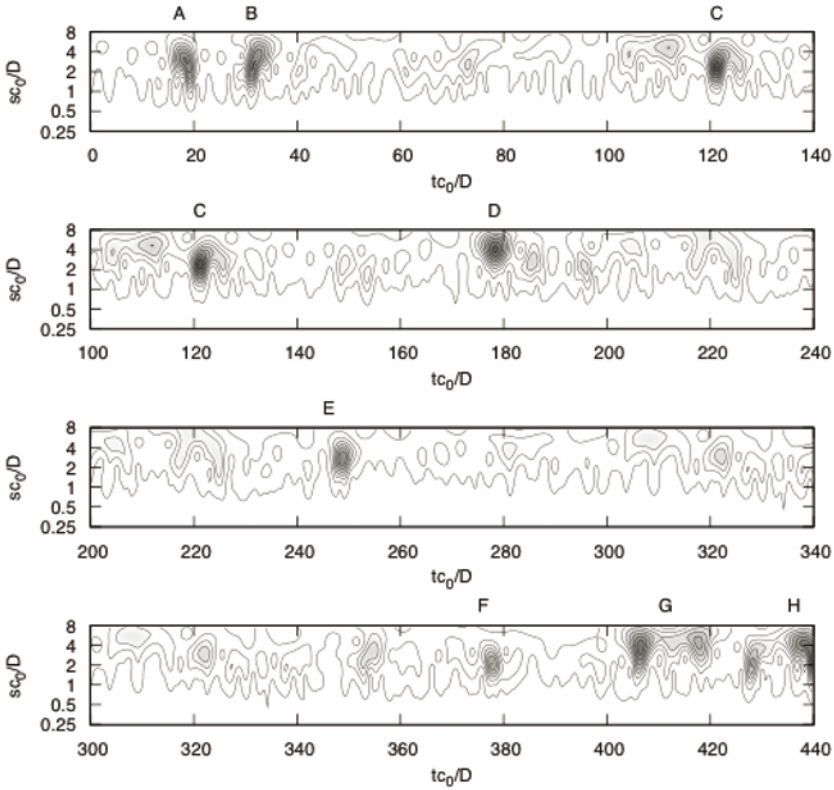


Figure 19. Scalogram computed from the time history of the axisymmetric acoustic mode at $r/D = 9$, $x/D = 17$

at this time. This propagating wave is the same observed in figure 20 at ($tc_0/D \approx 20$; $15 < x/D < 20$). After the emission of this wavefront the axisymmetric wavepacket extends axially, as seen in figure 21 at $t = 9.514$, and then undergoes a second truncation, at both the upstream and downstream ends ($t = 12.596$), at which point a second wavefront is released from the flow: this corresponds to the second depression observed, after wavelet transform, in figure 20, at ($tc_0/D \approx 25$; $15 < x/D < 20$). Finally, the axisymmetric wavepacket increases in both intensity and axial extent, as seen in figure 21 at $t = 16.48$, before collapsing a third time (not shown)

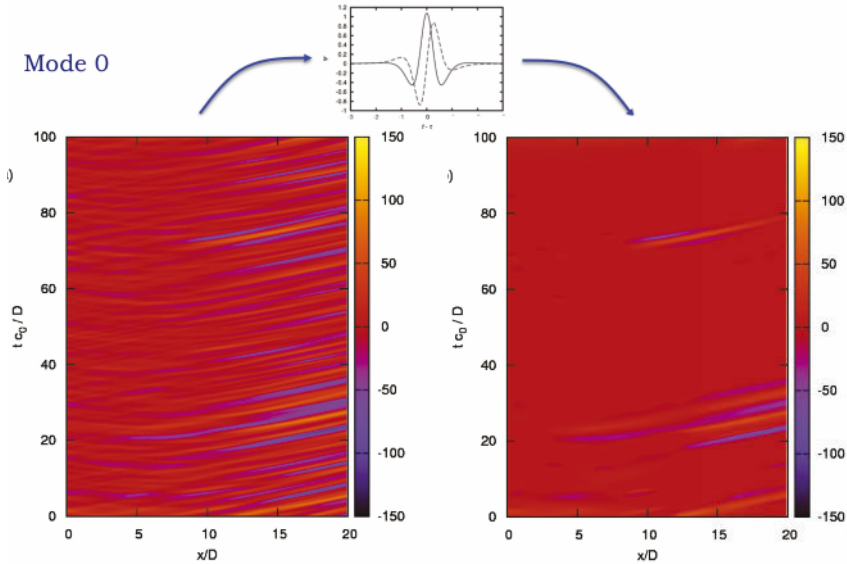


Figure 20. Left: space-time structure of axisymmetric component of sound field on cylindrical surface with $r/D = 9$. Right: same field after application of wavelet filtering; this serves to isolate high amplitude bursts.

and thereby releasing the third wavefront observed in figure 20.

The flow kinematics associated with the high-amplitude axisymmetric acoustic wavepacket is thus seen to comprise a drifting of the flow in and out of axially-extended axisymmetry; i.e. we have space-time modulation, or ‘jitter’ of an axisymmetric wavepacket. This behaviour is reminiscent of the observation of Crow and Champagne (1971) cited earlier: “three or four puffs form and induct themselves downstream, an interval of confused flow ensues, several more puffs form, and so on”. The third wavepacket *ansatz* proposed in section §3 would therefore appear to be appropriate. We recall the source model

$$T_{11}(\mathbf{y}, \tau) = 2\rho_0 U \tilde{u} \frac{\pi D^2}{4} \delta(y_2) \delta(y_3) A(\tau) e^{i(\omega\tau - ky_1)} e^{-\frac{y_1^2}{L^2(\tau)}}. \quad (109)$$

By application of a short-time Fourier series (figure 22), followed by the fitting of a Gaussian envelope function (figure 23), values of $A(\tau)$ and $L(\tau)$ are obtained. Inserting these into equation 109 and then solving the wave equation with this as source allows us to assess to what degree our kinematic

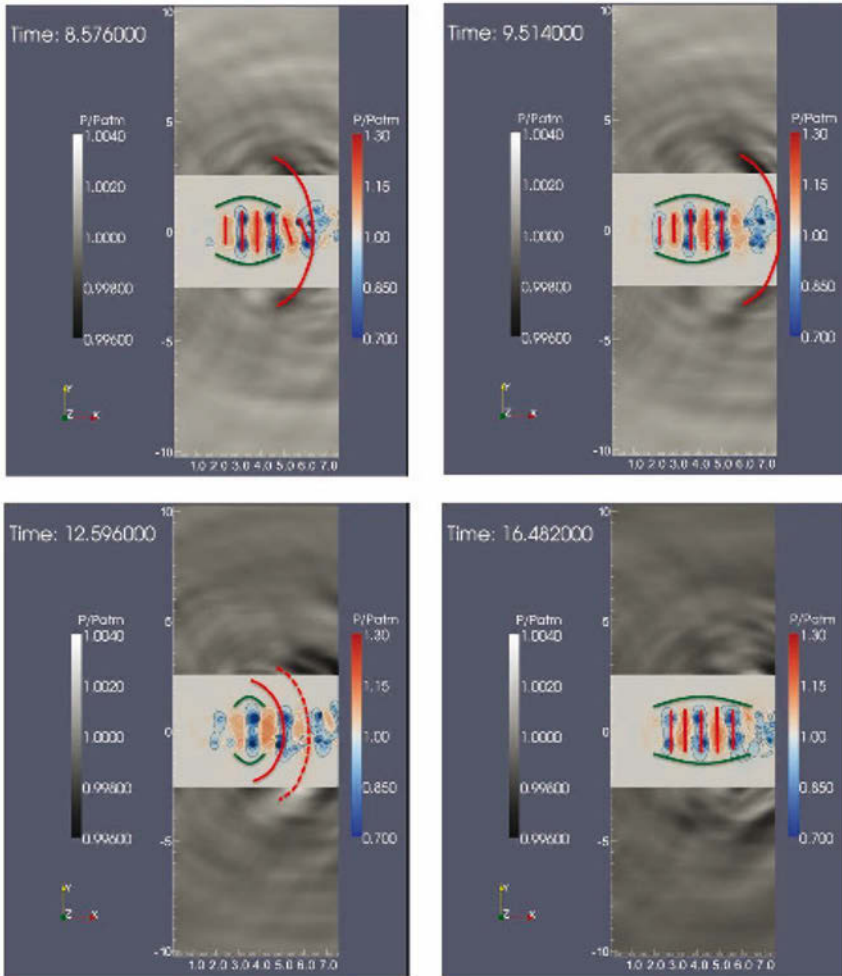


Figure 21. Visualisation of the hydrodynamic pressure within the jet at times corresponding to the acoustic wavepacket identified by wavelet transform in figure 20

source model, $s(\hat{\mathbf{q}}_D)$, reproduces a result, $\hat{\mathbf{q}}_A$, which is close to the acoustic observable \mathbf{q}_A . The result is shown in figure 24, where the result of the model is compared with both the OASPL of the axisymmetric mode of

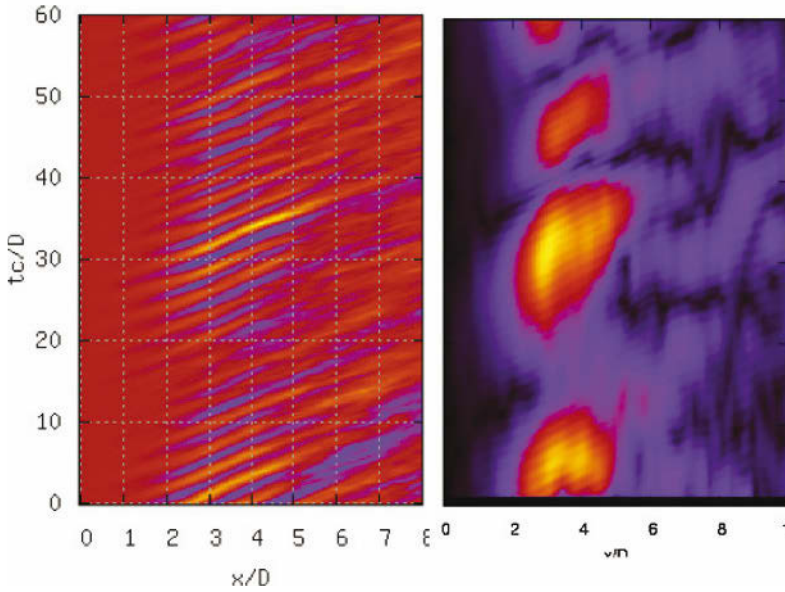


Figure 22. Left: space-time structure of axisymmetric component of axial velocity fluctuation at $r/D = 0.5$; right: short-time Fourier transform of the data in figure on the left.

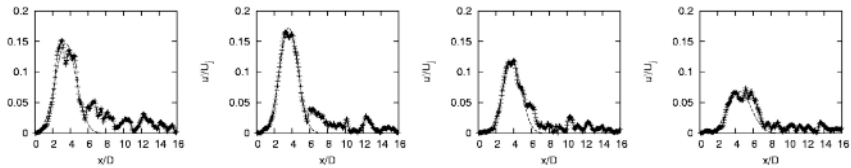


Figure 23. Gaussian functions are fitted to the result of projecting the flow data on the short-time Fourier series. In this way, values for the instantaneous wavepacket envelope amplitude, $A(\tau)$ and length scale, $L(\tau)$ can be obtained.

the LES, and a result obtained using a wavepacket *ansatz* where the time-averaged values of the $A(\tau)$ and $L(\tau)$ are used, i.e. a wavepacket that does not jitter. Whereas the non-jittering wavepacket shows a 12dB discrepancy

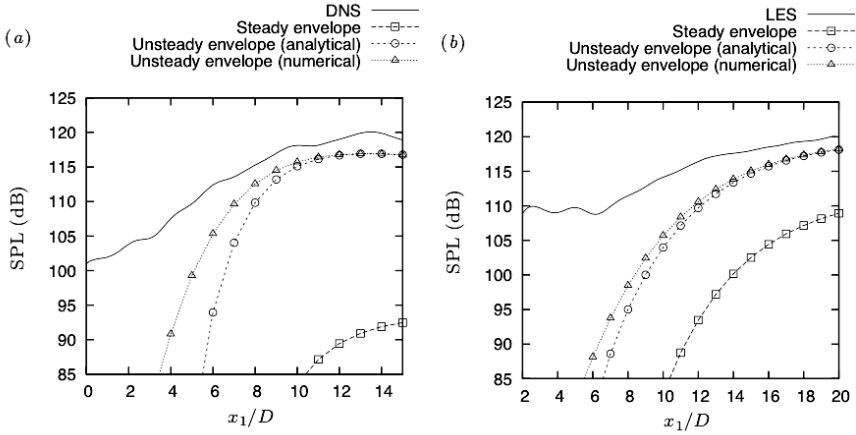


Figure 24. Comparison of the DNS and LES sound fields, left and right, respectively, with those obtained using simplified, jittering source models.

with the LES, showing it to be clearly incorrect, the jittering wavepacket is within 1.5dB, suggesting that this kinematic description is physically pertinent: this confirms that this behaviour comprises flow directions that are aligned with the propagation operator. The same procedure applied to the DNS database produced similar agreement, as can be seen in figure 24.

The next stage in the analysis methodology, which is work in progress, is to repeat the above analysis with respect to the other azimuthal Fourier modes of the sound field, in that way building up a composite, simplified kinematic description of the jet as a sound source, at which point it will be possible to address the question of the associated simplified dynamic law. Tools for reduced order dynamical modelling are outlined briefly in section §6.

4.2 Case study 2. High-resolution LES

The foregoing case study was considerably simplified by the relatively organised character of the flow solutions obtained using DNS and LES_{MR} . In this case study (taken from Kerhervé et al. (2010)) we consider a Large Eddy Simulation (Bogey et al. (2003)) with a higher order numerical scheme, which provides a flow solution with a broader range of turbulence scales in the noise producing region of the flow. This flow thus presents a greater

challenge in terms of flow feature education, and is in this respect a step closer to the high-Reynolds number experimental context.

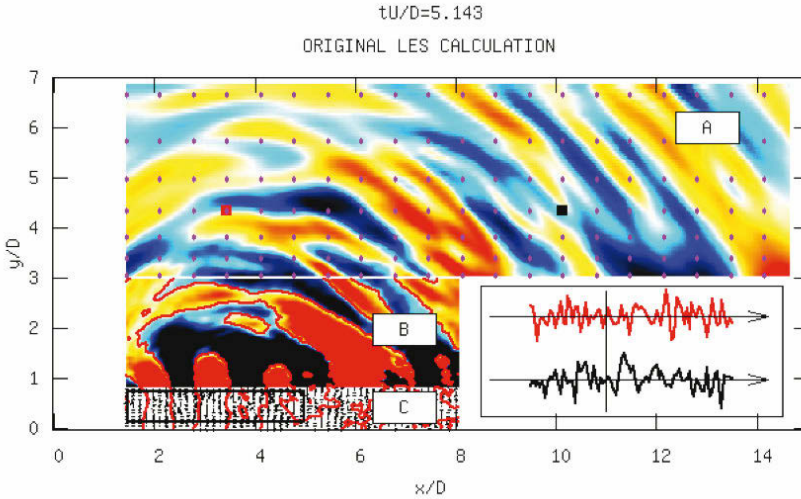


Figure 25. Large Eddy Simulation solution of Bogey et al. (2003), as used by Kerhervé et al. (2010). Zones *A*: linear acoustic region; zone *B*: nearfield, transition from non-linear hydrodynamics to linear acoustics; zone *C*: non-linear turbulent region.

A two-dimensional slice of the flow solution is shown in figure 25. Again, in the spirit of the analysis methodology outlined in section §3, we consider, separately, the acoustic region, where we define what is to be our observable, \mathbf{q}_A , and the flow region, where we are interested in reducing \mathbf{q}_D down to $\hat{\mathbf{q}}_D$. As seen in figure 25, the flow zone has been further split into zones *B* and *C*; the reason for this is that these zones present quite different behaviour. In zone *C* the flow is turbulent, non-linear, dominated by confused vortical motion, whereas in zone *B* fluctuations are predominantly irrotational, and a transition is observed, as we move radially through this region, the flow motions going from being dominated by hydrodynamics to being dominated by acoustics. It is often in this region of the flow, particularly in high Reynolds number experimental contexts, as the short historical note in section §3 outlined, that the signature of coherent structures is most easily observed.

Because of the greater complexity of both the flow and sound fields computed by this LES, we refine our definition of \mathbf{q}_A by filtering the sound field so as to only retain fluctuations associated with low-angle emission, which is believed to be predominantly contributed to by coherent structures. A frequency-wavenumber transform and subsequent filtering allows this to be achieved. The procedure works as follows. For each y - position in zone A, the pressure field is Fourier transformed from (x, t) to (k_x, ω) :

$$\tilde{p}(k_x, y, \omega) = \iint p(x, y, t) e^{-j(\omega t + k_x x)} dt dx. \quad (110)$$

A bandpass filter is then applied, which, for a given frequency, retains wavenumbers in the range $\omega/c(\theta_1) < k_x < \omega/c(\theta_2)$ where $c(\theta_i) = c_o/\cos(\theta_i)$ and θ_i denotes a given radiation direction. The bandpass filter is defined as

$$\Omega(\omega, k_x) = \begin{cases} 1 & \text{if } k_x < \omega/c(\theta_i) \\ \exp\left[-\frac{(k_x - |\omega|/c(\theta_i))^4}{\alpha^4}\right] & \text{otherwise} \end{cases}. \quad (111)$$

The filtered pressure is then recovered by inverse Fourier transform after application of the frequency-wavenumber filter,

$$p_f(x, y, t) = \iint \tilde{p}(k_x, y, \omega) \Omega(\omega, k_x) e^{j(\omega t - k_x x)} d\omega dk_x. \quad (112)$$

The results of the filtering are shown in figure 26. On the left the entire propagating field is shown in both frequency-wavenumber and physical space. The middle and right figures show, respectively, sound radiation in the angular sectors $0^\circ < \theta < 60^\circ$ and $60^\circ < \theta < 120^\circ$. The space-time field corresponding to the middle image is considered the acoustic observable, \mathbf{q}_A , and we now use this to construct a filter, $\mathcal{F}_{\mathbf{q}_A}$, by which we can eliminate, from the full flow solution, any information not directly associated with sound production. What remains is then considered the sound producing flow skeleton, which we can subsequently proceed to analyse and model.

Linear Stochastic Estimation The method used in order to perform the said filtering is based on Linear Stochastic Estimation, which provides a means by which an approximation of a conditional average

$$\hat{\mathbf{q}}(\mathbf{x}, t) = \langle \mathbf{q}(\mathbf{x}, t) | \mathbf{q}_A(\mathbf{x}, t + \tau) \rangle \quad (113)$$

can be obtained. For the specific case considered in this study, \mathbf{q} will be either the hydrodynamic pressure or the turbulent velocity, associated with

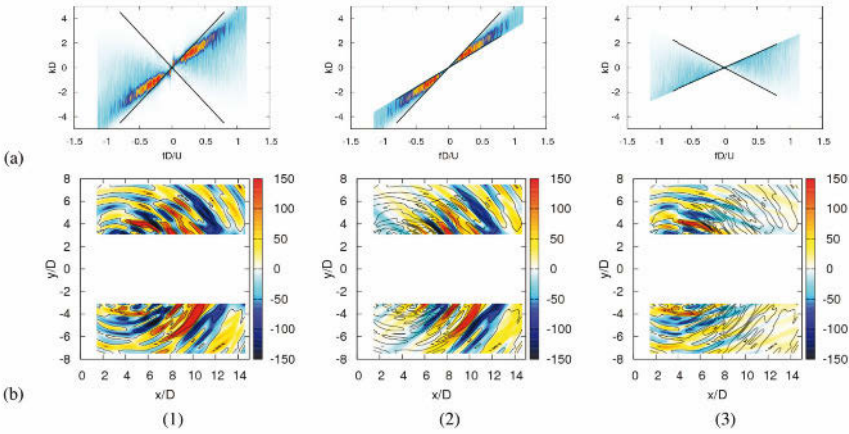


Figure 26. Top row: segments of frequency-wavenumber spectrum corresponding to radiation in different angular ranges; bottom row: corresponding instantaneous fields. Left column: $0^\circ < \theta < 180^\circ$; middle column: $0^\circ < \theta < 60^\circ$; right column: $60^\circ < \theta < 120^\circ$

the full LES solution, in zones B and C ; \mathbf{q}_A is the acoustic pressure, filtered so as to only retain components radiating in the angular range, $0 < \theta < 60$. The approach is used to determine, independently, conditional averages (which are here a function of space and of time) of the turbulent velocity and the pressure in zones B and C ¹⁴:

$$\hat{\mathbf{u}}(\mathbf{x}, t) = \langle \mathbf{u}(\mathbf{x}, t) | p_A(\mathbf{y}, t + \tau(\mathbf{x}|\mathbf{y})) \rangle \tag{114}$$

$$\hat{p}(\mathbf{x}, t) = \langle p(\mathbf{x}, t) | p_A(\mathbf{y}, t + \tau(\mathbf{x}|\mathbf{y})) \rangle, \tag{115}$$

where the time delay $\tau(\mathbf{x}|\mathbf{y})$ corresponds to the propagation time between each flow point and each observer (obtained by means of ray-tracing).

As LSE is comprehensively dealt with in section §5 we here simply recall the main result, which is that the above conditional average can be

¹⁴where the pressure is concerned it is, in zone C , predominantly hydrodynamic, while in zone B it contains an increasing proportion of acoustic fluctuation as we move radially away from the jet through zone B

approximated as

$$\hat{\mathbf{q}}(\mathbf{x}, t) = \sum_{i=1}^N a(\mathbf{x}, \mathbf{y}_i) p_A(\mathbf{y}_i, t + \tau(\mathbf{x}|\mathbf{y}_i)); \tag{116}$$

i.e. the value of the the filtered (conditional) flow variable, $\hat{\mathbf{q}}(\mathbf{x}, t)$, is obtained as the weighted linear combination of the values of the acoustic pressure, $p_A(\mathbf{y}_i, t + \tau(\mathbf{x}|\mathbf{y}_i))$; the acoustic domain, \mathbf{y} is discretised into an ensemble of discrete sensors. The coefficients $a(\mathbf{x}, \mathbf{y}_i)$ are obtained by solving a linear system of equations of the form $\mathbf{Q} = \mathbf{P} \cdot \mathbf{A}$ where,

$$\mathbf{Q} = \begin{bmatrix} \overline{q(\mathbf{x}, t) p_A(\mathbf{y}_1, t + \tau(\mathbf{x}|\mathbf{y}_1))} \\ \vdots \\ \overline{q(\mathbf{x}, t) p_A(\mathbf{y}_N, t + \tau(\mathbf{x}|\mathbf{y}_N))} \end{bmatrix} \quad \mathbf{A} = \begin{bmatrix} a(\mathbf{x}, \mathbf{y}_1) \\ \vdots \\ a(\mathbf{x}, \mathbf{y}_N) \end{bmatrix} \tag{117}$$

$$\mathbf{P} = \begin{bmatrix} \overline{p_A(\mathbf{y}_1, t) p_A(\mathbf{y}_1, t)} & \dots \\ \vdots & \ddots \\ \overline{p_A(\mathbf{y}_1, t) p_A(\mathbf{y}_N, t + \tau(\mathbf{x}|\mathbf{y}_N) - \tau(\mathbf{x}|\mathbf{y}_1))} & \dots \\ \dots & \overline{p_A(\mathbf{y}_N, t) p_A(\mathbf{y}_1, t + \tau(\mathbf{x}|\mathbf{y}_1) - \tau(\mathbf{x}|\mathbf{y}_N))} \\ \vdots & \vdots \\ \dots & \overline{p_A(\mathbf{y}_N, t) p_A(\mathbf{y}_N, t)} \end{bmatrix} \tag{118}$$

A sample of the result is shown in figure 27. Note the differences in flow field structure, in zones *B* and *C*, between the full Large Eddy Simulation solution ($\mathbf{q}(\mathbf{x}, t)$; figure on left) and the result obtained by Stochastic Estimation ($\hat{\mathbf{q}}(\mathbf{x}, t)$; figure on right). The quantity shown in zone *B* is pressure, while in zone *C* both pressure and velocity are shown (the bottom part of the figure shows a zoom on the section of zone *C* indicated by the black rectangle in the top part of the figure). In zone *C*, the velocity field is indicated by means of black arrows (showing the velocity vector in the plane), and the skeleton of the pressure field can be discerned by means of red iso-contours indicating $p(\mathbf{x}, t) = 0$ or $\hat{p}(\mathbf{x}, t) = 0$. In the case of $\hat{\mathbf{u}}(\mathbf{x}, t)$ the gamma criterion has been used to colour the velocity field. This quantity, often used as a visual aid for the study of coherent structures (Graftieaux et al. (2001),) is defined as:

$$\Gamma(\mathbf{P}) = \frac{1}{S} \int_S \frac{\mathbf{P} \mathbf{M} \wedge (\mathbf{U}_M - \mathbf{U}_P)] \cdot \vec{z}}{\|\mathbf{P} \mathbf{M}\| \cdot \|\mathbf{U}_M - \mathbf{U}_P\|} dS \quad \text{with} \quad \mathbf{U}_P = \frac{1}{S} \int_S \mathbf{U}_M dS, \tag{119}$$

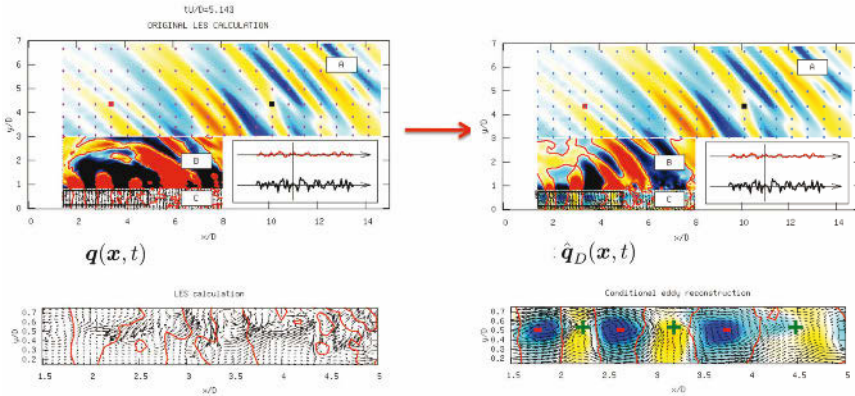


Figure 27. Left: Zone A: Low-angle filtered acoustic field; zones B and C: full LES solution. Right: Zone A Low-angle filtered acoustic field; zones B and C: conditional (filtered) flow, $\hat{\mathbf{q}}_D$

where P is the point where the function is evaluated, M lies in the region S centered on P —generally chosen as a rectangular area, \mathbf{z} is the unit vector normal to the measurement plane, \mathbf{U}_M and \mathbf{U}_P are the velocity vectors at point M and P respectively, and N is the number of point in S .

The result shown in figure 27 suggests the kind of wavepacket radiation observed in the previous studies. In zone C we observe a convected train of coherent vortical structures carrying a corresponding succession of positive and negative hydrodynamic pressures. The fact that the pressure and velocity fields are estimated independently, and yet produce a result that is, qualitatively, physically consistent (high and low hydrodynamic pressures carried, respectively, by vortical structures and saddle points), justifies our thinking about the result, $\hat{\mathbf{q}}(\mathbf{x}, t)$, as a sub-space of the flow.

We can now study this filtered field with a view to understanding what kind of simplified models might be appropriate where sound production is concerned. Two avenues appear worth pursuing: (1) We can decompose the field $\hat{\mathbf{q}}(\mathbf{x}, t)$ into orthogonal building blocks by means of Proper Orthogonal Decomposition; (2) we can study $\hat{\mathbf{q}}(\mathbf{x}, t)$ during periods of high-level sound emission in order to get a sense of what loud and quiet periods of flow activity look like. The first of these steps is of interest for two reasons. Firstly, the orthogonal building blocks constitute a basis that can help to characterise, and quantitatively assess the degree of complexity (the number

of degrees of freedom) of, the flow *kinematics*. And, secondly, the same basis provides a possible framework within which to begin studying the *dynamics* of the reduced-complexity flow skeleton.

Proper Orthogonal Decomposition Proper Orthogonal Decomposition (POD) is presented in some detail in section §5, we therefore here simply recall the main equations and results, before applying it to the both the complete flow solution, $\mathbf{q}(\mathbf{x}, t)$, and the reduced-complexity, filtered flow, $\hat{\mathbf{q}}(\mathbf{x}, t)$.

The snapshot POD is used in this situation. The eigenvalues and eigen-vectors of the two-time correlation function, $R(t, t')$, are first computed:

$$\int_T C(t, t') a^{(n)}(t') dt' = \lambda^{(n)} a^{(n)}(t) \quad (120)$$

where $a^{(n)}(t)$ are the eigen-vectors, $\lambda^{(n)}$ the eigenvalues and the two-time correlation function, $C(t, t')$, is defined as,

$$C(t, t') = \frac{1}{T} \iint_S \sum_{i=1}^{n_c} u_i(\mathbf{x}, t) u_i(\mathbf{x}, t') d\mathbf{x} \quad (121)$$

with $n_c = 3$ the number of components of the vector velocity field (when POD is effected on the pressure field, $n_c = 1$) and T the duration of the data set. An associated set of spatial functions $\Phi_i^{(n)}(\mathbf{x})$ can be obtained by projection of $a^{(n)}(t)$ onto the velocity or pressure fields:

$$\Phi_i^{(n)}(\mathbf{x}) = \int_T a^{(n)}(t) u_i(\mathbf{x}, t) dt \quad \text{with } i = 1, \dots, n_c. \quad (122)$$

The result of the POD can provide two pieces of information. The convergence of the eigenspectrum, shown in figure 28, gives a sense of how many POD modes are required to represent the flow: if the convergence is rapid a large portion of the flow energy is captured with relatively few modes, if it is slow we require a large number of modes to capture the same energy. The former situation indicates that the flow is relatively organised, while the latter indicates a more disorganised flow. The spatial modes $\Phi_i^{(n)}$ give us a sense of the characteristic spatial structures that dominate the flow.

The eigenspectrum, shown in figure 28, shows that while the eigenspectrum associated with \mathbf{q} has a slow convergence, 80 modes being required to capture 50% of the energy, that of $\hat{\mathbf{q}}$ is considerably more rapid, only 6 modes being necessary to represent the same percentage of the associated fluctuation energy.

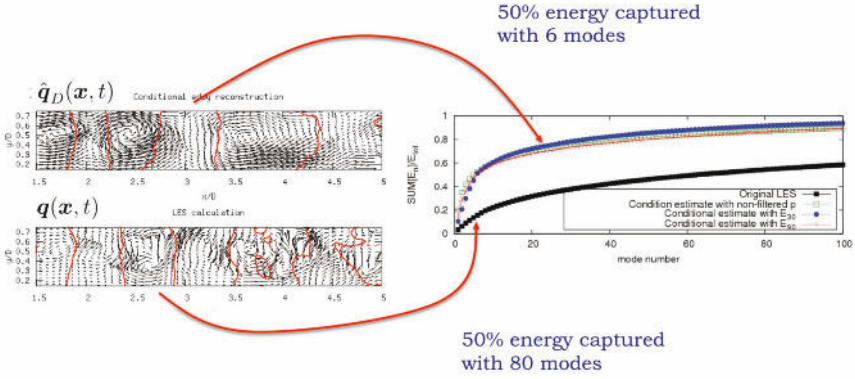


Figure 28. Eigenspectra associated with q and \hat{q}

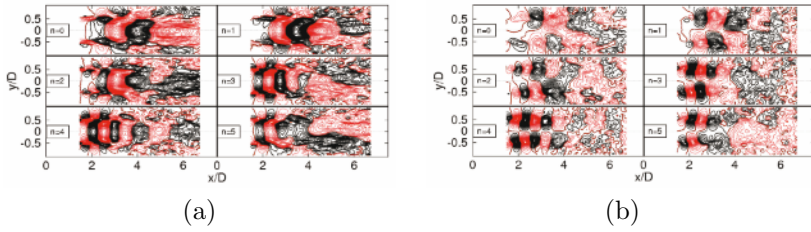


Figure 29. Eigenfunctions associated with \hat{q} ; (a): axial velocity; (b) radial velocity

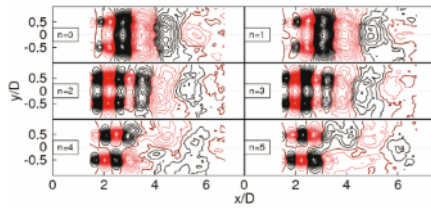


Figure 30. Eigenfunctions associated with \hat{q} : pressure.

The eigenfunctions, shown in figures 29 and 30, emphasise once again the orderly, wavelike character of $\hat{\mathbf{q}}$, in terms of both the velocity and the pressure fields, over the first five or so diameters. Two characteristic space scales can be distinguished in the velocity eigenfunctions: one is of the order of the jet diameter, manifest in modes 0 and 1, representative of activity towards the end of the potential core, and a second, smaller space scale is observed, in modes 2 through 5, representative of structures further upstream in the annular mixing-layer region of the flow. The pressure eigenfunctions are all characterised by similar scales; they peak farther upstream and there appears to be a distinction between modes 0 through 3, which have reflectional symmetry with respect to the jet axis, and modes 4 and 5 which are antisymmetric. These symmetries are most likely the two-dimensional signatures of axisymmetric and helical wavepackets.

Source mechanism analysis We now, finally, consider the space-time characteristics of $\hat{\mathbf{q}}$ associated with high- and low-level sound emission. Comparison of the pressure signature on the centerline of the jet gives a

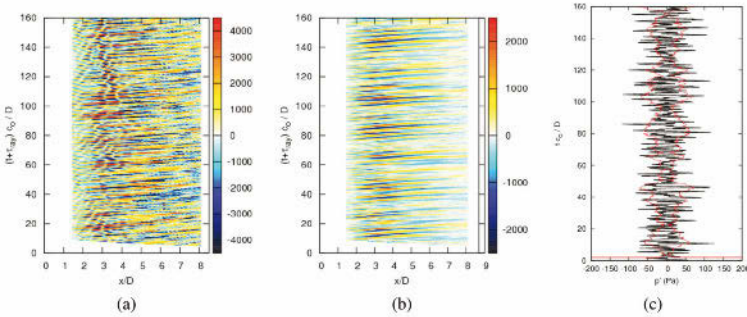


Figure 31. (a): (x, t) structure of full pressure (\mathbf{q}_p) on jet centerline; (b) (x, t) structure of reduced pressure ($\hat{\mathbf{q}}_p$) on jet centerline; (c): black line: acoustic pressure (\mathbf{q}_A) at 30° ; red line: short-time Fourier series of signal. Figure (c) has been time-shifted to account for propagation times, such that events at a given time are comparable with events in (a) and (b) at the same time-coordinate.

clearest indication of how the orderly component of the flow fields behave. Figure 31 shows this quantity for the full LES solution, $\mathbf{q}_p(x_1, t)$ and the reduced flow, $\hat{\mathbf{q}}_p(x_1, t)$, and these are compared with the acoustic signature,

$\mathbf{q}_A(t)$, sampled at an angle of 30° . The latter has been time-shifted such that a direct comparison can be made with the two signals. Furthermore, the acoustic signal has been transformed by means of a short-time Fourier series and the result is shown in red. This operation provides a means by which the loud portions of the signal can be more easily identified.

Examination of the figure shows the following. While it is difficult to discern any particular relationship between the hydrodynamic centerline signature of the full flow solution and the radiated sound, analysis of the same metric of the reduced field, $\hat{\mathbf{q}}_p$, reveals a clear correspondence between the growth and decay of wavepackets (modulation of both their amplitude and axial extent is observed) and high-amplitude sound radiation. The fitting procedure applied in the previous study is repeated here using the filtered flow field, $\hat{\mathbf{q}}$, and the jittering line source *ansatz*. The result is shown in figure 32. Good agreement is found between the acoustic observable, \mathbf{q}_A ,

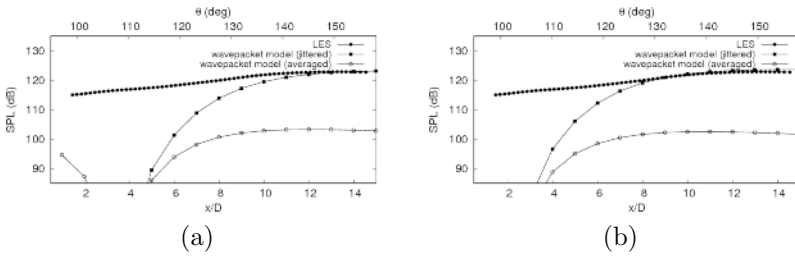


Figure 32. Comparison of sound field computed by Large Eddy Simulation with time-averaged and jittering wavepacket *ansatz*. (a) *ansatz* fitted with conditional field data, $\hat{\mathbf{q}}$, after radial integration; (b) *ansatz* fitted with conditiona field data, $\hat{\mathbf{q}}$ taken from mixing-layer axis.

and the modelled sound field, $\hat{\mathbf{q}}_A$, showing once again that the filtering procedure has been effective in the eduction of the sound-producing flow skeleton (kinematics).

4.3 Conclusions

Two case studies have been used, by way of example, in order to illustrate implementation of the analysis methodology outlined in section §3. In both cases, by following the methodology, kinematic models are constructed that mimic the sound-producing behaviour of the three different jets analysed. The quantitative accuracy is in all cases better than 1.5dB , showing the analysis methodology—which combines the data-analysis tools

presented in section §5 with the theoretical reasoning outlined in section §3—to be effective *with regard to the kinematics of sound source mechanism identification*. For the dynamic aspect further tools are necessary; these are presented briefly in section §6.

5 Data analysis / reduction

The complexity of most aeroacoustic systems—being associated with high Reynolds number turbulence—means that we frequently find ourselves faced with the task of making sense of large quantities of data; such databases may be the result of numerical simulation and/or experimental measurements. Some form of data synthesis, or reduction, is necessary. The data can be considerably compressed, for example, by considering only the time-averaged values of the dependent variables, but at the loss of a large quantity of information. Other time-averaged statistical moments, such as the root mean square (2nd order moment), skewness (3rd order moment) and kurtosis (4th order moment) can be computed—further information is thereby obtained regarding the state of the system.

Between such time-averaged quantities and the full space-time structure of the system considered there lie many intermediate possibilities for compressing the data into manageable and insight-providing forms. Four techniques by which such intermediate data compression can be obtained (Fourier transform, Wavelet transform, Proper Orthogonal Decomposition and Dynamic Mode Decomposition) are presented in this section, example implementations being found in section §4. Further to these data compression/decomposition tools we also present a technique, known as Linear Stochastic Estimation, for the computation of conditional averages. This can constitute a powerful complementary approach when used in conjunction with the said data compression/decomposition tools.

The four data compression techniques discussed have the following common property: they all involve the expansion of space-time data in terms of sets of basis functions. The interest in such an operation is that the very high dimensional flow data can be broken down into a more manageable number of ‘building blocks’, conducive to perspicacious analysis and modelling. In the case of spectral and wavelet analyses, the basis functions are analytic and specified *a priori*; in the case of Proper Orthogonal Decomposition the basis functions are empirical and thus intrinsic to the data; in the case of Koopman modes (obtained by Dynamic Mode Decomposition), the functions are associated with the dynamics of the system, in other words they contain information regarding the temporal evolution of the system.

5.1 The Fourier transform

The Fourier transform is probably the best known and most commonly used data analysis tool in the domain of fluid mechanics and aeroacoustics (and indeed in engineering in general) - the Fourier power spectrum of the sound field radiated by an aeroacoustic system is the quantity that mod-

elling tools are required to reproduce; it is the quantity by which we most often endeavour to assess and understand the behaviour of the system. We recall it briefly in this section, simply so as to have it appear in juxtaposition with a number of alternative, but less commonly used, data-processing tools. We do so because three of the latter (the wavelet transform, Proper Orthogonal Decomposition, and Dynamic Mode Decomposition), as evoked above, bear certain similarities to the Fourier transform in terms of the way their result can be useful as an aid to understanding and modelling; indeed these alternative processing techniques might be best thought of as surrogate tools for assessing complex data in situations where the Fourier transform may not necessarily be the best choice.

The Fourier transform involves the expansion of a given data set in terms of analytical basis functions that are specified *a priori*; there is no flexibility in this choice. The Fourier transform and its inverse are defined as

$$\tilde{q}(f) = \int_{-\infty}^{\infty} q(a) \exp(-2\pi i a f) da \quad (123)$$

$$q(f) = \int_{-\infty}^{\infty} \tilde{q}(f) \exp(2\pi i a f) df. \quad (124)$$

When the signal $q(a)$ is periodic in the variable a it can be expanded as a Fourier *series*:

$$q(a) = \frac{1}{2}A_0 + \sum_{n=1}^{\infty} A_n \cos(na) + \sum_{n=1}^{\infty} B_n \sin(na), \quad (125)$$

where

$$A_0 = \frac{1}{\pi} \int_{-\pi}^{\pi} q(a) da \quad (126)$$

$$A_n = \frac{1}{\pi} \int_{-\pi}^{\pi} q(a) \cos(na) da \quad (127)$$

$$B_n = \frac{1}{\pi} \int_{-\pi}^{\pi} q(a) \sin(na) da. \quad (128)$$

5.2 The wavelet transform

The wavelet transform provides additional flexibility on two levels when compared with the Fourier transform. (1) The transformed quantity is local in both frequency (or wavenumber) and time (or space); (2) many different kinds of basis function are available, and indeed it is possible to create new functions, provided certain mathematical constraints are satisfied.

The continuous wavelet transform of a signal $q(\alpha)$ is written:

$$\tilde{q}(s, a) = \int_{-\infty}^{\infty} q(\alpha)\psi(s, a - \alpha)d\alpha. \quad (129)$$

This amounts to the convolution of a signal of interest with a set of wavelet functions ψ . This set of functions is generated by dilation and translation of a basic form known as the mother wavelet: dilation is achieved by varying the scale, s , translation being effected by means of the variable, a , which could be a space or time coordinate, for example. The mother wavelet function must satisfy the mathematical constraints of admissibility and regularity; however, provided these constraints are satisfied a good deal of flexibility remains for the design of new mother wavelet functions.

The main difference between the wavelet transform and the Fourier transform is that the former allows space- or time-localised characteristics of a signal to be more clearly identified: the transformed signal is local in both space (and/or time) and scale, whereas its Fourier transformed counterpart is local only in frequency, being infinitely extended in space (and/or time).

The following are some relations between the fluctuation energy of a signal, its wavelet transform and its Fourier transform.

1. The relationship between the fluctuation energy, E of the signal $q(a)$ and the wavelet transform of the signal is given by:

$$E = \int_{\mathbb{R}} |q(a)|^2 da = C_{\psi}^{-1} \int_{\mathbb{R}^+} \int_{\mathbb{R}} |\tilde{q}(s, a)| \cdot |\tilde{q}^*(s, a)| \frac{ds da}{s^2} \quad (130)$$

where C_{ψ} is a constant associated with the mother wavelet function used.

2. A global wavelet energy spectrum can be defined as:

$$e_{\text{global}}(s) = \int_{\mathbb{R}} e(s, a) da \quad (131)$$

where $e(s, a)$ is the energy density as a function of scale, s and the space or time dimension, a .

3. This can also be expressed in terms of the Fourier energy spectrum $E(f) = |\hat{q}(f)|^2$:

$$e_{\text{global}}(s) = \int_{\mathbb{R}} E(f) |\hat{\psi}(sf)|^2 df \quad (132)$$

where $\hat{\psi}(sf)$ is the Fourier transform of the wavelet. This shows that the global wavelet energy spectrum corresponds to the Fourier energy spectrum smoothed by the wavelet spectrum at each scale.

4. The total fluctuation energy of the signal can be obtained by

$$E = C_\psi^{-1} \int_{\mathbb{R}^{+*}} e_{\text{global}}(s) \frac{ds}{s} \quad (133)$$

5.3 Proper Orthogonal Decomposition

The Proper Orthogonal Decomposition is a data processing technique which is known by this name when used in the field of turbulence analysis, following its introduction for such usage by Lumley (1967). It can also be found referred to as Karhunen-Loève decomposition, principal component analysis (Jolliffe (1986)) and singular value decomposition (Golub and Van Loan (1996)). The presentation of POD given here follows that of Delville (1995).

Consider a flow system for which we possess the information $\mathbf{q}(\mathbf{a}, \mathbf{b})$. The vector \mathbf{q} could contain, for example, the values of the three components of velocity on the four-dimensional grid, (\mathbf{x}, t) ; in this case \mathbf{a} would represent three-dimensional cartesian space, and \mathbf{b} the time direction. We retain the notation \mathbf{a} and \mathbf{b} in order to keep the derivation as general as possible, because different variants of the POD can be derived from different specific choices of \mathbf{a} and \mathbf{b} , and associated definitions of the inner product and averaging operations that are applied, respectively, with respect to these coordinates.

POD consists in searching for the function, $\phi(\mathbf{a})$, that is best aligned, on average, with the field $\mathbf{q}(\mathbf{a}, \mathbf{b})$, the averaging operation being with respect to the coordinate \mathbf{b} .¹⁵ Both $\mathbf{q}(\mathbf{a}, \mathbf{b})$ and $\phi(\mathbf{a})$ are indefinitely differentiable, have compact support, and belong to the space of square integrable functions. The problem is considered in Hilbert space, and so it is possible to define the inner product $(\mathbf{q}, \phi)_{\mathbf{a}}$ with respect to \mathbf{a} :

$$(\mathbf{q}, \phi)_{\mathbf{a}} = \int_{\mathbf{a}} \mathbf{q}(\mathbf{a}, \mathbf{b}) \phi^*(\mathbf{a}) d\mathbf{a} = \sum_{i=1}^{n_c} \int_{\mathbf{a}} q_i(\mathbf{a}, \mathbf{b}) \phi_i^*(\mathbf{a}) d\mathbf{a} \quad (134)$$

where n_c denotes the number of components of the vector \mathbf{q} (the three components of velocity for example).

The search for the function ϕ amounts to a search, over the ensemble of realisations of \mathbf{q} , for the ϕ that most closely resembles \mathbf{q} on average. This means maximising the projection $\mathbf{q}(\mathbf{a}, \mathbf{b})$ on the function $\phi(\mathbf{a})$ with respect to the inner product defined above: we must find the function ϕ

¹⁵Note that \mathbf{a} could comprise both space and time coordinates, and the averaging operation, over \mathbf{b} , could be, for example, a phase- or ensemble-average.

that maximises

$$\frac{\langle (\mathbf{q}(\mathbf{a}, \mathbf{b}), \phi(\mathbf{a}))^2 \rangle_{\mathbf{b}}}{\|\phi(\mathbf{a})\|} \quad (135)$$

The numerator can be expressed as

$$\langle (\mathbf{q}, \phi)^2 \rangle = \langle \int_{\mathbf{a}} \mathbf{q}(\mathbf{a}, \mathbf{b}) \phi^*(\mathbf{a}) d\mathbf{a} \int_{\mathbf{a}} \mathbf{q}(\mathbf{a}', \mathbf{b}) \phi^*(\mathbf{a}') d\mathbf{a}' \rangle_{\mathbf{b}} \quad (136)$$

$$= \int_{\mathbf{a}} \left(\int_{\mathbf{a}} \langle \mathbf{q}(\mathbf{a}, \mathbf{b}) \mathbf{q}^*(\mathbf{a}', \mathbf{b}) \rangle_{\mathbf{b}} \phi(\mathbf{a}') d\mathbf{a}' \right) \phi^*(\mathbf{a}) d\mathbf{a}, \quad (137)$$

the averaging being applied only to the (two-point correlations of the) data, $\mathbf{q}(\mathbf{a}, \mathbf{b})$, as ϕ is, by definition, independent of this direction. Denoting the two point correlation as $R_{ij}(\mathbf{a}, \mathbf{a}') = \langle \mathbf{q}(\mathbf{a}, \mathbf{b}) \mathbf{q}^*(\mathbf{a}', \mathbf{b}) \rangle_{\mathbf{b}}$ and introducing the Hermitian operator, A , such that

$$A \cdot \phi_i = \sum_{j=1}^{n_c} \int_{\mathbf{a}} R_{ij}(\mathbf{a}, \mathbf{a}') \phi_j(\mathbf{a}') d\mathbf{a}' \quad (138)$$

means that we can write

$$\langle (\mathbf{q}, \phi)_{\mathbf{a}}^2 \rangle = \sum_{i=1}^{n_c} (A \cdot \phi_i, \phi_i)_{\mathbf{a}}, \quad (139)$$

and so the POD problem comes down the maximising of

$$\frac{(A \cdot \phi_i, \phi_i)_{\mathbf{a}}}{\|\phi\|^2}. \quad (140)$$

This maximisation problem corresponds to a constrained optimisation: *find ϕ that maximises equation 140 subject to the constraint $\|\phi\|^2 = 1$* . This side-constraint is chosen because we are only interested in the shape of the functions, ϕ . The optimisation problem, which can be solved using the technique of Lagrange multipliers, or by variational analysis, leads to the following eigenvalue problem

$$A \cdot \phi_i = \lambda \phi_i, \quad (141)$$

or, in integral form

$$\sum_{j=1}^{n_c} \int_{\mathbf{a}} R_{ij}(\mathbf{a}, \mathbf{a}') \phi_j(\mathbf{a}') d\mathbf{a}' = \lambda \phi_i(\mathbf{a}), \quad (142)$$

¹⁶The notation $\langle \rangle_{\mathbf{b}}$ indicates that the averaging operation is with respect to the direction \mathbf{b}

an equation known as the Fredholm integral.

Solution of the integral eigenvalue problem is obtained by means of the theory of Hilbert-Schmidt Lovitt (1950). The details are not given here, but we recall some of the main results:

1. As with most eigenvalue problems, rather than admitting a unique solution, the equation yields a set of solutions:

$$\int_{\mathbf{a}} R_{ij}(\mathbf{a}, \mathbf{a}') \phi_j^{(n)}(\mathbf{a}') d\mathbf{a}' = \lambda^{(n)} \phi_i^{(n)}(\mathbf{a}) \quad n = 1, 2, 3, \dots \quad (143)$$

2. The ensemble of solutions can be chosen such that the eigenfunctions are orthonormal:

$$\int_{\mathbf{a}} \phi_i^{(p)}(\mathbf{a}) \phi_i^{(q)}(\mathbf{a}) d\mathbf{a} = \delta_{pq} \quad (144)$$

3. Any field, $q_i(\mathbf{a}, \mathbf{b})$, can be expanded in terms of these eigenfunctions, $\phi_i^{(n)}(\mathbf{a})$:

$$q_i(\mathbf{a}, \mathbf{b}) = \sum_{n=1}^{\infty} a^{(n)}(\mathbf{b}) \phi_i^{(n)}(\mathbf{a}) \quad (145)$$

where the coefficients, $a^{(n)}(\mathbf{b})$, are obtained by the projection of $q_i(\mathbf{a}, \mathbf{b})$ onto $\phi_i^{(n)}(\mathbf{a})$:

$$a^{(n)}(\mathbf{b}) = \int_{\mathbf{a}} q_i(\mathbf{a}, \mathbf{b}) \phi_i^{(n)}(\mathbf{a}) d\mathbf{a} \quad (146)$$

4. The series converges in a least mean square sense and the coefficients, $a^{(n)}(\mathbf{b})$, are mutually uncorrelated:

$$\langle a^{(n)} \cdot a^{(m)} \rangle = \delta_{mn} \lambda^{(n)} \quad (147)$$

5. The eigenvalues are real, positive, their sum finite and they form a convergent series:

$$\lambda^{(1)} > \lambda^{(2)} > \lambda^{(3)}, \dots \quad (148)$$

The most common experimental implementation of POD involves space-time velocity or pressure fields: $\mathbf{q}(\mathbf{a}, \mathbf{b}) = \mathbf{u}(\mathbf{x}, t) = \mathbf{u}(x, y, z, t)$ or $\mathbf{q}(\mathbf{a}, \mathbf{b}) = p(\mathbf{x}, t) = p(x, y, z, t)$ in which case expansion of the data in terms of the POD eigenfunctions reads

$$u_i(x, y, z, t) = \sum_{n=1}^{\infty} a^{(n)}(t) \phi_i^{(n)}(x, y, z) \quad (149)$$

or (150)

$$p(x, y, z, t) = \sum_{n=1}^{\infty} a^{(n)}(t) \phi^{(n)}(x, y, z). \quad (151)$$

The space-time structure of the measured field is thus separated into spatial (*topos*) and temporal (*chronos*) functions. Example implementations are provided in section §4.

5.4 Koopman modes / Dynamic mode decomposition

The *Dynamic Mode Decomposition* is a procedure for estimating the eigenvectors and eigenvalues of the *Koopman operator*. The latter provides a means by which the dynamics of a flow can be analysed, this analysis being effected through some associated observable. An assumption central to the approach is that the flow can be considered as a dynamical system evolving on a manifold Ω of dimension N . A manifold—the locus of points that comprise the state-space trajectory of a dynamical system—is a generalisation, to the non-linear case, of the eigenspace associated with the linear instability of dynamical system in the vicinity of a fixed point : while in a linearised system eigenvectors denote the directions in which that system will move, exponentially, either to or from a fixed point (or equilibrium point), in the non-linear context the manifold amounts to a continuation of these eigenvectors, which continually change direction as the system evolves non-linearly.

This section provides an introduction to both the Koopman operator and the dynamic mode decomposition. The exposition combines elements taken from Rowley et al. (2009), Schmid (2010) and Pastur (2011).

The Koopman operator Let X be a point on Ω , corresponding to the state of the system at some given time, and let f_t be a propagator (frequently referred to as a ‘flow’ or a ‘map’ in dynamical systems or control theory textbooks) that evolves, propagates, or maps, the flow from one time-step to the next; i.e. from $X(t_0) \in \Omega$ to $X(t_0 + t) \in \Omega$:¹⁷

$$X(t_0 + t) = f_t\{X(t_0)\}. \quad (152)$$

In an experiment we never have access to the full flow state; at best we may have access to the velocity field on a two-dimensional spatial section (from a PIV measurement for example), with restricted temporal resolution, or single-point information with higher temporal resolution (from a hot-wire, Laser Doppler Velocimeter or microphone for instance). Such an incomplete sample of the flow can be referred to as an *observable*. We denote this observation by means of a function, $q(X)$, which gives us the observable

¹⁷In the case of fluid flow the propagator is the right hand side of the Navier Stokes equations; i.e. the dynamic law governing the time evolution of the fluid flow.

corresponding to the full state X . q belongs to a Hilbert space, \mathcal{H} , and so we can define the norm:

$$\|q\| = \sqrt{(q, q)_\Omega} = \sqrt{\int_\Omega |q|^2 d\Omega} < \infty. \quad (153)$$

The *Koopman operator*, U_t , acts in \mathcal{H} , such that:

$$U_t\{q(X)\} = q(f_t\{X\}). \quad (154)$$

In other words, the Koopman operator is a map that describes the evolution of the *observable*, q (which is a function of the full flow state X), from one time-step to the next. The non-linear dynamics associated with the evolution of the full flow leaves its signature in the evolution of the observable; the essence of Koopman/DMD analysis is here: by considering the evolution of the observable we seek to gain insight regarding the nature of the evolution law that underpins the dynamics of the full flow.

The Koopman operator has the following important property. Let ϕ_j and λ_j be, respectively, eigenfunctions and associated eigenvalues of U_t .¹⁸ If we denote by X_k the state of the system at some time $k\Delta t$ after an initial time t_0 : $X_k \equiv X(t_0 + k\Delta t)$, then:

$$\begin{aligned} q(X_{k+1}) &= U\{q(X_k)\} = U\left\{\sum_{j \geq 1} \phi_j(X_k)\nu_j\right\} \\ &= \sum_{j \geq 1} U\{\phi_j(X_k)\nu_j\} = \sum_{j \geq 1} \lambda_j \phi_j(X_k)\nu_j \end{aligned} \quad (155)$$

The first equality simply corresponds to the definition of the Koopman operator—it evolves the observable, q , from its value when the system is in the state X_k to its value when the system is in the state X_{k+1} . In the second equality the observable, q , has been expanded in terms of the eigenfunctions of the Koopman operator (chosen here as a suitable set of basis functions); ν_j are the associated expansion coefficients, obtained by projecting the observable, q , onto the eigenfunctions, ϕ_j . In the third equality the Koopman operator has simply been moved inside the summation, while in the fourth, as ϕ_j are eigenfunctions of U , $U\{\phi_j\}$ can be written as $\lambda_j\phi_j$.

ν_j are the Koopman modes (sometimes referred to as Koopman coefficients, or dynamic modes), λ_j the Koopman eigenvalues and ϕ_j the Koopman eigenfunctions. The Dynamic Mode Decomposition constitutes a

¹⁸In what follows we will drop the the subscript t .

methodology, similar to the Arnoldi algorithm used in the solution of global stability problems, whereby these quantities can be *estimated* using *limited data sets*.

Now, as the evolution of the system from some initial state, X_0 to a later state X_{k+1} is given by $U^k(X_0)$ (because $U(X_k) = UU(X_{k-1}) = U^3(X_{k-2}) = \dots$), the state of the observable, $q(X_{k+1})$, can be expressed in terms of the state at some initial time, X_0 , as:

$$q(X_{k+1}) = \sum_{j \geq 1} \lambda_j^k \phi_j(X_0) \nu_j. \quad (156)$$

This equation shows that any value of the observable, q , can be deduced from knowledge of the projection of the initial condition $q(X_0)$ onto the eigenfunctions, ϕ_j , of the Koopman operator, provided the eigenvalues, λ_j are known; this property is important in what follows. Furthermore, if the dynamics considered evolve on a non-degenerated attractor—the dynamics continue to evolve on the manifold, Ω —then the Koopman operator, U , is a unit operator: the eigenvalues lie on the unit circle and the eigenvectors, ϕ_j , are orthogonal.

Krylov sub-space Consider the following set of successive snapshots of data:

$$Q_0^{N-1} = \{q(X_0), q(X_1), q(X_2), \dots, q(X_{N-1})\}, \quad (157)$$

the sub- and super-scripts on Q indicate the first and last snapshots. Expressed in terms of the Koopman operator this reads:

$$Q_0^{N-1} = \{q(X_0), U\{q(X_0)\}, U^2\{q(X_0)\}, \dots, U^{N-1}\{q(X_0)\}\}, \quad (158)$$

which is an N^{th} -order Krylov subspace. And we know that the Koopman operator applied to this subspace gives:

$$U\{Q_0^{N-1}\} = Q_1^N : \quad (159)$$

the action of the Koopman operator is inherently contained in Q_1^N .

To this point the observable has been considered a single-point scalar; however, the generalisation to multi-valued observables (for example a velocity field obtained from PIV) is straightforward. In this case the ν_j are multi-valued and complex.

Dynamic mode decomposition DMD is one possible technique, based on what is known as a companion Matrix, by which the eigenvalues and eigenvectors of U can be estimated; the technique is similar to that used

for the computation of global modes from the Hessenberg matrix using the Arnoldi method.

In what follows we will consider multi-valued observables, represented by the vector $\mathbf{q}(\mathbf{x}, t_k)$. A Krylov subspace is first constructed from sampled data, where the time-step is small enough to resolve all of the dynamics:

$$Q_0^{N-1} = \{\mathbf{q}_0, \mathbf{q}_1, \mathbf{q}_2, \dots, \mathbf{q}_{N-1}\}. \tag{160}$$

The indices correspond to the successive times, $t_0, t_1, t_2, \dots, t_{N-1}$. The assumption underpinning the companion matrix approach is that the first N fields (where $N < M$, M being the dimension of the observable \mathbf{q} , i.e. the number of spatial points in the snapshot) are sufficient to describe any later realisation of the field \mathbf{q} ; thus, the N^{th} snapshot can be expressed as a linear combination of all previous snapshots:

$$\mathbf{q}_N = c_0\mathbf{q}_0 + c_1\mathbf{q}_1 + c_2\mathbf{q}_2 + \dots + c_{N-1}\mathbf{q}_{N-1}, \tag{161}$$

or

$$\mathbf{q}_N = Q_0^{N-1}\mathbf{c}, \tag{162}$$

where $\mathbf{c} = (c_0, c_1, c_2, \dots, c_{N-1})^T$ and the superscript T denotes hermitian transpose. From equation 158 we know that

$$U \{Q_0^{N-1}\} = Q_1^N, \tag{163}$$

i.e. application of the Koopman operator to the Krylov subspace propagates all of the fields by one time-step. In light of this observation, and equation 162, equation 163 can be written as

$$UQ_0^{N-1} = Q_1^N = Q_0^{N-1}C + \mathbf{r}^T \mathbf{e}_N, \tag{164}$$

where C is the companion matrix. $\mathbf{e}_N = (0, 0, \dots, 1)^\dagger \in \mathbb{R}^{N+1}$ and \mathbf{r} is a residual vector, orthogonal to the Krylov subspace V_0^{N-1} . The residual goes to zero when condition 162 is satisfied.

The following example will help illustrate this. Consider that we have the data:

$$Q_1^4 = \begin{bmatrix} q_{11} & q_{12} & q_{13} & q_{14} \\ q_{21} & q_{22} & q_{23} & q_{24} \\ q_{31} & q_{32} & q_{33} & q_{34} \end{bmatrix}$$

where the first and second indices on the matrix entries denote spatial and temporal coordinates, respectively: each column is a snapshot. We know that the Koopman operator, U , will map from Q_1^3 to Q_2^4 :

$$\begin{bmatrix} U_{11} & U_{12} & U_{13} \\ U_{21} & U_{22} & U_{23} \\ U_{31} & U_{32} & U_{33} \end{bmatrix} \begin{bmatrix} q_{11} & q_{12} & q_{13} \\ q_{21} & q_{22} & q_{23} \\ q_{31} & q_{32} & q_{33} \end{bmatrix} = \begin{bmatrix} q_{12} & q_{13} & q_{14} \\ q_{22} & q_{23} & q_{24} \\ q_{32} & q_{33} & q_{34} \end{bmatrix}.$$

But, we are also making the assumption that \mathbf{q}_{i4} can be expressed as a linear combination of \mathbf{q}_{i1} , \mathbf{q}_{i2} and \mathbf{q}_{i3} :

$$\begin{bmatrix} q_{14} \\ q_{24} \\ q_{34} \end{bmatrix} \approx \begin{bmatrix} c_1 q_{11} + c_2 q_{21} + c_3 q_{31} \\ c_1 q_{12} + c_2 q_{22} + c_3 q_{32} \\ c_1 q_{13} + c_2 q_{23} + c_3 q_{33} \end{bmatrix}.$$

Substituting into the previous equation gives,

$$\begin{bmatrix} U_{11} & U_{12} & U_{13} \\ U_{21} & U_{22} & U_{23} \\ U_{31} & U_{32} & U_{33} \end{bmatrix} \begin{bmatrix} q_{11} & q_{12} & q_{13} \\ q_{21} & q_{22} & q_{23} \\ q_{31} & q_{32} & q_{33} \end{bmatrix} \approx \begin{bmatrix} q_{12} & q_{13} & (c_1 q_{11} + c_2 q_{21} + c_3 q_{31}) \\ q_{22} & q_{23} & (c_1 q_{12} + c_2 q_{22} + c_3 q_{32}) \\ q_{32} & q_{33} & (c_1 q_{13} + c_2 q_{23} + c_3 q_{33}) \end{bmatrix},$$

which is the same as

$$\begin{bmatrix} U_{11} & U_{12} & U_{13} \\ U_{21} & U_{22} & U_{23} \\ U_{31} & U_{32} & U_{33} \end{bmatrix} \begin{bmatrix} q_{11} & q_{12} & q_{13} \\ q_{21} & q_{22} & q_{23} \\ q_{31} & q_{32} & q_{33} \end{bmatrix} \approx \begin{bmatrix} q_{11} & q_{12} & q_{13} \\ q_{21} & q_{22} & q_{23} \\ q_{31} & q_{32} & q_{33} \end{bmatrix} \begin{bmatrix} 0 & 0 & c_1 \\ 1 & 0 & c_2 \\ 0 & 1 & c_3 \end{bmatrix}.$$

In the more general case, the companion matrix takes the form:

$$C = \begin{pmatrix} 0 & \dots & \dots & 0 & c_0 \\ 1 & 0 & & \vdots & c_1 \\ 0 & 1 & \ddots & \vdots & c_2 \\ \vdots & \ddots & \ddots & 0 & \vdots \\ 0 & \dots & 0 & 1 & c_{N-1} \end{pmatrix}. \quad (165)$$

DMD consists in computing the eigenmodes of the companion matrix, which are then considered as approximations of the eigenmodes of the Koopman operator (when the residual is zero the correspondence is exact). The matrix C has dimension $N \times N$, and its unknown elements, c_j , can be computed by minimising the norm

$$\mathbf{c}_{opt} = \min_{\mathbf{c}} \left\| \mathbf{q}_N - \sum_{j=1}^{N-1} c_j \mathbf{q}_j \right\|_2.$$

Having computed the eigenvalues and eigenvectors of the companion matrix we are finally in a position to write

$$\tilde{\mathbf{q}}_k = \sum_{j=1}^N \lambda_j^{k-1} \phi_j(X_0) \mathbf{v}_j. \quad (166)$$

The initial conditions $\phi_j(X_0)$ are obtained by projecting the initial field, \mathbf{q}_0 , on to the ν_j . The eigenfunctions, ϕ_j , are Fourier modes, $\phi_j = \exp(i\omega_j t)$ if the dynamics are periodic.

5.5 Conditional analysis techniques: Stochastic estimation

The following exposition is based on that of Adrian (1996). Consider some variable, \mathbf{q} , which is unknown, and another vector quantity $\mathbf{E} = E_i$, $i = 1..N$ which is somehow related to \mathbf{q} . We are interested in identifying the functional relationship, $\mathbf{q} = g(\mathbf{E})$, which provides some approximation of \mathbf{q} in terms of \mathbf{E} . This kind of estimation of one variable in terms of another is known as stochastic estimation and is widely used in information theory (Papoulis (1984)). When such a relationship cannot be usefully derived from first principals, we frequently revert to statistics: the *joint* probability density between \mathbf{q} and \mathbf{E} is:

$$f_{\mathbf{q},\mathbf{E}}d\psi d\phi = \text{Prob}\{\psi \leq \mathbf{q} < \psi + d\psi \text{ and } \phi \leq \mathbf{E} < \phi + d\phi\}; \tag{167}$$

the *conditional* probability density of \mathbf{q} given \mathbf{E} is

$$f_{\mathbf{q}|\mathbf{E}}(\psi|\phi) = \frac{f_{\mathbf{q},\mathbf{E}}(\psi, \phi)}{f_{\mathbf{E}}(\phi)}. \tag{168}$$

Three estimates of \mathbf{q} given \mathbf{E} are: (1) the *maximum likelihood estimate*, defined as the most probable value of \mathbf{q} given \mathbf{E} , i.e. the value at which $f_{\mathbf{q}|\mathbf{E}}$ is a maximum; (2) the *conditional average* of \mathbf{q} given \mathbf{E} , given by the centroid of the *conditional probability*

$$\langle \mathbf{q}|\mathbf{E} \rangle = \int \psi f_{\mathbf{q}|\mathbf{E}}(\psi|\phi) d\psi; \tag{169}$$

and, (3) the *mean square estimate*, i.e. the estimate $\hat{\mathbf{q}} = f(\mathbf{E})$ that minimises $\langle |\mathbf{q} - f(\mathbf{E})|^2 \rangle$. It can be shown that the best mean square estimate of \mathbf{q} given \mathbf{E} is the conditional average $\langle \mathbf{q}|\mathbf{E} \rangle$. In other words, $\langle |\mathbf{q} - f(\mathbf{E})|^2 \rangle$ is a minimum when $f(\mathbf{E}) = \langle \mathbf{q}|\mathbf{E} \rangle$.

In this section we outline a technique by which the conditional average can be *estimated*; in other words we wish to estimate the best estimate: $\hat{\mathbf{q}} \approx \langle \mathbf{q}|\mathbf{E} \rangle$. The conditional average is approximated by means of a truncated Taylor series expansion about $\mathbf{E} = 0$:

$$\hat{\mathbf{q}} \approx \langle \mathbf{q}|\mathbf{E} \rangle \equiv f(\mathbf{E}) \equiv f(0) + \frac{\partial f}{\partial \mathbf{E}} \frac{\mathbf{E}}{1!} + \frac{\partial^2 f}{\partial \mathbf{E}^2} \frac{\mathbf{E}^2}{2!} + \frac{\partial^3 f}{\partial \mathbf{E}^3} \frac{\mathbf{E}^3}{3!} + \dots \tag{170}$$

As we do not know the function $f(\mathbf{E})$ we cannot evaluate the derivatives $\frac{\partial^n f}{\partial \mathbf{E}^n}$ and so these are unknowns of the problem. So, considering that the

mean value is zero, ($f(0) = 0$), the expansion can be written

$$\hat{\mathbf{q}} \approx \langle \mathbf{q} | \mathbf{E} \rangle \equiv f(\mathbf{E}) \equiv A\mathbf{E} + B\mathbf{E}^2 + C\mathbf{E}^3 + \dots \quad (171)$$

and we are required to determine the value of the coefficients A, B, C, \dots . When truncation is performed after the linear term this expression is known as *Linear stochastic estimation*, when the quadratic term is included we speak of *quadratic stochastic estimation*, and so on...

Let us now see how to calculate the coefficients, A , in the case where truncation is performed after the linear term. We have

$$\hat{\mathbf{q}} \approx A\mathbf{E}, \quad (172)$$

and we would like to obtain a best estimate for $\langle \mathbf{q} | \mathbf{E} \rangle$; i.e. we need to minimise the error

$$e = \langle |\langle \mathbf{q} | \mathbf{E} \rangle - \hat{\mathbf{q}}|^2 \rangle \quad (173)$$

$$= \langle |\langle \mathbf{q} | \mathbf{E} \rangle - A\mathbf{E}|^2 \rangle, \quad (174)$$

we therefore require the solution to

$$\frac{\partial e}{\partial A} = 2 \langle -\langle \mathbf{q} | \mathbf{E} \rangle \mathbf{E} \rangle + 2A \langle \mathbf{E}\mathbf{E} \rangle = 0, \quad (175)$$

which is given by

$$A = \frac{\langle \langle \mathbf{q} | \mathbf{E} \rangle \mathbf{E} \rangle}{\langle \mathbf{E}\mathbf{E} \rangle} \quad (176)$$

$$= \frac{\langle \langle \mathbf{q}\mathbf{E} | \mathbf{E} \rangle \rangle}{\langle \mathbf{E}\mathbf{E} \rangle} \quad (177)$$

$$= \frac{\langle \mathbf{q}\mathbf{E} \rangle}{\langle \mathbf{E}\mathbf{E} \rangle}, \quad (178)$$

where \mathbf{E} has been brought inside the conditional average on account of its being constant with respect to the latter, and, in the final step, the conditional average has been performed over all values of \mathbf{E} , reducing the conditional average $\langle \langle \mathbf{q}\mathbf{E} | \mathbf{E} \rangle \rangle$ to the conventional average $\langle \mathbf{q}\mathbf{E} \rangle$.

So, the linear stochastic estimate of \mathbf{q} given some related event \mathbf{E} , which provides a best approximation to the conditional average $\langle \mathbf{q} | \mathbf{E} \rangle$, is:

$$\hat{\mathbf{q}} = \frac{\langle \mathbf{q}\mathbf{E} \rangle}{\langle \mathbf{E}\mathbf{E} \rangle} \mathbf{E}. \quad (179)$$

This shows the close relationship between the conditional average and the correlation function $\langle \mathbf{q}\mathbf{E} \rangle$. In the context of aeroacoustics, where \mathbf{E} is the

radiated acoustic pressure and \mathbf{q} the turbulence velocity, such correlations can be shown to provide an approximation to the integral solution of the acoustic analogy (Lee and Ribner (1972)). An example implementation of this technique is provided in section §4.

6 Reduced Order Modelling

6.1 Introduction

It was shown in section §4 how the analysis tools presented in section §5 can provide a useful means by which the analysis methodology outlined in section §3 can help guide kinematic modelling. However, the final goal, as evoked in the introduction, is to understand and model the dynamic law associated with sound production, as it is only then that one can really claim to have identified source mechanisms.

In this section we provide a very brief introduction to reduced order modelling. For a more complete treatment the reader is encouraged to refer to Noack et al. (2011).

6.2 Two approaches for reduced order dynamical modelling

The governing dynamic law of the full flow system is:

$$\mathcal{N}\mathbf{q} = 0. \quad (180)$$

The objective of reduced order modelling, the final stage of the analysis methodology outlined in section §3, is to construct a simplified dynamic law governing the evolution of a simplified kinematic field, $\hat{\mathbf{q}}$:

$$\hat{\mathcal{N}}\hat{\mathbf{q}} = 0. \quad (181)$$

Two reduced-order dynamic modelling strategies will be outlined here. The first is useful when relatively complete space-time data is available, from a numerical simulation for example, the second being useful in an experimental context, where more limited data is available. In both cases the objective is to write down an Ordinary Differential Equation that mimics either the dynamics of the Navier Stokes operator, or of some reduced sub-space of the system.

This can be achieved once the flow has been expanded in terms of a set of orthogonal basis functions, which can be obtained, for example, by means of POD:¹⁹

$$\hat{\mathbf{q}}(\mathbf{x}, t) = \sum_{n=1}^N a_n(t)\phi(\mathbf{x}). \quad (182)$$

The temporal evolution of the flow is here contained in $a_i(t)$, and so it is via these, the *topos*, that we can attempt to write down a simplified

¹⁹See section §5 for details.

evolution equation, in the form of an ODE:

$$\frac{da_i}{dt} = L_{ij}a_j + Q_{ijk}a_ja_k, \quad (183)$$

which mimics both linear and non-linear aspects of the dynamics, via, respectively, the first and second terms on the right hand side. The goal is to compute the coefficients, L_{ij} and Q_{ijk} , that best reproduce the (known) temporal structure of $a_i(t)$; we then have a simplified dynamic model for the flow (or flow sub-space) considered.

The difference between the two said approaches is in the way that the coefficients L_{ij} and Q_{ijk} are computed.

Galerkin projection In this approach, the Navier Stokes equations are projected onto the basis functions, $\phi(\mathbf{x})$, giving, directly

$$\frac{da_i}{dt} = \nu L_{ij}a_j + (Q_{ijk}^c + Q_{ijk}^p)a_ja_k \quad (184)$$

where

$$L_{ij} = (\phi_i, \Delta\phi_j) = \int_{\mathbf{x}} \phi_i \Delta\phi_j d\mathbf{x} \quad (185)$$

$$Q_{ijk}^c = (\phi_i, \nabla \cdot (\phi_j \otimes \phi_k)) = \int_{\mathbf{x}} \phi_i \nabla \cdot (\phi_j \otimes \phi_k) d\mathbf{x} \quad (186)$$

$$Q_{ijk}^p = (\phi_i, \phi_{jk}^p) = \int_{\mathbf{x}} \phi_i \phi_{jk}^p d\mathbf{x}. \quad (187)$$

$$(188)$$

Q_{ijk}^c is here associated with the non-linear convection term of the Navier-Stokes equations, Q_{ijk}^p is associated with the pressure term²⁰, while L_{ij} is associated with viscous and linear convection terms.

Polynomial identification This technique, proposed by Perret et al. (2006) is useful when only limited experimental data is available. The polynomial form

$$\frac{da_i}{dt} = L_{ij}a_j + Q_{ijk}a_ja_k \quad (189)$$

is chosen as a suitable generic dynamic *ansatz*; then, knowing the values of a_i , we have a linear system of equations with unknowns, L_{ij} and Q_{ijk} . By solving this linear system, the coefficients can be identified.

²⁰see Noack et al. (2011) for details

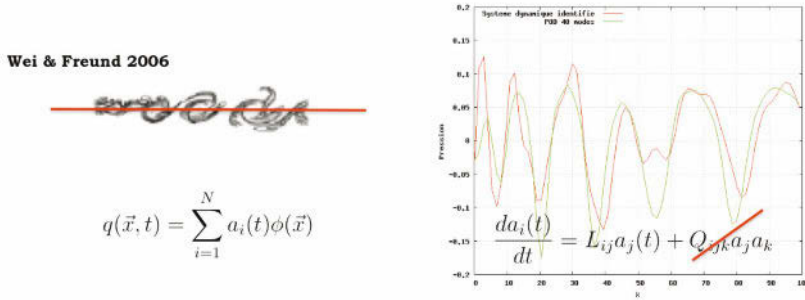


Figure 33. Left: instantaneous image of DNS of 2-D mixing-layer of Wei and Freund (2006): pressure fluctuations are sampled along the red line, and this field is then decomposed using POD; Right: green line shows a truncated representation of the DNS solution for the spatial structure of the pressure field on the red line at some given instant in time, while the red line shows the structure predicted by the simplified dynamic model given by the ODE—the quadratic term has been neglected in this example.

6.3 Example

Figure 33 shows an example implementation of the polynomial identification technique. The DNS computation of a two-dimensional shear-layer, performed by Wei & Freund, is used. The pressure field is sampled along the red line shown on the left of the figure. This sampled pressure field is then decomposed using Proper Orthogonal Decomposition, allowing it to be represented in terms of a set of temporal functions, $a_i(t)$, and spatial functions, $\phi(x)$. Using the polynomial identification technique, truncated to only include the linear term, the coefficients, L_{ij} are determined. The ODE is then integrated in time and the result compared with a truncated representation (using 40 POD modes, a number found sufficient to reproduce the full DNS field with good accuracy) of the original pressure field.

The integrated ODE, a snapshot of which is shown in figure 33, was found to follow the DNS very closely for about three convective time units. After this the two solutions begin to differ, although the simplified dynamic model continues to behave in a qualitatively similar manner to the DNS.

Bibliography

- G. K. Batchelor. *The theory of homogeneous turbulence*. Cambridge University Press, 1953. ISBN 0521041171.
- GK Batchelor and AE Gill. Analysis of the stability of axisymmetric jets. *Journal of Fluid Mechanics*, 14(04):529–551, 1962. ISSN 1469-7645.
- KA Bishop, JE Williams, and W. Smith. On the noise sources of the unsuppressed high-speed jet. *Journal of Fluid Mechanics*, 50(01):21–31, 1971. ISSN 1469-7645.
- D. J. Bodony and S. K. Lele. On using large-eddy simulation for the prediction of noise from cold and heated turbulent jets. *Physics of Fluids*, 17(8):085103, 2005.
- C. Bogey, C. Bailly, and D. Juvé. Noise investigation of a high subsonic, moderate Reynolds number jet using a compressible large eddy simulation. *Theoretical and Computational Fluid Dynamics*, 16(4):273–297, 2003. ISSN 0935-4964.
- G. L. Brown and A. Roshko. On density effects and large structure in turbulent mixing layers. *Journal of Fluid Mechanics*, 64(4):775–816, 1974.
- B.J. Cantwell. Organized motion in turbulent flow. *Annual Review of Fluid Mechanics*, 13(1):457–515, 1981. ISSN 0066-4189.
- A. V. G. Cavalieri, G. Daviller, P. Comte, P. Jordan, G. Tadmor, and Y. Gervais. Using LES to explore sound-source mechanisms in jets. In *IUTAM Symposium on Computational Aero-Acoustics for Aircraft Noise Prediction*, Southampton, UK, March 29-31 2010a.
- A. V. G. Cavalieri, P. Jordan, A. Agarwal, and Y. Gervais. Jittering wavepacket models for subsonic jet noise. In *AIAA Paper 2010-3957, 16th AIAA/CEAS Aeroacoustics Conference and Exhibit*, Stockholm, Sweden, June 7-9 2010b.
- A. V. G. Cavalieri, P. Jordan, A. Agarwal, and Y. Gervais. Jittering wavepacket models for subsonic jet noise. *Journal of Sound and Vibration*, accepted for publication, 2011a.
- A. V. G. Cavalieri, Jordan P., Y. Gervais, and T. Colonius. Axisymmetric superdirectivity in subsonic jets. In *AIAA Paper 2011-NNNN, 17th AIAA/CEAS Aeroacoustics Conference and Exhibit*, Portland, USA, June 7-9 2011b.
- Y.Y. Chan. Spatial waves in turbulent jets. *Physics of Fluids*, 17:46, 1974.
- B.T. Chu and L.S.G. Kovásznyay. Non-linear interactions in a viscous heat-conducting compressible gas. *Journal of Fluid Mechanics*, 3(05):494–514, 1958. ISSN 1469-7645.
- T. Colonius, A. Samanta, and K. Gudmundsson. Parabolized stability equation models of large-scale jet mixing noise. *Procedia Engineering*, 6: 64–73, 2010. ISSN 1877-7058.

- D. G. Crighton. Basic principles of aerodynamic noise generation. *Progress in Aerospace Sciences*, 16(1):31–96, 1975.
- D. G. Crighton and M. Gaster. Stability of slowly diverging jet flow. *Journal of Fluid Mechanics*, 77(2):397–413, 1976. ISSN 0022-1120.
- D. G. Crighton and P. Huerre. Shear-layer pressure fluctuations and superdirective acoustic sources. *Journal of Fluid Mechanics*, 220:355–368, 1990.
- S. C. Crow. Acoustic gain of a turbulent jet. *Phys. Soc. Meeting, Univ. Colorado, Boulder*, 6(paper IE), 1972.
- S. C. Crow and F. H. Champagne. Orderly structure in jet turbulence. *Journal of Fluid Mechanics*, 48(3):547–591, 1971.
- J. Delville. *La decomposition orthogonale aux valeurs propres et l'analyse de l'organisation tridimensionnelle des ecoulements turbulents cisailles libres*. PhD thesis, Universite de Poitiers, 1995.
- P.E. Dimotakis and G.L. Brown. The mixing layer at high Reynolds number: large-structure dynamics and entrainment. *Journal of Fluid Mechanics*, 78(03):535–560, 1976. ISSN 1469-7645.
- J. E. Ffowcs Williams and A. J. Kempton. The noise from the large-scale structure of a jet. *Journal of Fluid Mechanics*, 84(4):673–694, 1978. ISSN 0022-1120.
- J. B. Freund. Noise sources in a low-Reynolds-number turbulent jet at Mach 0.9. *Journal of Fluid Mechanics*, 438:277–305, 2001.
- HV Fuchs. Space correlations of the fluctuating pressure in subsonic turbulent jets. *Journal of Sound and Vibration*, 23(1):77–99, 1972. ISSN 0022-460X.
- W. K. George, P. D. Beuther, and R. E. A. Arndt. Pressure spectra in turbulent free shear flows. *Journal of Fluid Mechanics*, 148:155–191, 1984. ISSN 0022-1120.
- M. E. Goldstein. A generalized acoustic analogy. *Journal of Fluid Mechanics*, 488:315–333, 2003.
- M. E. Goldstein. On identifying the true sources of aerodynamic sound. *Journal of Fluid Mechanics*, 526:337–347, 2005. ISSN 0022-1120.
- G.H. Golub and C.F. Van Loan. *Matrix computations*. Johns Hopkins Univ Pr, 1996. ISBN 0801854148.
- L. Graftieaux, M. Michard, and N. Grosjean. Combining PIV, POD and vortex identification algorithms for the study of unsteady turbulent swirling flows. *Measurement Science and Technology*, 12:1422, 2001.
- A. Hussain and K. Zaman. The preferred mode of the axisymmetric jet. *Journal of fluid mechanics*, 110(-1):39–71, 1981. ISSN 1469-7645.
- IT Jolliffe. Principal component analysis., 1986.

- F. Kerhervé, P. Jordan, C. Bogey, and D. Juvé. Jet turbulence characteristics associated with downstream and sideline sound emission. In *AIAA Paper 2010-3964, 16th AIAA/CEAS Aeroacoustics Conference and Exhibit*, Stockholm, USA, June 2010.
- H.K. Lee and HS Ribner. Direct correlation of noise and flow of a jet. *The Journal of the Acoustical Society of America*, 52:1280, 1972.
- L. Lesshafft, P. Huerre, and P. Sagaut. Aerodynamic sound generation by global modes in hot jets. *Journal of Fluid Mechanics*, 647:473–489, 2010. ISSN 0022-1120.
- M. J. Lighthill. On sound generated aerodynamically. I. General theory. *Proceedings of the Royal Society of London. Series A, Mathematical and Physical Sciences*, pages 564–587, 1952.
- G. M. Lilley. On the noise from jets. *AGARD CP-131*, pages 13–1, 1974.
- W.V. Lovitt. *Linear integral equations*. Dover Publications, 1950.
- JL Lumley. The structure of inhomogeneous turbulent flows. *Atmospheric turbulence and radio wave propagation*, pages 166–178, 1967.
- R. Mankbadi and JTC Liu. Sound generated aerodynamically revisited: large-scale structures in a turbulent jet as a source of sound. *Philosophical Transactions of the Royal Society of London. Series A, Mathematical and Physical Sciences*, 311(1516):183–217, 1984. ISSN 0080-4614.
- A. Michalke. A wave model for sound generation in circular jets. Technical report, Deutsche Luft- und Raumfahrt, November 1970. URL <http://elib.dlr.de/63062/>.
- A. Michalke. Instabilität eines Kompressiblen Runden Freistrahls unter Berücksichtigung des Einflusses der Strahlgrenzschichtdicke. *Z. Flugwiss*, 19:319–328; English translation: NASA TM 75190, 1977, 1971.
- A. Michalke. On the effect of spatial source coherence on the radiation of jet noise. *Journal of Sound and Vibration*, 55(3):377–394, 1977. ISSN 0022-460X.
- A. Michalke and H. V. Fuchs. On turbulence and noise of an axisymmetric shear flow. *Journal of Fluid Mechanics*, 70:179–205, 1975.
- A. Michalke and A. Timme. On the inviscid instability of certain two-dimensional vortex-type flows. *Journal of Fluid Mechanics*, 29(04):647–666, 1967. ISSN 1469-7645.
- U. Michel. The role of source interference in jet noise. In *15th AIAA/CEAS Aeroacoustics Conference(30th Aeroacoustics Conference)*, pages 1–15, 2009.
- E. Mollo-Christensen. Measurements of near field pressure of subsonic jets. Technical report, ADVISORY GROUP FOR AERONAUTICAL RESEARCH AND DEVELOPMENT PARIS (FRANCE), 1963.

- E. Mollo-Christensen. Jet noise and shear flow instability seen from an experimenter's viewpoint (Similarity laws for jet noise and shear flow instability as suggested by experiments). *Journal of Applied Mechanics*, 34:1–7, 1967.
- E. Mollo-Christensen and R. Narasimha. Sound emission from jets at high subsonic velocities. *Journal of Fluid Mechanics*, 8(01):49–60, 1960. ISSN 1469-7645.
- C. J. Moore. The role of shear-layer instability waves in jet exhaust noise. *Journal of Fluid Mechanics*, 80(2):321–367, 1977.
- B.R. Noack, M. Morzynski, and G. Tadmor. *Reduced-Order Modelling for Flow Control. CISM Courses and Lectures 528*. Springer-Verlag Berlin (in press), 2011.
- L. Pastur. personal communication, 2011.
- L. Perret, E. Collin, and J. Delville. Polynomial identification of POD based low-order dynamical system. *Journal of Turbulence*, 7(17):1–15, 2006.
- O.M. Phillips. On the generation of sound by supersonic turbulent shear layers. *Journal of Fluid Mechanics*, 9(1):1–28, 1960. ISSN 0022-1120.
- C.W. Rowley, I. Mezić, S. Bagheri, P. Schlatter, and D.S. Henningson. Spectral analysis of nonlinear flows. *Journal of Fluid Mechanics*, 641(-1): 115–127, 2009. ISSN 1469-7645.
- A. Samanta, J. B. Freund, M. Wei, and S. K. Lele. Robustness of acoustic analogies for predicting mixing-layer noise. *AIAA Journal*, 44(11):2780–2786, 2006.
- P.J. Schmid. Dynamic mode decomposition of numerical and experimental data. *Journal of Fluid Mechanics*, 656:5–28, 2010. ISSN 0022-1120.
- S. Sinayoko, A. Agarwal, and Z. Hu. Flow decomposition and aerodynamic sound generation. *Journal of Fluid Mechanics*, 668:335–350, 2011. ISSN 1469-7645.
- T. Suzuki and T. Colonius. Instability waves in a subsonic round jet detected using a near-field phased microphone array. *Journal of Fluid Mechanics*, 565:197–226, 2006.
- C. K. W. Tam and P. J. Morris. The radiation of sound by the instability waves of a compressible plane turbulent shear layer. *Journal of Fluid Mechanics*, 98(2):349–381, 1980. ISSN 0022-1120.
- C.K.W. Tam and D.E. Burton. Sound generated by instability waves of supersonic flows. Part 2. Axisymmetric jets. *Journal of Fluid Mechanics*, 138(-1):273–295, 1984. ISSN 1469-7645.
- C. E. Tinney and P. Jordan. The near pressure field of co-axial subsonic jets. *Journal of Fluid Mechanics*, 611:175–204, 2008.
- M. Wei and J. B. Freund. A noise-controlled free shear flow. *Journal of Fluid Mechanics*, 546:123–152, 2006.